For Reference

NOT TO BE TAKEN FROM THIS ROOM

For Reference

NOT TO BE TAKEN FROM THIS ROOM

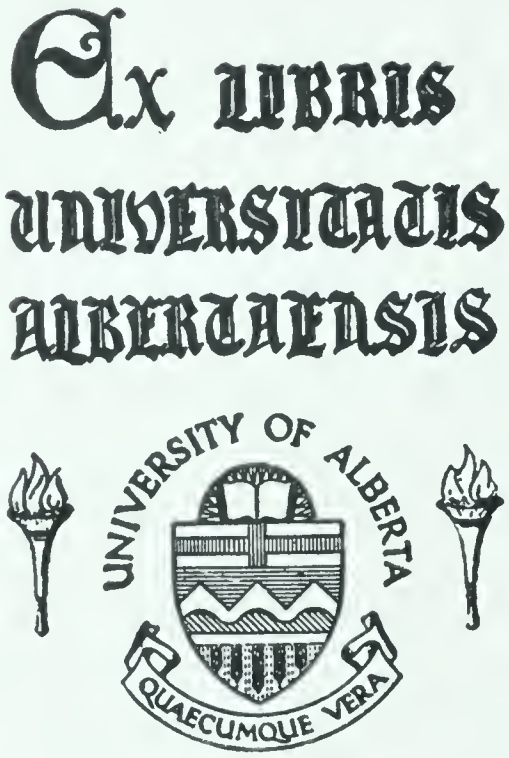

University of Alberta
Printing Department

Digitized by the Internet Archive
in 2019 with funding from
University of Alberta Libraries

https://archive.org/details/studyoflinearste00rjha

Thesis
1963
#21

THE UNIVERSITY OF ALBERTA

"A STUDY OF LINEAR, STEADY STATE, GAS FLOW THROUGH CONSOLIDATED POROUS MEDIA"

BY

R.J. HAMILTON

A THESIS

SUBMITTED TO THE FACULTY OF GRADUATE STUDIES

IN PARTIAL FULFILLMENT OF

THE REQUIREMENTS FOR THE DEGREE OF

MASTER OF SCIENCE IN PETROLEUM ENGINEERING

FACULTY OF ENGINEERING

DEPARTMENT OF CHEMICAL AND PETROLEUM ENGINEERING

EDMONTON, ALBERTA

FEBRUARY, 1963

ABSTRACT

Experimental and published results, on the flow of gas through consolidated porous media, have been correlated on a log log plot in terms of the permeability, porosity and an inertial resistance coefficient β . This plot indicates that an assumed linear relationship between the three factors is justified based on the experimental data available. An equation for this relationship is proposed.

The limited data obtained, for the flow of a gas through a porous media when the temperature of the media and of the flowing gas was varied, indicate that the permeability is a function of the temperature. An early investigation reported in the literature indicated that no dependence on temperature was apparent. Further investigation of this effect needs to be carried out.

Experimental evidence, from the use of large core samples, points out the need for the proper design of the equipment and the use of proper core mounting methods. Significantly different calculated results can be obtained on the same porous core when data measuring points are incorrectly located. An example showing the magnitude of the error caused by incorrectly located pressure measuring points is shown.

ACKNOWLEDGEMENT

The writer wishes to express his appreciation to Dr. D.L. Flock, Department of Chemical and Petroleum Engineering, University of Alberta, under whose guidance and direction this research project was completed, and to the Pan American Petroleum Corporation for making available their Fellowship in Petroleum Engineering.

A debt of gratitude is certainly due my wife whose encouragement and understanding eased the task of completing this thesis.

TABLE OF CONTENTS

	Page
LIST OF TABLES	i
LIST OF FIGURES	ii
INTRODUCTION	1
THEORY	5
EXPERIMENTAL EQUIPMENT	13
EXPERIMENTAL PROCEDURE	19
Sample Preparation	19
Porosity Measurement	21
Flow Measurement	25
DISCUSSION of EXPERIMENTAL RESULTS	27
CONCLUSIONS and RECOMMENDATIONS	58
NOMENCLATURE	61
BIBLIOGRAPHY	63
APPENDIX I	66
APPENDIX II	113
APPENDIX III	118

LIST OF TABLES

Table	Title	Page
1	Small Core Physical Properties	24
2	P^2 - pressure squared at points equi-spaced along the length of the Alundum core	32
3	Summary of Porosity and Flow Data for Consolidated Porous Media	42
4	Comparison of Permeabilities determined from both Flow Data and Klinkenberg plots	47
5-20	Gas Flow Data	67 to 87
21-35	Summarized Calculations of the Experimentally Determined Flow Characteristics of Consolidated Porous Media	88 to 108

LIST OF FIGURES

Figure	Title	Page
1	Small Core Holder	15
2	Diagram of Experimental Apparatus	16
3	Core Fracturing Device	20
4	Oilwell Research Porosimeter	22
5	P^2 - Pressure Squared Profile	30
6	P^2 - Pressure Squared Profile	31
7	Flow Data Plot to Obtain α and β - Alundum Core	36
8	Flow Data on Consolidated Porous Cores	37
9	Flow Data Plot to Obtain α and β - Cardium Cores	39
10	Flow Data Plot to Obtain α and β - Sturgeon Lake Cores	40
11	Flow Data Plot to Obtain α and β - Viking Cores	41
12	Flow Data on Consolidated Porous Cores	44
13	Reynolds number - Friction Factor Plot	45
14	Reynolds number - Friction Factor Plot	46
15	Klinkenberg Permeability Plot	48
16	Klinkenberg Permeability Plot	48
17	Correlation of β Factor with Permeability and Porosity	50
17a	Correlation of β Factor with Permeability and Porosity	53
18	Flow Data Plot to Obtain α and β - effect of temperature	56
19	Flow Data Plot to Obtain α and β - Cardium Core	109
20	Flow Data Plot to Obtain α and β - Belly River Core	109
21	Flow Data Plot to Obtain α and β - Indiana Core	110

LIST OF FIGURES (continued)

Figure	Title	Page
22	Flow Data Plot to Obtain α and β - Berea Core	110
23	Flow Data Plot to Obtain α and β - Blairmore Core	111
24	Flow Data Plot to Obtain α and β - Indiana Core	112
25	Klinkenberg Permeability Plot	112
26	Compressibility factor of Nitrogen	119
27	Viscosity of Nitrogen	120
28	Vapour Pressure of Water	121
29	Relative Density of Mercury	122
30	Relative Density of Water	123

INTRODUCTION

A review of the literature concerned with the flow of a gas through a porous media was carried out. The experimental and theoretical evidence indicates, that when the range of validity of Darcy's law has been exceeded, an equation of the form proposed by Forchheimer will describe the flow of a gas through a porous media. This takes place when the inertial effects due to the complicated nature of the flow path become significant.

$$\frac{dP}{dL} = \alpha v + \beta v^2$$

A nomenclature defining the terms used in all equations is shown at the end of this work. Equations similar to the Forchheimer equation have been developed based on different theories. The final form of the equation used in this study, for the flow of a perfect gas with account taken of the compressibility, is the one developed by Green and Duwez but expressed in a slightly different form.

$$\frac{\Delta(P^2)}{2} \frac{M}{L} \frac{g_c}{(ZRT)\mu G} = \alpha + \beta\left(\frac{G}{\mu}\right)$$

The terms in the equation are

$\Delta(P^2)$ = difference of squared pressures

M = molecular weight of gas

g_c = conversion factor

L = length of porous sample

Z = compressibility

R = gas constant

T = temperature

μ = viscosity

G = mass velocity

α = coefficient of laminar term of flow equation

β = coefficient of inertial resistance term of flow equation

The factors α and β are a measure of the pressure loss which can be attributed to the viscous resistance and inertial energy loss respectively. This equation is linear and when plotted will yield the values of α and β for the rock being studied. The factor α is seen to be the inverse of the permeability K.

This was the procedure followed during this study in which 14 short core samples and 2 long core samples were used to obtain experimental data. A similar procedure was used by previous investigators. Cornell and Katz obtained flow characteristic data on 24 sandstone samples. A log log plot of the flow characteristics, K and β, indicated an apparent linear relationship between them. They expressed this relationship as

$$\beta = \frac{4.11 \times 10^{10}}{K^{4/3}}$$

A recorrelation of the data of Cornell and Katz by Janicek and Katz resulted in a relationship relating permeability, porosity and the inertial resistance coefficient β as

$$\beta = \frac{5.5 \times 10^7}{K^{5}/_{4}\ \phi^{3}/_{4}}$$

which resulted in a set of porosity lines on a log log plot of K against β. One of the aims of this investigation was to attempt to justify or disprove the use of such a relationship with additional experimental data. An immediate observation was that the porosity lines proposed by Janicek and Katz did not appear to correlate the experimental data with any consistency. For this reason the basis of the correlation was reexamined, and an alternative correlation proposed which fits the experimental data with much more consistency.

The permeability, as determined from a Klinkenberg plot, is compared to that determined from a flow data plot, for several of the rock samples studied. The agreement is quite good, but there appears to be justification for obtaining flow data plots at different constant mean pressures. Such plots would ensure that what is assumed to be the straight line flow region of the flow data plots is not being affected by gas slippage.

The dependence of the permeability on temperature was examined by Johnston and Taliaferro for the flow of gas through consolidated porous cores. Their findings indicated that no

such dependence was apparent. Greenberg and Weger, when investigating the possible dependence of β and K on temperature for gas flow through porous sintered metals, found that β was unaffected but that with increased temperature the permeability decreased. It was felt that increased temperature might have an effect on the permeability of a consolidated porous rock and for this reason a series of experimental runs were carried out on one of the small cardium sandstone samples. The results appear to agree with the findings of Greenberg and Weger.

THEORY

The flow of gas through porous materials has been extensively investigated both theoretically and experimentally. Molecular streaming, viscous flow and non Darcy or "turbulent" flow are the regions of flow which have been considered separately. An excellent summarization of the significant theoretical and experimental work carried out in the three flow regions has been compiled by Scheidegger[27].

Deviations from Darcy's law have been observed and studied at low flow rates. As the radius of the flow channels becomes smaller the viscous flow of the gas will undergo a transition to slip flow and thence to molecular streaming. This flow regime has been successfully described by Grunberg and Nissan[16], Klinkenberg[21] and Carman[7]. When the mean free path of the gas molecules approaches the dimensions of the flow path, the rate of flow exceeds that calculated by Darcy's law. This increase is attributed to slippage at the walls of the pores. At very low pressures the mean free path will be greater than the dimensions of the flow path and viscosity will no longer be a factor in the flow process. The gas molecules will collide only with the walls of the flow path and not with each other, leading to a form of diffusion flow.

As flow rates are increased, a deviation from viscous flow takes place. Opinion varies as to the mechanism of the energy loss causing the deviation and as a consequence the

terms "turbulent", "quasi turbulent", "non Darcy" and "inertial" have been applied to the flow region. It has been shown that the dependence of the pressure drop on the flow rate becomes non linear as soon as the pressure loss due to inertia becomes significant[17][18][27]. In curved tubes this is long before the onset of turbulence. Numerous authors have proposed theories based on their concept of the energy loss mechanism in porous media[1][6][9][17][24].

Hubbert[17] proposed an "inertial resistance" where the distortion of the streamlines due to the inertial forces increases the velocity gradient, which increases the frictional forces over what they would have been had no distortion occurred. Green and Duwez[14] support the theory that distortion of the flow lines and the possible formation of stationary vortices can be expected. Tek, Coates and Katz[32] state that the abrupt transition from streamline flow to turbulent eddies has been observed by one of the authors in media with large pores but conclude that the irreversibilities occur due to extra fluid motion consuming energy, probably in the absence of turbulent eddies. Turbulence can be defined as the random variation with time of the velocity, at any point in the flow stream. In terms of this definition the general opinion is that true turbulence is unlikely in fine grained porous material. The initial deviation from a linear relationship undoubtedly takes place in the laminar flow region when inertial effects become appreciable due to the distribution of pore sizes with their

rapidly changing directions and cross sections. The term "non Darcy" will be used to describe the condition of gas flow where the difference of squares of pressures are more than proportional to increases in flow rates.

Because of the assumption of an analogy between the flow of fluids in tubes and in porous media, much effort has been directed toward finding the universal Reynolds number at which a deviation from Darcy's law will occur in all porous media. Since the Reynolds number and friction factor are both dimensionless groups one must be a numerical function of the other. However, the usual representation of the flow system by a Reynolds number - friction factor correlation depends on the definition of a characteristic length for the media, which for consolidated media is difficult to establish. Such correlations have been achieved for special systems[1][4][11] and are useful when dealing with such systems. However there does not appear to be any justification for assuming flow to be analogous when the Reynolds number, for different systems, are the same. If the porosity, tortuosity and cross section were the same, different results would still be obtained if the curvature of the flow paths differed.

Experimental evidence has shown that rather than an empirical correlation between the friction factor and Reynolds number an equation of the type suggested by Forchheimer, will

$$-\frac{dP}{dL} = \frac{\mu}{K} v + b v^2$$

correlate the flow data results for one dimensional flow.

A nomenclature listing and defining the terms used in all equations is shown at the end of this work. The results of attempts to develop an equation to explain non Darcy flow show that an equation of this type should describe the flow data when inertial effects are significant.

Johnston and Taliaferro[19] found the empirical equation

$$\frac{P_1^2 - P_2^2}{L} = a\left(\frac{Q}{A}\right) + b\left(\frac{Q}{A}\right)^n \qquad (2)$$

would express the resultant gas flow data curve for both consolidated and unconsolidated porous samples. Green and Duwez[14] developed a similar equation from the dimensional considerations proposed by Muskat[24] as

$$-\frac{dP}{dL} = \alpha\mu v + \beta\rho v^2 \qquad (3)$$

where α and β define the viscous and inertial resistance of the porous system. These two factors, which have the dimensions of length, were considered independent of the mechanical properties of the fluid but characterize the structure of the porous system. The factor α is the inverse of the permeability factor K.

The theories based on the Kozeny theory of capillaric models are restrictive in nature and were not normally applied to consolidated media. Ergun and Orning[11] developed a quadratic equation describing flow through unconsolidated media based on this theory. Their equation was developed from the

Reynolds theory of resistance to flow and the Kozeny assumption that the media can be considered analogous to a bundle of parallel capillaries with a common hydraulic radius. α and β were used to indicate the part of the pressure drop which was due to viscous and inertial energy loss and they are necessarily different for each media. Just as it has not been possible to determine the Reynolds number on a universal basis, so are α and β dependent on the structure of the porous media.

A similar approach was used by Cornell and Katz[9] to obtain a quadratic equation of flow for consolidated media. A Kozeny type equation was written in terms of the hydraulic radius and the tortuosity, as measured electrically. The problem of determining their factors k_1 and k_2 on a universal basis remains and they have to be determined for each rock sample. The equation they developed is

$$\frac{\Delta(P^2)g_c}{L} = \left(\frac{32F}{k_1 D_E^2}\right) 2\mu \frac{ZRT}{M} G + \left(\frac{32 F^{3/2}}{k_2 D_E \phi^{1/2}}\right) \frac{2ZRT}{M} G^2 \quad (4)$$

Equation (3) proposed by Green and Duwez[14] can be rewritten for the flow of gas by using the perfect gas law with a compressibility coefficient and assuming that under steady state conditions the mass velocity of the gas $\rho v = G$ is a constant. The resulting equation is

$$-\frac{M}{2ZRT} \frac{d(P^2)}{dL} = \alpha \mu G + \beta G^2$$

When the integration is carried out the final equation becomes

$$\frac{\Delta(P^2)\ M\ g_c}{2\ L(ZRT)\mu G} = \alpha + \beta\left(\frac{G}{\mu}\right) \qquad (5)$$

This equation when plotted yields a straight line with an intercept of α and a slope of β. When compared to the Cornell and Katz equation it can be seen that

$$\alpha = \frac{32F}{k_1\ D_E{}^2}$$

$$\text{and } \beta = \frac{32F^{3/2}}{k_2\ D_E\ \phi^{1/2}}$$

Equation (5) was the one used by Cornell and Katz and by Greenberg and Weger[15] in analysing their flow data. It is the equation that was used in this study to analyse similar flow data. Appendix II contains an example calculation, showing the calculations necessary for each flow rate data point. All of the equations, with their constants determined for the units of measurement used in this study, are included with the example calculation in Appendix II. The data, on the physical properties of gases and liquids, necessary for the calculations are shown in Appendix III.

By definition the Reynolds number of a flow system represents the ratio of the inertia forces to the viscous forces[17]. From equation (5) this can be seen to be

$$N_{Re} = \left(\frac{\beta}{\alpha}\right)\left(\frac{G}{\mu}\right) \qquad (8)$$

Similarly the friction factor is defined by the ratio of the total pressure loss to the inertia energy loss, which from the same equation is

$$f = \frac{\Delta(P^2)\ M\ g_c}{\beta\ L\ (ZRT)\ G^2} \tag{9}$$

Equation (5) can then be written as

$$f = \frac{2}{N_{Re}} + 2 \tag{10}$$

For a consolidated system it is impossible at present to describe the geometry of the system in detail. Factors such as porosity, tortuosity, pore size distribution, flow path curvature, particle size and roughness are just some of the factors which govern the values of α and β. Green and Duwez suggest that the friction factor correlation using equations (8) and (9), which requires two characteristic length parameters, is the only one that can be successfully applied to consolidated materials.

α and β are usually assumed to be constant for specific porous systems. The validity of this assumption was investigated by Greenberg and Weger for gas flow through porous sintered metals. There was no apparent effect on either coefficient due to pressure but with increased temperature the value of α was found to increase. This has not been investigated to any extent for porous rock systems. While a temperature effect would not be significant in an essentially isothermal reservoir, the

usual practice is to determine the permeability at room temperature without taking account of the reservoir temperature.

EXPERIMENTAL EQUIPMENT

As part of the experimental investigation it was initially decided that large core samples would be mounted in lucite and in steel cylinders, in which pressure taps could be fitted for the determination of pressure drop along the length of the core under conditions of high and low flow rates. It was considered possible that the point of deviation from Darcy's equation could be observed along the length of the core under high flow rates.

The mounting of the cores proved difficult. An epoxy resin mounting material, Shell epon 828 with a filler material and curing agent, similar to that used by Greenburg and Weger[15] was employed. This material was generally unsuccessful for cores of greater than one inch diameter. Its apparent shortcomings were that it contracted on cooling leaving a void space between the solidified material and the casing. Further additions of material did not fill these voids completely leaving permanent spaces next to the casing wall. Examination also showed that considerable air was entrapped in the material in the form of bubbles. A further source of difficulty was in attempting to effect a seal between the end plates and the mounted core. The best method appeared to be "O" rings, when the end faces provided a good seating surface and did not have large air bubbles exposed.

Under high pressure the resin material permanently deformed and cracks invariably developed. Often these cracks were propagated into the porous core. The holes drilled for the pressure

taps were a point of weakness which together with the void spaces next to the casing wall were considered suspect as possible means of pressure communication. Flow data and results of such a mounting procedure are discussed in a later section.

The use of a non shrink concrete, used commercially as a grouting material, was investigated as a core mounting material. Any size of core can be mounted at one pouring but extreme care is necessary to remove all of the entrained air. When the cement mixture sets the permeability was found to be less than 0.1 millidarcies and decreased with time. Prior to mounting cores in this cement they were given a thin coat of the previously mentioned epoxy resin material.

The major experimental data were obtained on small core samples of consolidated porous media. Various methods of holding such samples are described in the literature[9][15][18]. A modification of the method described by Johnston and Taliaferro[18] was used and is shown in Figure 1. The holder was machined as shown from solid stock. The rubber stoppers used were #26 extra long, drilled to one inch diameter, which fitted in the tapered section of the holder. Pressures up to 1900 psia were imposed across the short core samples without difficulty.

Figure 2 is a composite diagram of the experimental apparatus used for obtaining data on both long and short core samples. Nitrogen cylinders were manifolded through a pressure

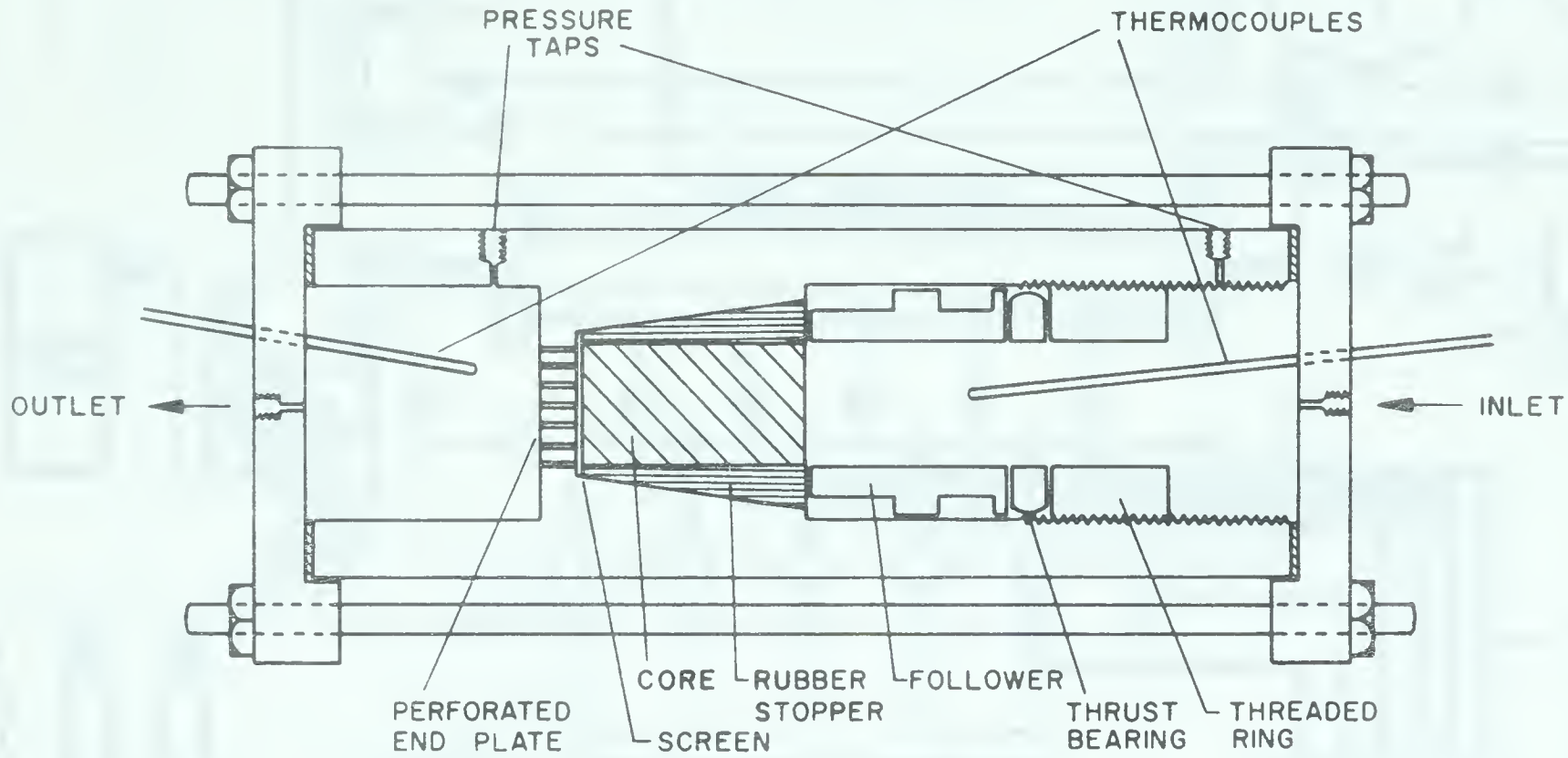

SMALL CORE HOLDER

FIG. 1

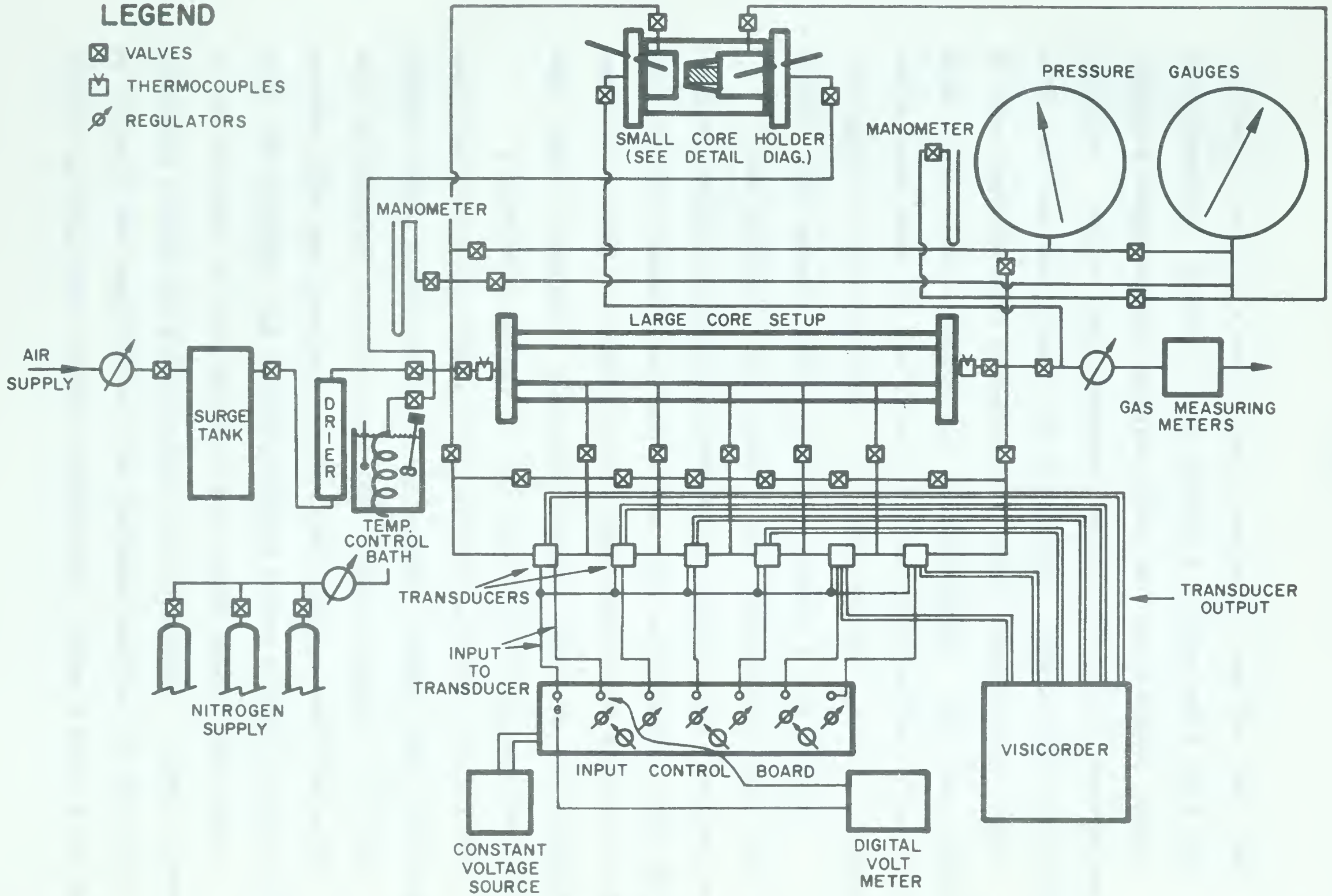

DIAGRAM OF EXPERIMENTAL APPARATUS

FIG. 2

regulator to give a sufficient source of gas for the flow measurements. Bourdon tube pressure gauges were used for pressure measurements greater than two atmospheres gauge pressure. Below that pressure, water or mercury manometers were used for the measurement of pressures. Temperature measurement of the upstream and downstream flowing temperatures were made using iron - constantan thermocouples. Gas flow measurements were made at low flow rates using burettes, from 1 to 25 cfm using a wet test meter and above 25 cfm using a diaphragm meter. The meters were calibrated using a gas prover.

The pressure drop profile was obtained on long core samples using calibrated transducers which were recorded on a continuously recording visicorder plot as pressure drop per section in psi. A constant voltage source and digital voltmeter were used to ensure a constant voltage input to the transducers.

A possible defect in the core holding apparatus used, was that gas might bypass the core in some way during the experimental runs, either between the rubber stopper and the holder wall or between the core and the rubber stopper. To help prevent the gas passing between the stopper and the holder wall the stopper was greased before being placed in the holder. In an attempt to determine if gas could bypass the core a machined lucite plug was placed in the holder. When a pressure of 60 psig was applied to the upstream section of the core holder no flow was evident immediately, then a very slow seepage

was apparent which built up to a static pressure of 4 inches of water in three minutes. The flow rate was in effect negligible. It is felt that this seepage may have been due to the surface of the lucite cylinder, which is extremely smooth, making it an extremely poor gripping surface. The rock samples however offered a rougher surface allowing a firm contact between the rubber and the rock material. Care was taken that the follower in the core holder was screwed down as tightly as possible for all of the experimental runs. As far as could be determined there would not have been any significant error in the flow data due to the core being bypassed by the gas flowing through the core holder.

EXPERIMENTAL PROCEDURE

Sample Preparation

Small cylindrical samples of the porous media investigated were cut from bulk samples using a one inch diamond drill. All samples were cut parallel to the bedding planes. They were then cleaned of any loose surface material and extracted in Soxhlet extractors using benzene. The extraction was continued for at least 12 hours after which time the samples were left to soak in benzene for a further period of 12 hours. If after this time the benzene was found to be clear, the sample was dried in a constant temperature oven for three hours at 200°F. If the benzene was found to be oil stained after the soaking period, the extraction was continued until the benzene was found to be clear after soaking for 12 hours. After drying, the samples were allowed to cool, and kept stored, in a dessicator until used.

The samples were cut to approximately 1½ inches in length, with the exposed faces produced by fracturing. Figure 3 shows the details of the apparatus used to break off the ends of the sample. The sample was held tightly in the apparatus while pressure was applied to the knife blades. The fracturing can be caused in two ways, by sharp blows to the knife blades, and by applying the pressure slowly to the blades using a bench vise. Both methods gave satisfactory results. The softer

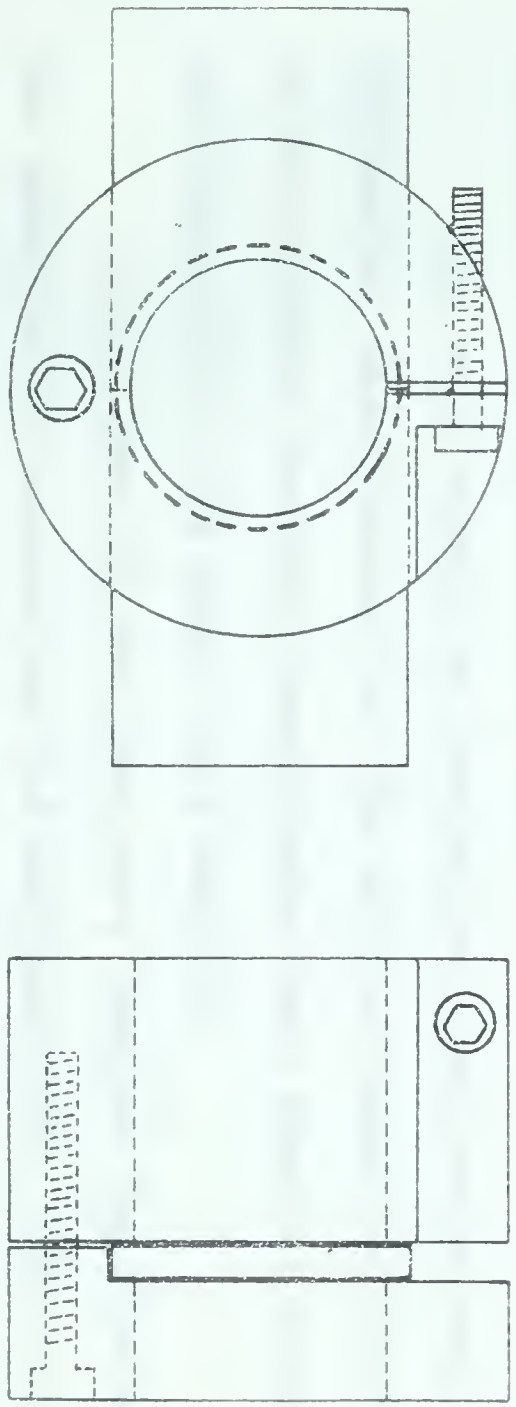

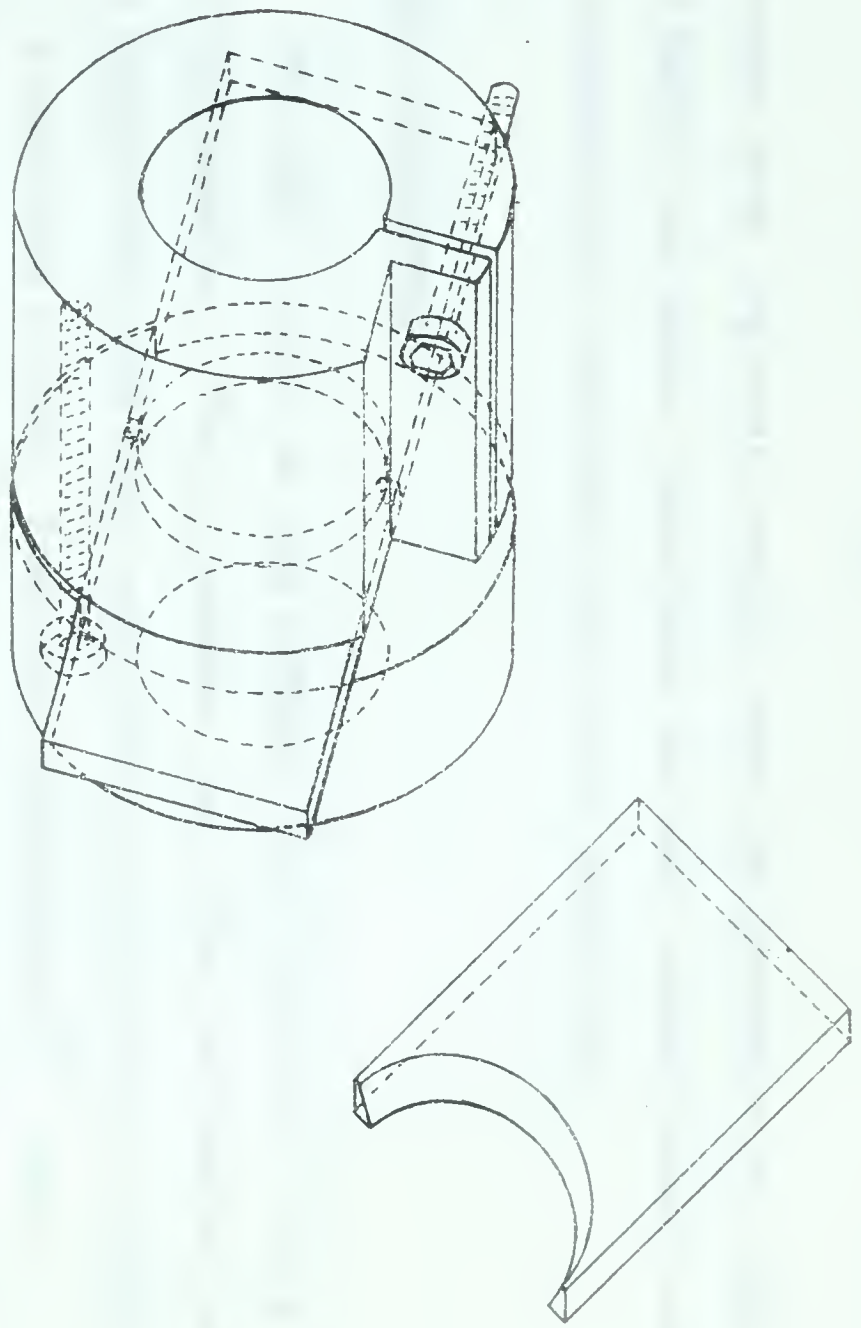

FIGURE 3 CORE FRACTURING DEVICE

sandstones gave the best results when the pressure was applied slowly while the dense limestones and well consolidated sands were successfully fractured using both techniques.

Porosity Measurement

The bulk volume of the samples was determined using a mercury pycnometer. The pycnometer was first calibrated using lucite plugs which had been machined to the required dimensions.

A modified Oilwell Research Porosimeter[2] using Helium gas was used to determine the matrix volume of the samples. This apparatus is shown in figure 4. Machined steel blanks were used to calibrate the porosimeter.

The average diameter of the samples was determined by averaging five different diameter measurements along the length of the sample as measured using a micrometer. The length of each sample was computed from the data on its volume and calculated cross sectional area.

The bulk volume as determined from the mercury pycnometer measurements and the matrix volume as determined by the Oilwell Research porosimeter were used to determine the porosity of the small core samples.

In the case of the long core samples the pore volume was measured by evacuating the weighed cores, saturating them with water and reweighing. The bulk volumes were determined by measurement of their length and cross sectional areas.

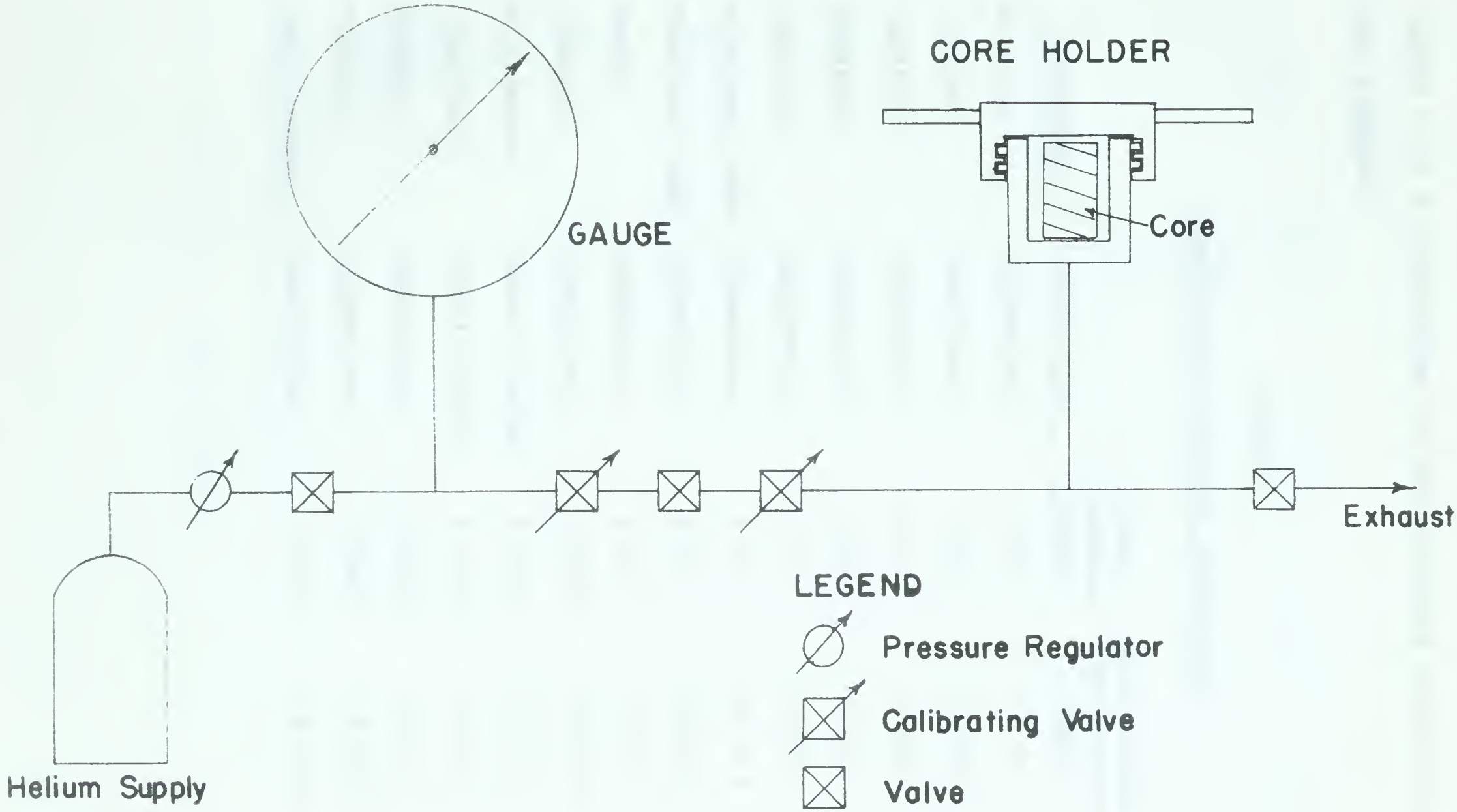

FIGURE 4 OILWELL RESEARCH POROSIMETER
(after Beeson[2])

Table 1 is a tabulation of the physical properties of the small core samples.

Table 1

Small Core Physical Properties

Core	Formation	Rock Type	Core Diameter (cm)	Bulk Volume (Pycnometer) (cc)	Equivalent Length (cm)
1	Cardium	Sandstone	2.532	18.751	3.723
2	Cardium	Sandstone	2.535	18.886	3.742
3	Cardium	Sandstone	2.535	19.094	3.783
4	Cardium	Sandstone	2.532	18.690	3.711
5	Cardium	Sandstone	2.530	18.664	3.713
6	Sturgeon Lake	Limestone	2.522	19.571	3.917
7	Sturgeon Lake	Limestone	2.531	19.150	3.806
8	Berea	Sandstone	2.529	18.806	3.745
9	Indiana	Limestone	2.529	18.208	3.626
10	Blairmore	Basal Quartz	2.579	19.165	3.670
11	Blairmore	Basal Quartz	2.579	17.793	3.405
12	Viking	Sandstone	2.579	18.757	3.590
13	Viking	Sandstone	2.580	19.472	3.726
14	Belly River	Sandstone	2.579	19.629	3.758

Table 1 - continued

Core	Pore Volume (cc)	Porosity (%)	Length Inches	Area Inches^2
1	3.656	19.50	1.466	.781
2	.446	2.36	1.473	.782
3	3.593	18.82	1.490	.782
4	3.945	21.11	1.461	.781
5	3.202	17.16	1.462	.779
6	2.848	14.55	1.542	.774
7	2.605	13.60	1.498	.780
8	3.646	19.39	1.474	.778
9	3.543	19.46	1.428	.778
10	3.825	19.96	1.445	.810
11	3.628	20.39	1.341	.810
12	1.842	9.82	1.414	.810
13	2.002	10.28	1.467	.810
14	3.701	18.85	1.480	.810

Core diameter - average of 5 measurements

Bulk volume - average of 3 measurements

$$\text{Equivalent length} = \frac{\text{Bulk Volume}}{\text{Area}}$$

$$\text{Porosity} = \frac{\text{Pore Volume}}{\text{Bulk Volume}}$$

Flow Measurement

Flow data were obtained on 14 small core samples and 2 large core samples using the experimental setup shown in figure 2. The small cores were placed in the core holder as shown in figure 1. The gas supply was connected to the upstream end of the holder and the flow measuring equipment to the downstream end. Connections were made for the measurement of upstream and downstream pressure. The thermocouples used for the determination of upstream and downstream flowing temperatures were connected to a Leeds and Northrup potentiometer. All connections were tested under pressure with a soap solution, particular care being taken to ensure that all downstream connections and pressure measuring connections were gas tight.

Two flow measurements were taken at each data point to ensure that stable conditions of flow had been established. A period of 5 to 10 minutes was allowed to elapse between the two measurements. Any significant change in upstream pressure meant a further period of flow was required to attain stable conditions. Only at highflow rates was any difficulty experienced in attaining stable conditions. This could have been minimized by having a larger gas supply or a method of maintaining the pressure of the gas supply at a constant value.

No attempt was made to maintain a constant upstream and downstream flowing gas temperature for the majority of the runs. The gas inlet line was ¼ inch copper tube which between

the regulator and the inlet connection had a coil of several feet immersed in a water bath to bring the temperature of the gas up to the room temperature after the cooling caused by expansion through the regulator.

Data on one of the core samples were obtained at three different temperatures. A constant temperature water bath and heating tapes were used to stabilize the core temperature and the flowing gas temperature at the desired value. Extreme difficulty was experienced in stabilizing the temperature at the low flow rates. It was necessary to allow a lengthy period of flow after every minor heating tape adjustment, to ensure that a stable temperature condition was attained.

All measured flow data, and calculated flow characteristic data, are tabulated in Appendix I and are not included in the body of this report. Tables referred to by number, in the discussion following, are located in Appendix I.

DISCUSSION OF EXPERIMENTAL RESULTS

Flow tests were carried out initially on two large cores. An Indiana limestone core was mounted in a steel casing using an epoxy resin mounting material. Attempts to determine the porosity of this core using saturation techniques were unsuccessful. The porosity calculated using a representative small core sample was assumed correct due to the homogeneity of the Indiana limestone. The results of the flow tests on this core are recorded in table 5 in Appendix I and are shown on figure 24. These were flow tests carried out prior to drilling pressure taps along the length of the core. The plotted flow data would appear to indicate that the straight line predicted by equation (5) had been established. A comparison of figure 24 with figure 21, which shows results obtained from flow tests using a small Indiana limestone core sample, would indicate that the flow data were probably still in the flow region affected by molecular streaming. This would result in a permeability value which would be too high and a β value which would be too high. While the small core sample may well be of lower permeability than the long core sample, it would appear necessary to take flow data over a more extended range of flow rates before the permeability determined on the long core sample could be assumed to be correct. No further data was taken on this core because of the trouble experienced with epoxy resin mounted cores.

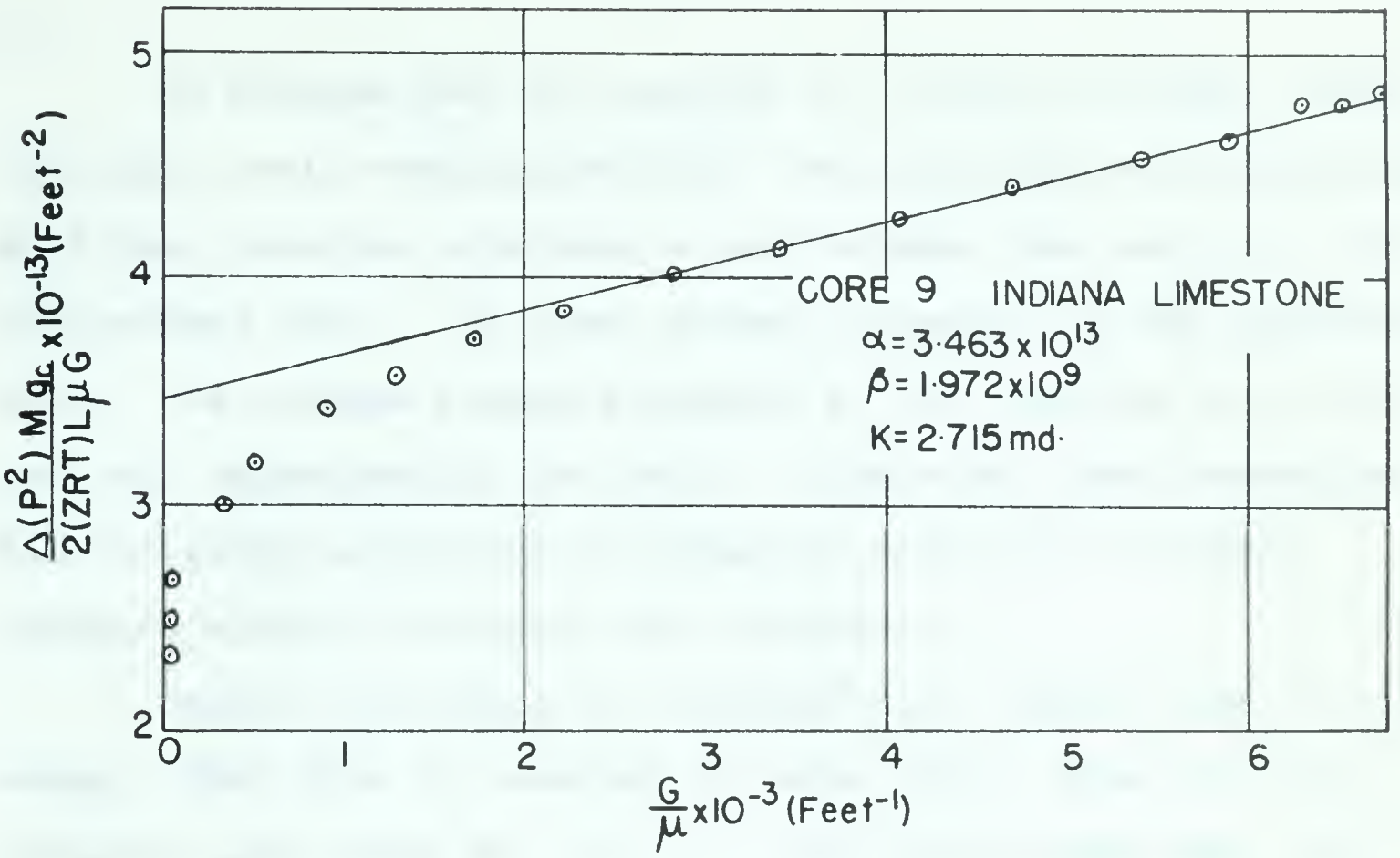

FIGURE 21 FLOW DATA PLOT TO OBTAIN α AND β

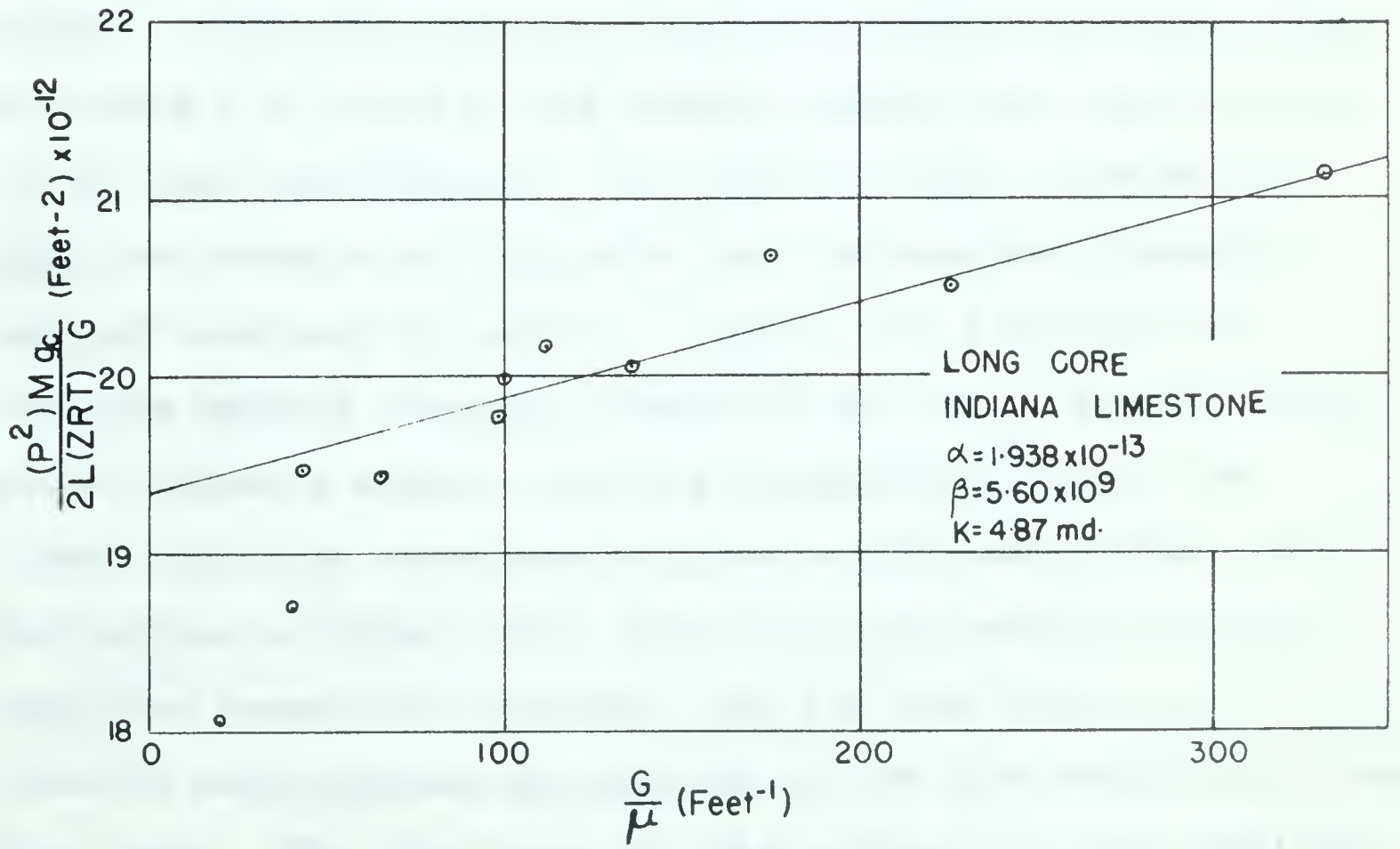

FIGURE 24 FLOW DATA PLOT TO OBTAIN α AND β

An Alundum core was mounted in a lucite cylinder using the epoxy resin mounting method. The main difficulty, experienced with this core, was obtaining a seal between the end plates and the mounted core. "O" rings proved successful at the pressures used. The maximum pressure applied at the upstream end of the core was approximately 240 psig. At this and lower pressures the "O" rings maintained an effective seal and no visible cracking within the epoxy resin occurred.

Initial flow data were obtained for a small range of flow rates. That data is recorded in table 4(A). After drilling pressure taps along the length of the core further data runs were carried out, these are recorded in table 4(B). Until this time the upstream and downstream pressure taps were located in the flow line just upstream and downstream of the end plates. Using the pressure taps and recording apparatus shown in figure 2 a record of the pressure drop across each section of the core was obtained. These data were then converted to absolute pressure at each point and the resultant pressure squared tabulated in table 2. Figure 5 is a plot of the pressure squared along the length of the core. The increasing outlet pressure squared, and the increasing slope of the lines, indicates measurements taken at increasing flow rates. The decreasing slope lines, with the inlet pressure squared remaining essentially constant, are for runs where an increasing back pressure was applied to the core resulting in lower flow rates. The flow rates for the plotted runs are tabulated in table 2.

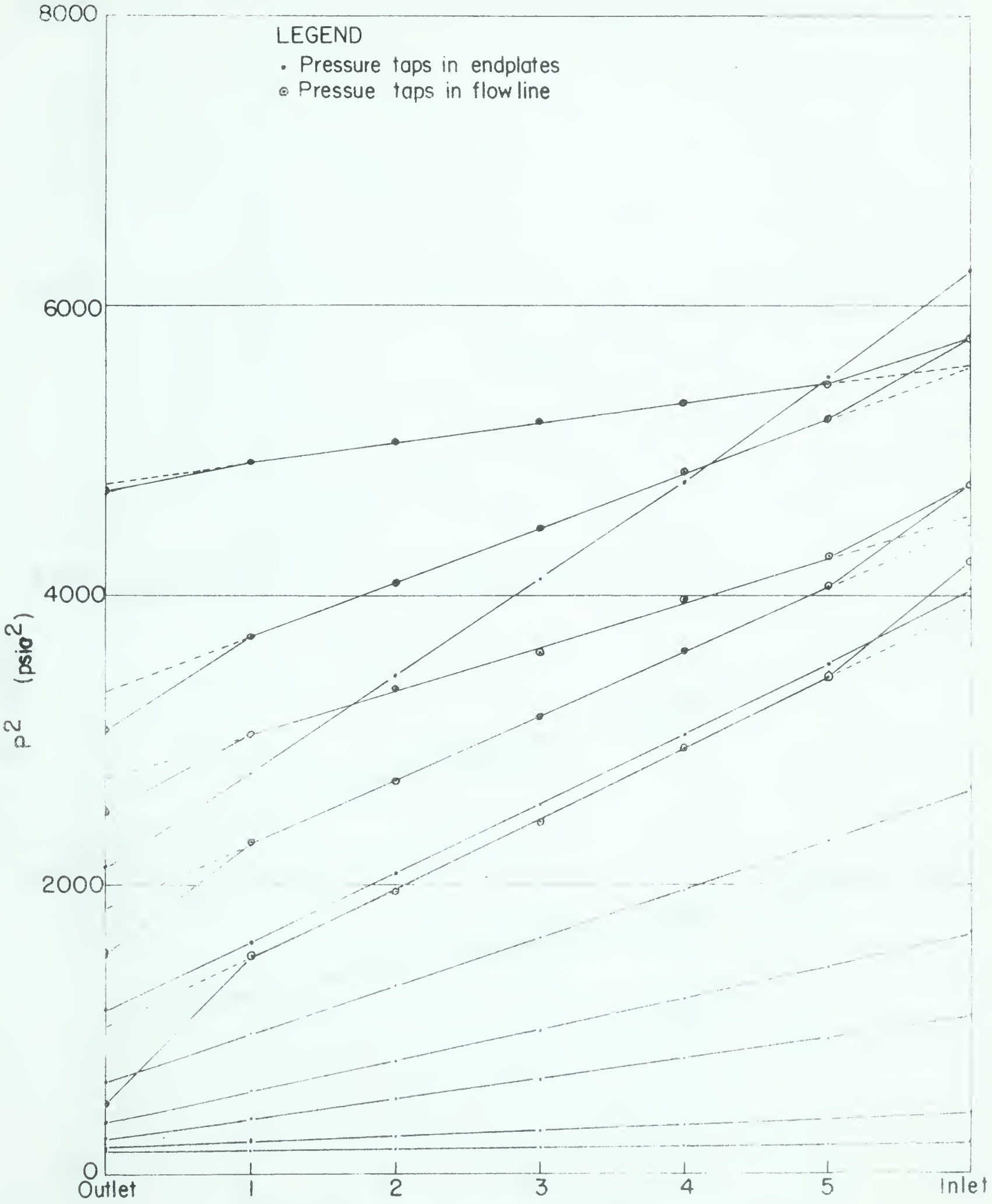

FIGURE 5 P^2- PRESSURE SQUARED PROFILE

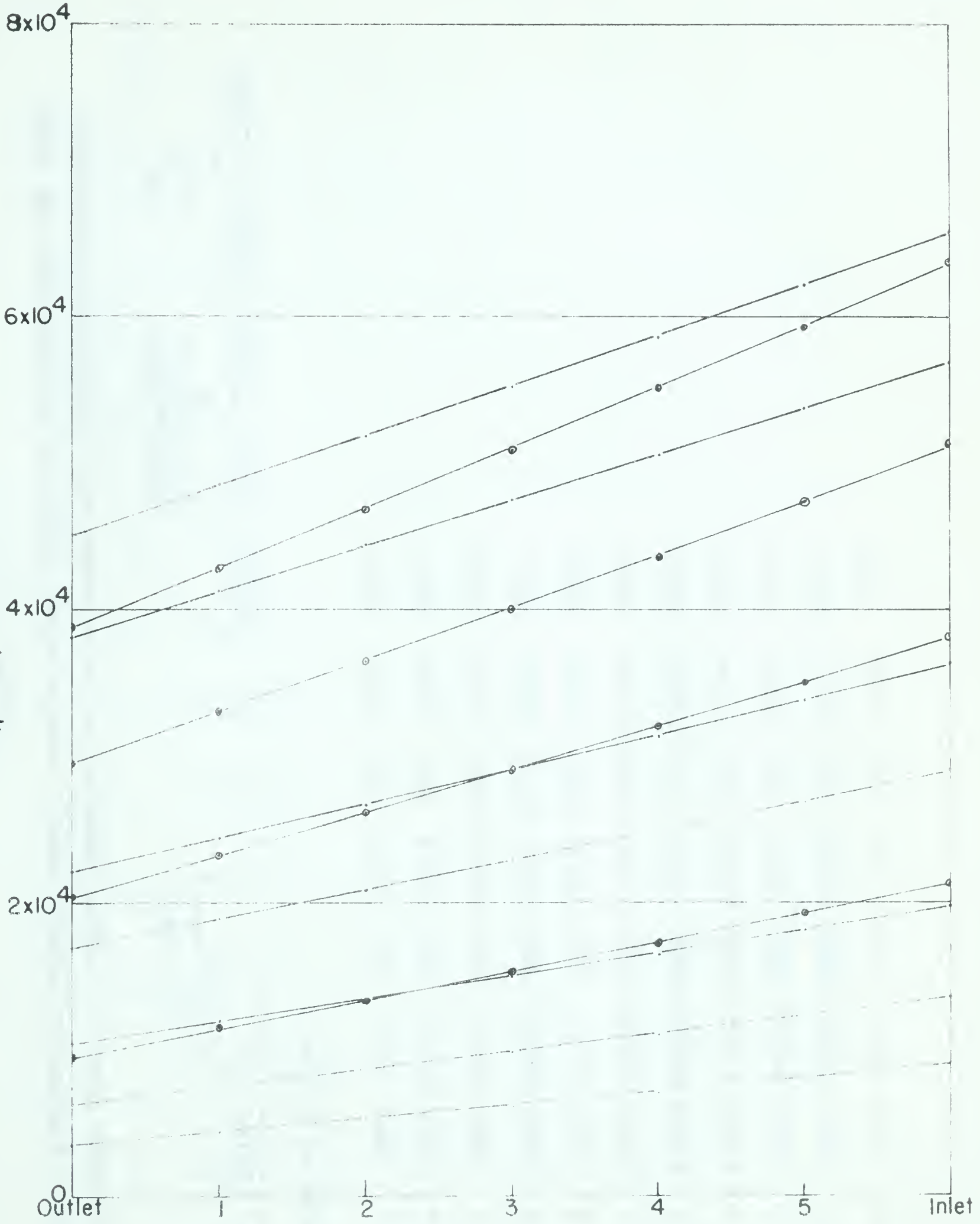

FIGURE 6 P^2 - PRESSURE SQUARED PROFILE

Table 2

Pressure squared at points equally spaced along length of Alundum Core (TA 7921)
(Calculated from ΔP values measured by Transducers and recorded on Visicorder)

Q	P_i^2 (psi^2)						Extrapolated		ΔP_i	
SCFH	P^2_{inlet}	P^2_5	P^2_4	P^2_3	P^2_2	P^2_1	P^2_{outlet}	P^2_{inlet}	P^2_{outlet}	ΔP_{inlet}	ΔP_{outlet}
Plotted on Figure 6											
31.7	8892	7920	6990	6070	5230	4340	3490				
40.4	13430	12140	10920	9742	8575	7430	6273				
53.2	19680	18010	16410	14880	13360	11860	10320				
67.9	28930	26700	24680	22710	20770	18850	16930				
80.2	36180	33670	31260	28930	26600	24340	22050				
106.2	57070	53680	50490	47390	44270	41210	38140				
116.2	65740	62050	58520	55130	51710	48400	45030				
121.6	51080	47260	43560	40000	36440	32940	29450				
100.9	38140	34970	31930	29000	26080	23230	20360				
139.7	63710	59290	55040	50900	46790	42770	38730				
68.3	21370	19270	17240	15330	13390	11490	9584				

Table 2 - continued

Q	P_i^2 (psi^2)						Extrapolated		ΔP_i	
SCFH	P^2_{inlet}	P^2_5	P^2_4	P^2_3	P^2_2	P^2_1	P^2_{outlet}	P^2_{inlet}	P^2_{outlet}	ΔP_{inlet}	ΔP_{outlet}
Plotted on Figure 5											
16.7	4040	3520	3030	2550	2080	1600	1150				
23.2	6240	5510	4790	4110	3450	2770	2125				
1.39	416	372	335	299	262	225	182				
4.98	1089	930	790	650	520	388	250				
7.7	1665	1430	1205	992	784	571	357				
11.6	2660	2295	1955	1630	1300	973	640				
0.19	202	193	188	185	180	174	161				
*15	4225	3435	2940	2430	1955	1515	484	3900	1000	2.6	9.6
*12	4760	4058	3610	3160	2715	2295	1521	4493	1825	2.0	3.7
*10	5776	5213	4845	4460	4083	3710	3070	5585	3325	1.3	2.3
* 7	4760	4264	3970	3660	3350	3035	2500	4575	2718	1.3	2.1
* 6	5776	5460	5330	5220	5055	4915	4720	5596	4776	1.2	0.4

* approximate

Figure 5 shows that a pressure drop in the two end sections, greater than would be predicted, was experienced. Because of this result the pressure measuring points were changed to the end plates and further flow data were obtained. The resultant plots of the pressure squared along the length of the core are shown in figure 5 and figure 6. Two separate plots were necessary because of the range of flow rates covered. Figure 5 shows the low flow rate data while Figure 6 shows the high flow rate data. Straight lines resulted from the plot of these data which is in accordance with the predicted result for Darcy flow. Very slight deviation from the straight line was observed at the higher rates of flow, shown on Figure 6, but it was not sufficiently pronounced to indicate a definite deviation from Darcy flow.

The relocation of the pressure taps indicated that a straight line relationship, of pressure squared along the length of the core, existed for the range of flow rates covered. The flow rates, when the pressure taps were located in the flow lines, were low enough to have given a similar linear result. For this reason the plots of those data, shown on figure 5, were extrapolated to give predicted inlet and outlet pressures squared. From these extrapolated pressures squared, the predicted pressures at the inlet and outlet faces of the core were calculated. Table 2 shows the error in the measured pressure drop, in the two end sections, due to the measurement

of the inlet and outlet pressure in the flow line. The error due to the inclusion of the short lengths of flow line is seen to be of significant magnitude.

Also shown in figure 6 is the result that was obtained when the length of line, from the end plate outlet, to the gas flow measuring apparatus was shortened. The reduction in back pressure allowed a higher flow rate to be acheived for the same upstream or inlet pressure.

The plotted flow data for the Alundum core is shown in figure 7. Curve A represents the condition where the pressure taps were in the flow line, for curve B the pressure taps were still in the flow line but additional pressure taps had been drilled along the length of the core and curve C shows the result when the pressure taps were moved from the flow line to the end plates of the mounted core. A significant change in the measured flow characteristics is apparent. The curves for run A and B in figure 8 indicate that the greater part of the flow was in the transition region while curve C indicates almost continuous laminar flow for the range of flow rates covered. The plot of the pressure squared along the length of the core, shown in figure 6,verifies that laminar flow existed through the range of flow rates covered.

From the results of the experimental data obtained on the long core samples it is apparent that it is necessary to measure the flowing upstream and downstream pressures at the core face. While in liquid flow tests the error due to measuring

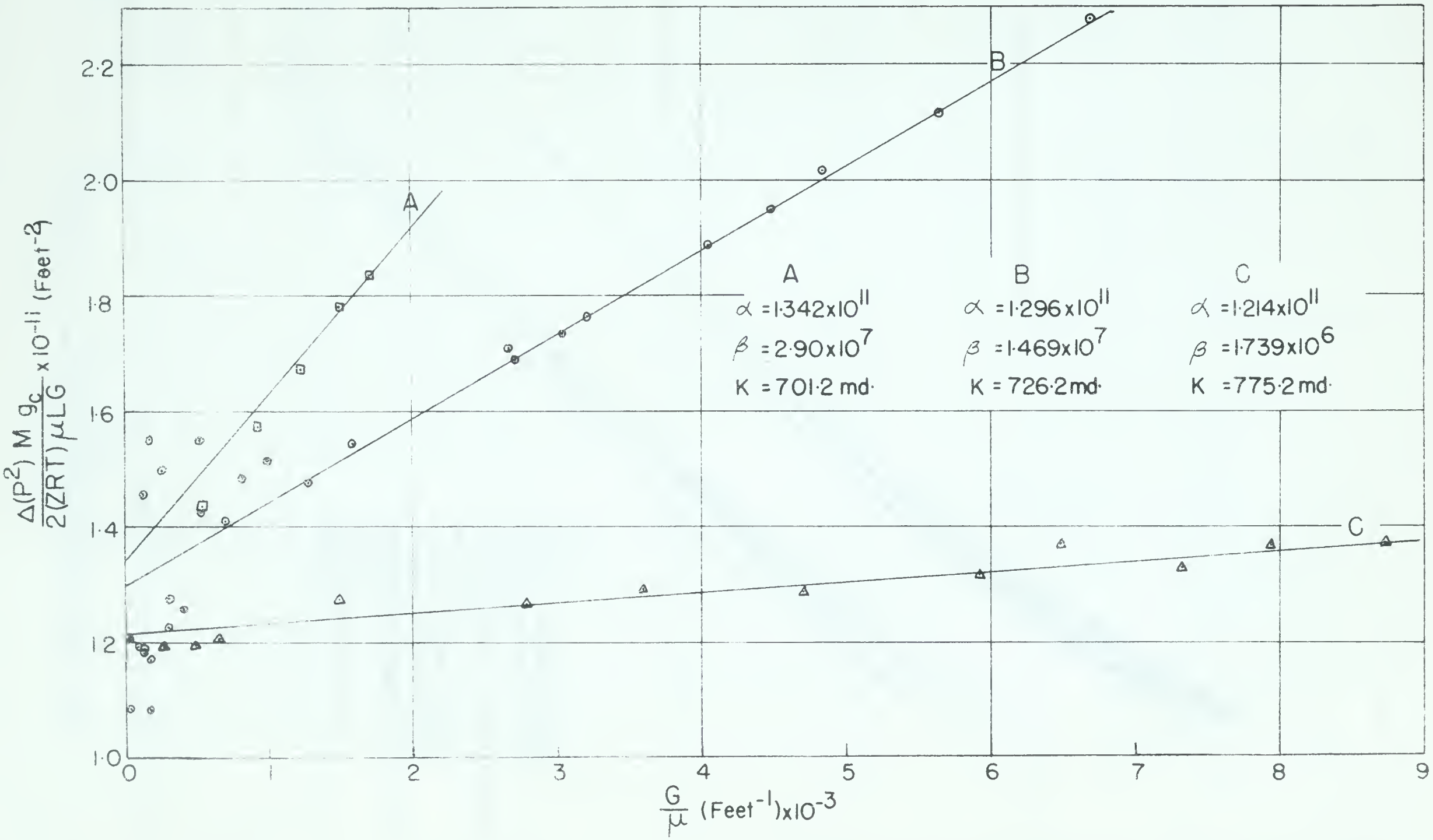

FIGURE 7 FLOW DATA PLOT TO OBTAIN α AND β - ALUNDUM CORE

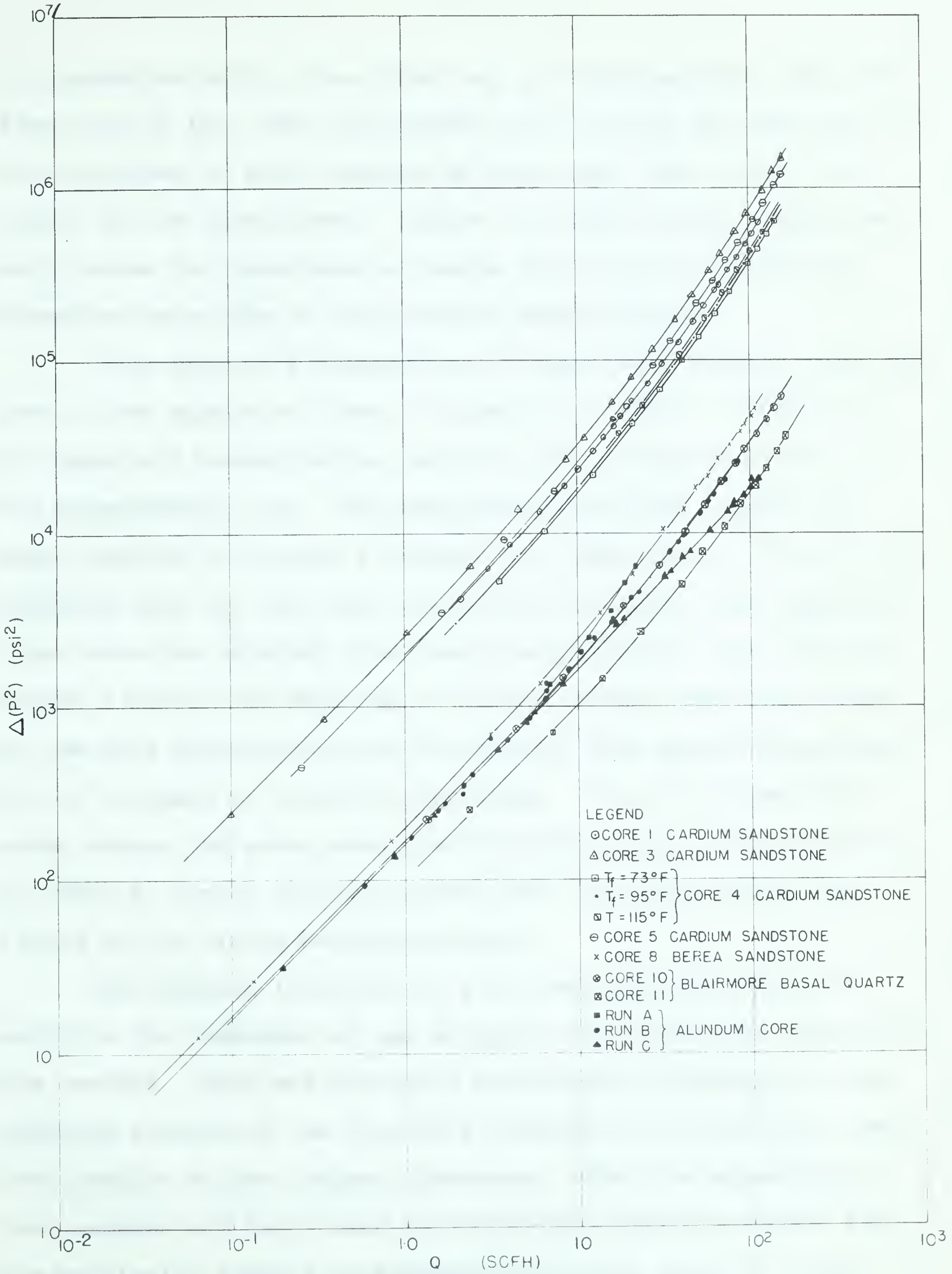

FIGURE 8 FLOW DATA ON CONSOLIDATED POROUS CORES

the pressures in the flow lines may not be significant when the flow rate is low, when the flowing fluid is gas the error due to the inclusion of short lengths of flow line, even at low flow rates, can be significant. Figure 7 is ample proof of this fact as it shows the considerable change in the experimental flow characteristics due to the pressure measuring point.

Flow data were obtained on 14 small core samples using the core holder apparatus shown in figure 1. Tables 5 through 36 in Appendix I summarize the measured and calculated results of the experimental runs. The calculated flow data results are shown plotted in Figures 7 through 25. The values of α and β are obtained from the flow data plotted in accordance with Equation 5 and show the straight line result predicted by that equation. Figure 9 shows flow data for the three cardium sandstone cores. At low mean pressures all of the plotted data showed deviations due to slippage or molecular streaming. The low permeability cores showed the more pronounced deviations due to the phenomena as shown in Figure 10 for Sturgeon Lake limestone cores, and Figure 11 for Viking sandstone cores.

The Indiana limestone is a low permeability rock and exhibits the phenomena of gas slippage until high mean pressures are reached. This was discussed previously in relation to the compared results of the flow data obtained on the long and short core samples of the Indiana limestone. When low permeability core samples are being used to obtain flow characteristics for the particular rock, it is necessary to attain rates of flow,

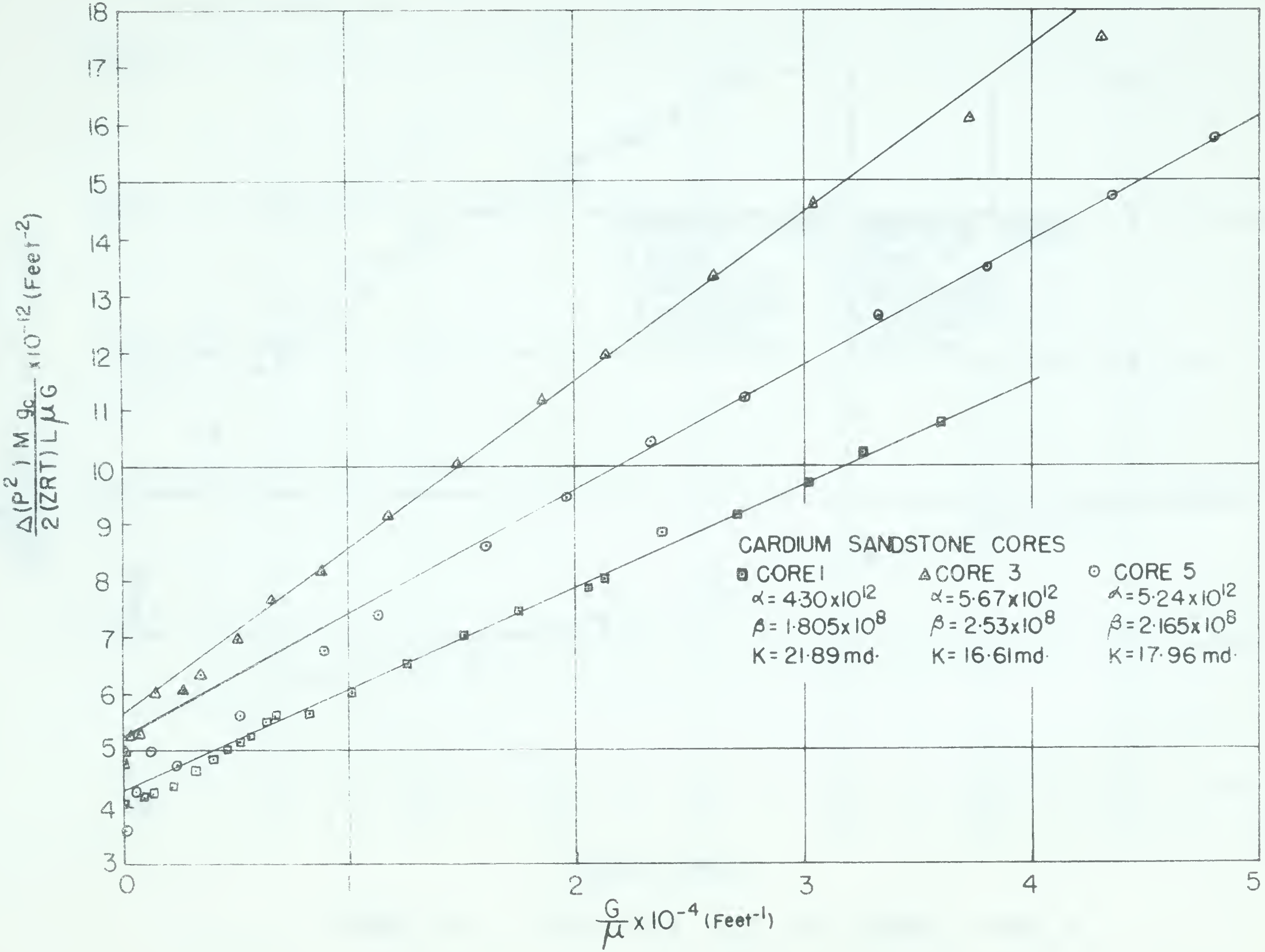
$\frac{\Delta(P^2)}{2(ZRT)}\frac{M}{L}\frac{g_c}{\mu G} \times 10^{-12}$ (Feet^{-2})
$\frac{G}{\mu} \times 10^{-4}$ (Feet^{-1})
CARDIUM SANDSTONE CORES
CORE 1
$\alpha = 4.30 \times 10^{12}$
$\beta = 1.805 \times 10^{8}$
K = 21.89 md.
CORE 3
$\alpha = 5.67 \times 10^{12}$
$\beta = 2.53 \times 10^{8}$
K = 16.61 md.
CORE 5
$\alpha = 5.24 \times 10^{12}$
$\beta = 2.165 \times 10^{8}$
K = 17.96 md.

FIGURE 9 FLOW DATA PLOT TO GET α AND β

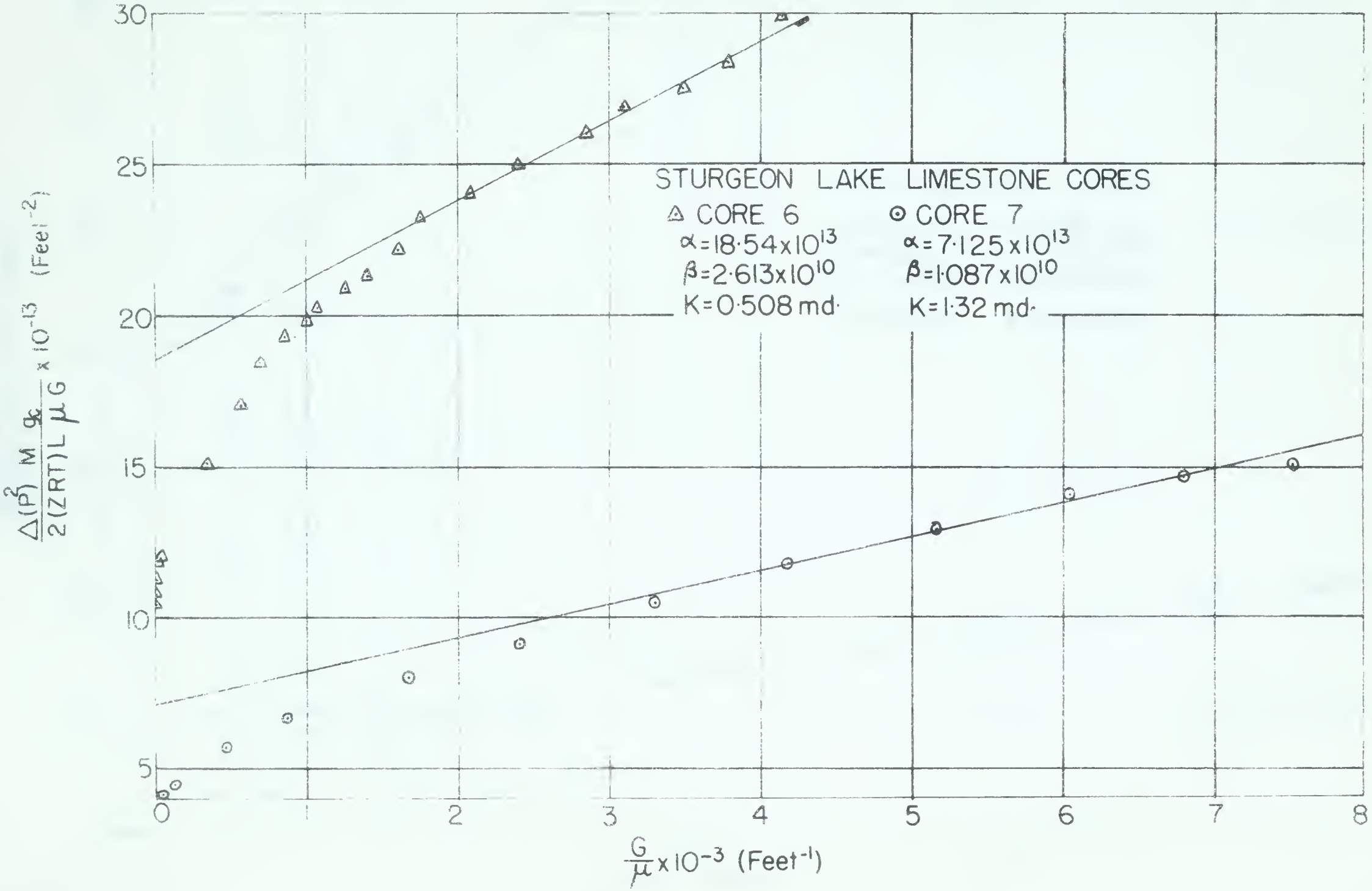

FIGURE 10 FLOW DATA PLOT TO OBTAIN α AND β

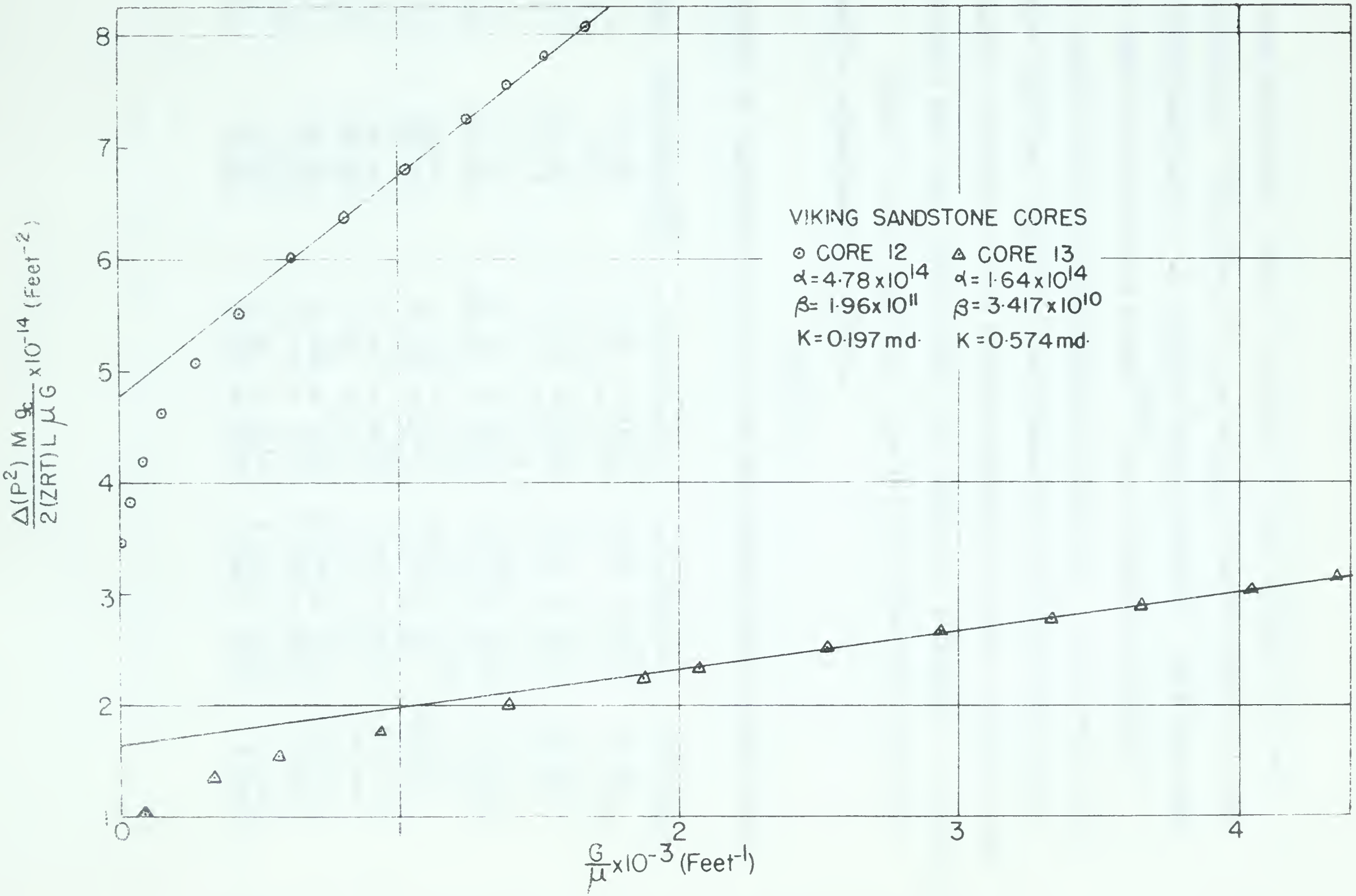

FIGURE 11 FLOW DATA PLOT TO OBTAIN α AND β

or mean pressures, where the effect of gas slippage is not significant. The effect of gas slippage can be held constant by obtaining data at a constant mean pressure. This approach was used by Stewart and Owens[29] in a study of turbulent and laminar flow in heterogeneous limestones. Flow data plots where different constant mean pressures are used should show a series of curves which become asymptotic to the straight line covering the flow region where the effect of slippage is negligible.

Table 3 summarized the porosity and flow data obtained from the experimental results.

Table 3

SUMMARY OF POROSITY AND FLOW DATA FOR CONSOLIDATED POROUS MEDIA

Core	Porosity (%)	α (ft^{-2})	β (ft^{-1})	K (md)
1	19.50	4.30×10^{12}	1.805×10^{8}	21.89
2	2.36	1.922×10^{16}	1.07×10^{14}	0.0049
3	18.82	5.665×10^{12}	2.533×10^{8}	16.61
4	21.11	3.18×10^{12}	1.85×10^{8}	29.59
5	17.16	5.24×10^{12}	2.165×10^{8}	17.96
6	14.55	18.54×10^{13}	2.613×10^{10}	0.508
7	13.60	7.125×10^{13}	1.807×10^{10}	1.32
8	19.36	5.745×10^{11}	1.144×10^{7}	163.81
9	19.46	3.463×10^{13}	1.972×10^{9}	2.715
10	19.96	3.85×10^{11}	1.107×10^{7}	244.44
11	20.39	2.265×10^{11}	5.689×10^{6}	415.50
12	9.82	4.778×10^{14}	1.962×10^{11}	0.197
13	10.28	1.64×10^{14}	3.417×10^{10}	0.574
14	18.85	1.568×10^{14}	1.264×10^{10}	0.6002

Figures 8 and 12 show the plotted flow data of flow rate against the difference of the squared upstream and downstream flowing pressures. The higher permeability cores gave a laminar flow result at low flow rates but a gradual departure from the linear relationship was soon apparent. This gradual transition zone was the flow regime in which all the remainder of the flow data were obtained. The expected fully developed turbulent region in which the slope of the plotted results would have a constant value of 2 was not achieved. For the low permeability cores the pressure necessary to attain that region would have been far beyond the safety limits of the equipment, while for the high permeability cores the flow rate necessary would be greater than the rated capacity of the flow meters which were used. Certainly the plotted curves were still in the transition region, however a greater coverage of the flow regions could be obtained with a large gas supply and high flow rate measuring equipment.

A common method of plotting flow data is the Reynolds number - friction factor correlation. Figures 13 and 14 show the flow data plotted as such a correlation, with the Reynolds number and friction factor determined from equations (8) and (9). The work of Cornell and Katz[9] contains a similar plot with the results of Green and Duwez[14] for flow through porous metals included. Friction factor - Reynolds number data for four sandstones were extracted from reference (9) and plotted on figure 13. It can be seen that all the data are consistent, falling on

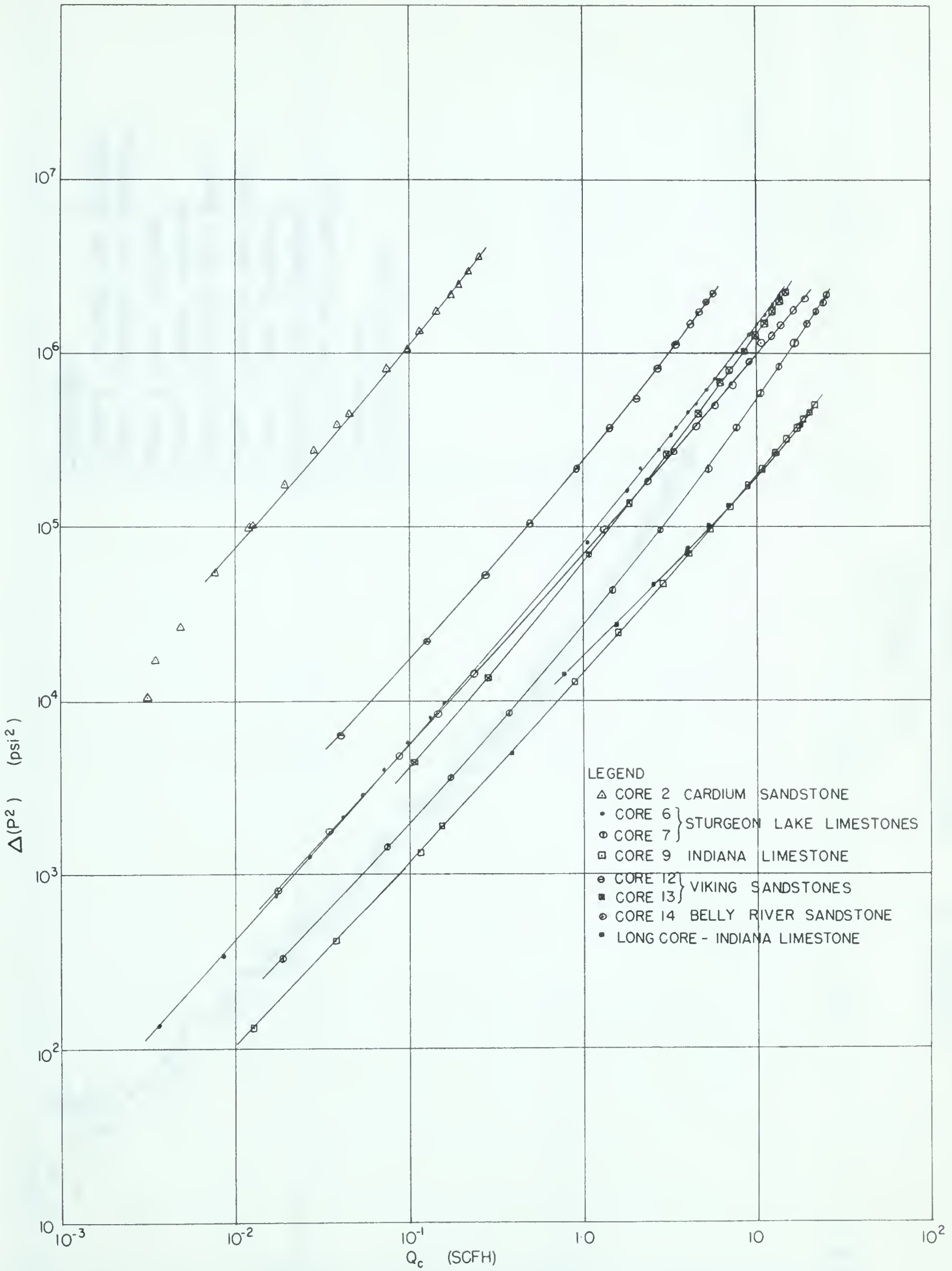

FIGURE 12 FLOW DATA ON CONSOLIDATED POROUS CORES

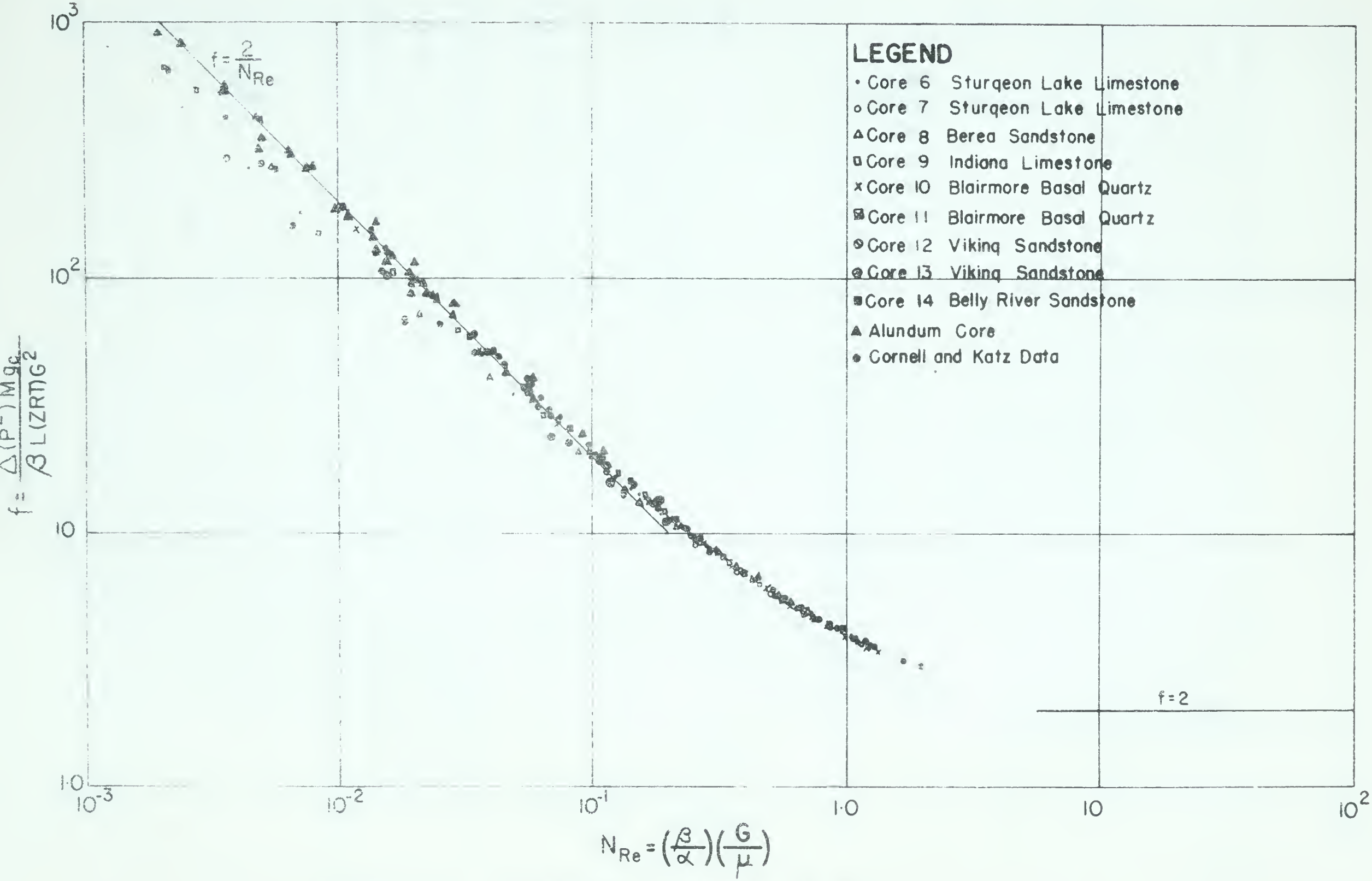

FIGURE 13 REYNOLDS NUMBER – FRICTION FACTOR PLOT

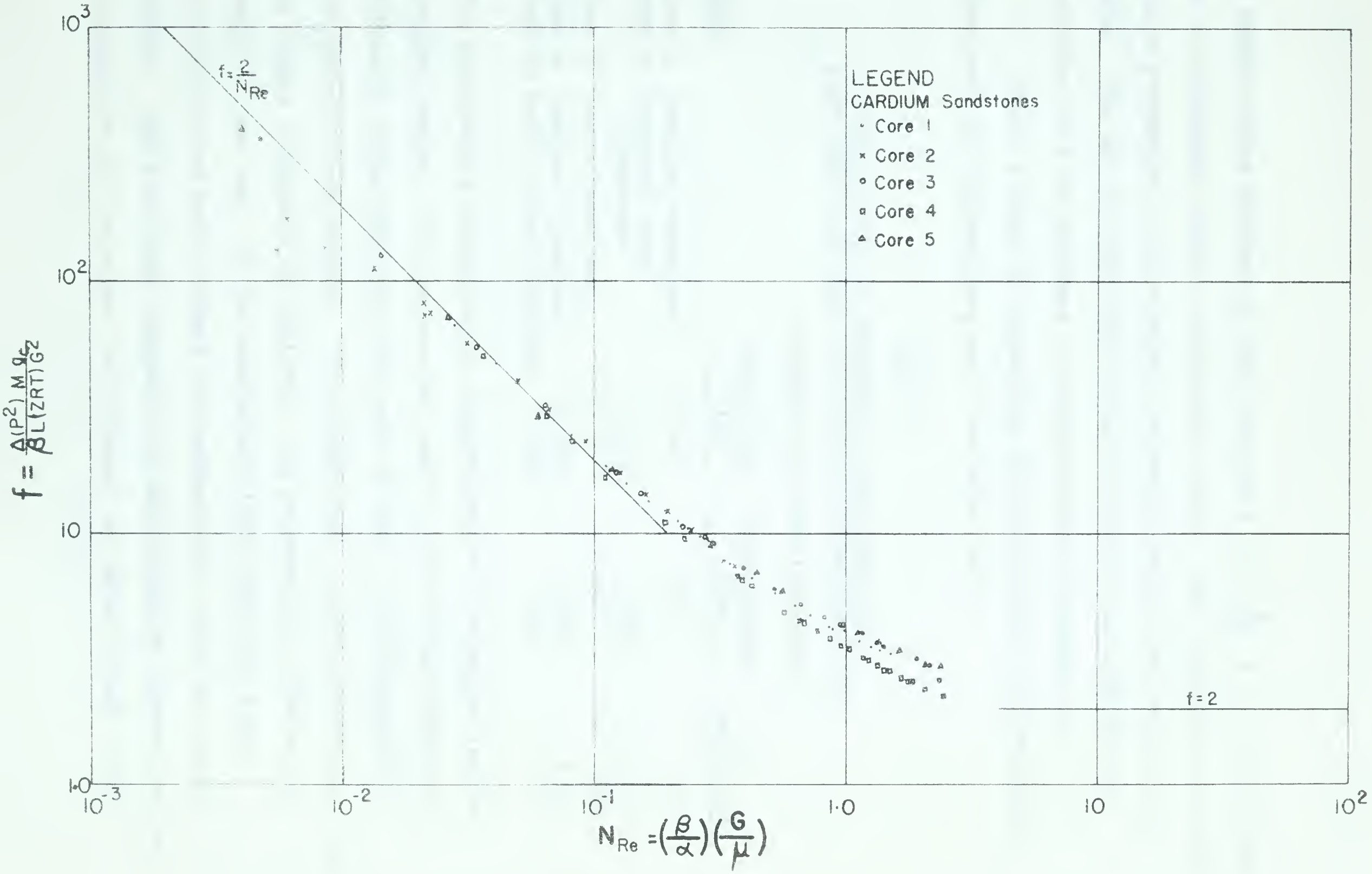

FIGURE 14 REYNOLDS NUMBER - FRICTION FACTOR PLOT

a smooth curve defined by the equation $f = \frac{2}{Re} + 2$. The forms of the friction factor and Reynolds number used for the correlation plots presented in this paper are useful mainly for correlating data. The way in which this type of plot can be used in the solution of flow problems is explained in reference 30.

Table 4 shows a comparison of the permeability determined from both the Klinkenberg and flow data plots.

Table 4

COMPARISON OF PERMEABILITIES DETERMINED
FROM BOTH FLOW DATA PLOTS AND KLINKENBERG PLOTS

Core		Permeability (millidarcies) Flow Data Plot	Klinkenberg Plot	% Deviation
Core 1	Cardium Sandstone	21.89	20.2	- 7.72
Core 6	Sturgeon Lake Limestone	0.508	0.557	+ 11.22
Core 8	Berea Sandstone	163.8	179	+ 9.28
Core 9	Indiana Limestone	2.715	2.68	- 1.29
Core 14	Belly River Sandstone	0.600	0.643	+ 7.17

The Klinkenberg permeability depends on the flow being in the laminar region. In the case of core 1, the Cardium sandstone, figure 16 shows that the flow was, at best, just bordering on the laminar flow region. If it were still in the transition region, as figure 8 appears to indicate, the permeability determined would be too low. It is considered likely that had lower mean pressures been reached the permeability would have been higher. The flow data permeability determination depends on the elimination of the effect of slippage, an effect which is not

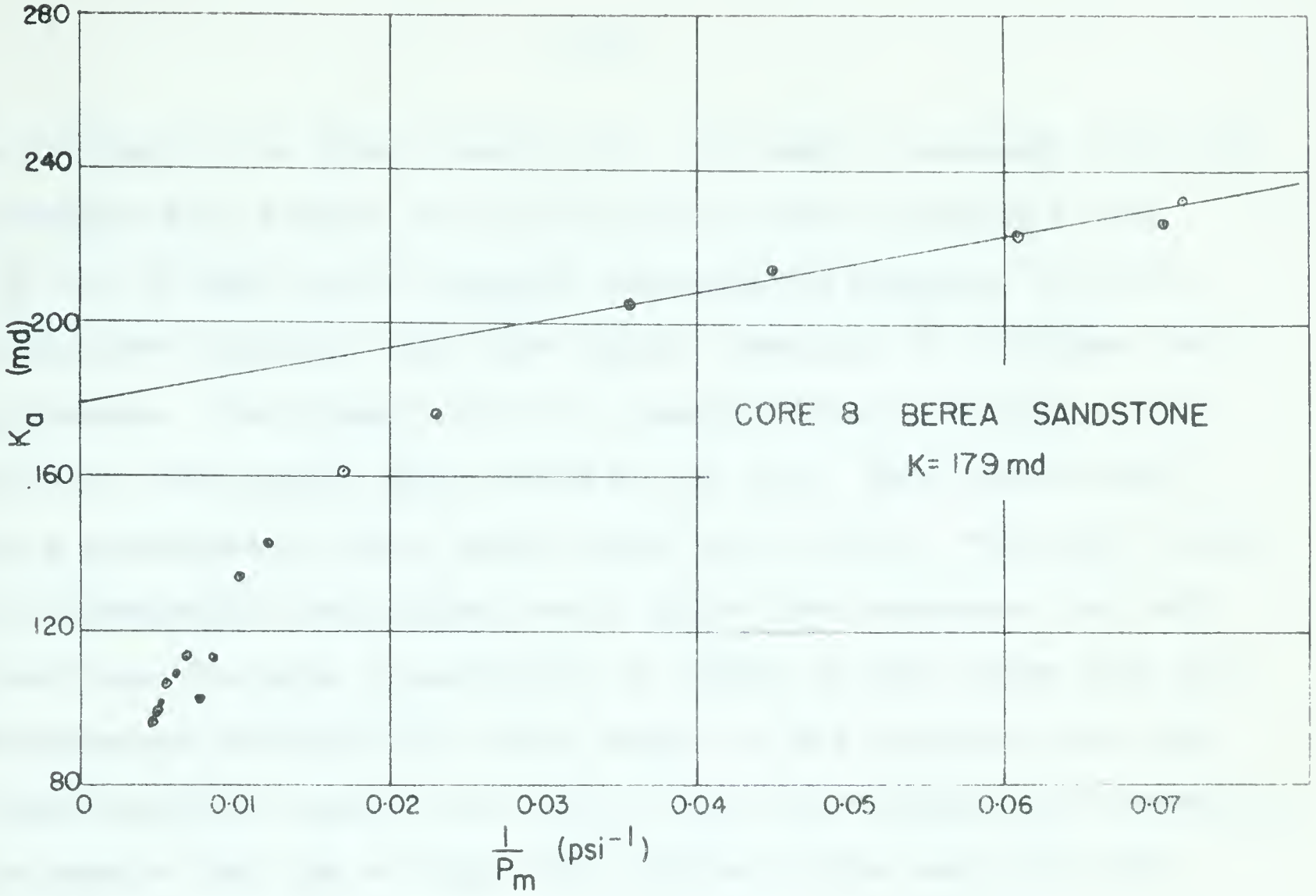

FIGURE 15 KLINKENBERG PERMEABILITY PLOT

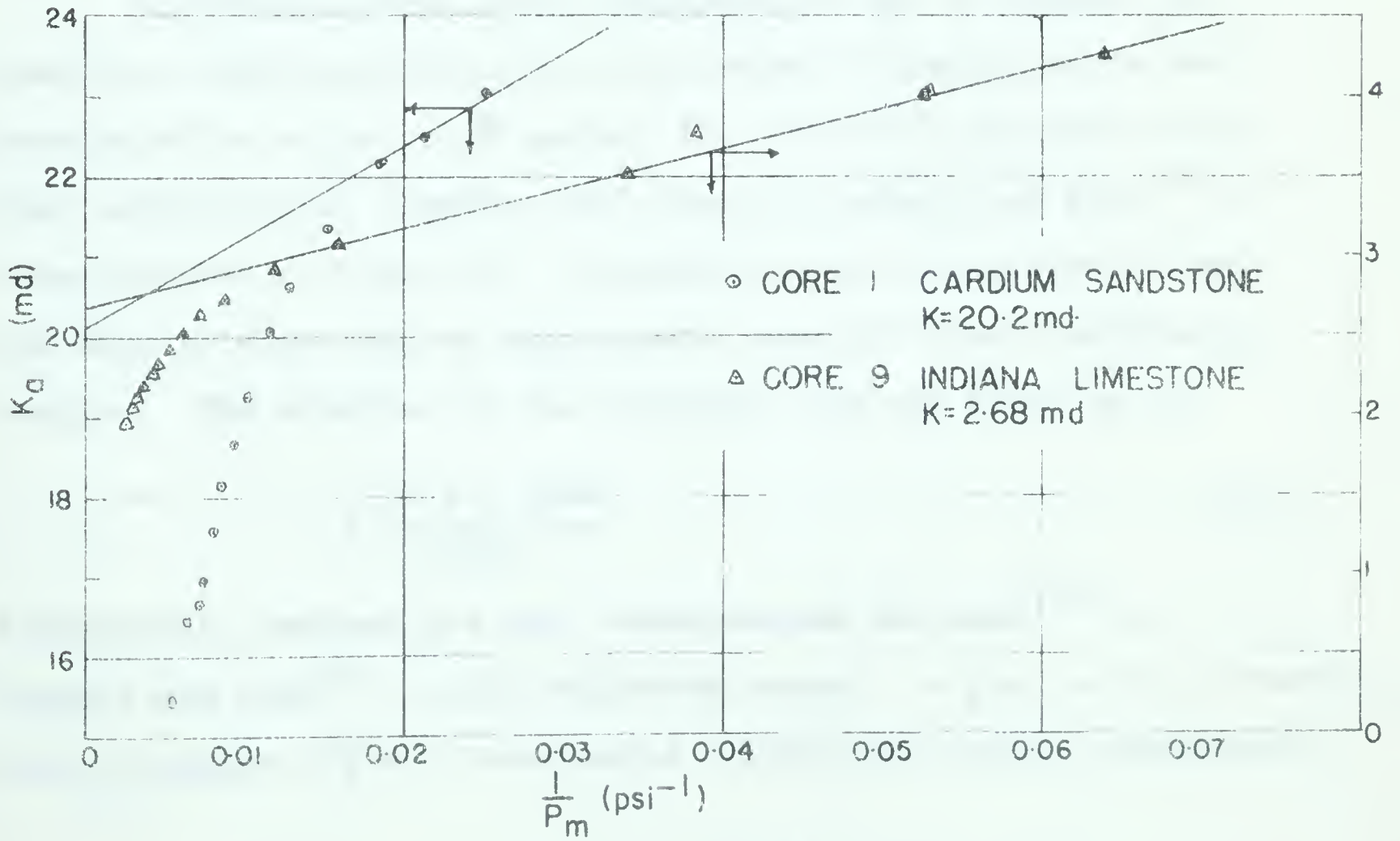

FIGURE 16 KLINKENBERG PERMEABILITY PLOT

accounted for in flow equation (5). If what is assumed to be the straight line region, on the flow data plots to obtain α and β, is in fact still slightly influenced by slippage, the flow data curve would in fact have slight curvature up to higher mean pressures. The visual fit of a straight line to the data would give an intercept α which would be too low. This would result in a permeability value which would be too high. While the values of permeability determined are in quite good agreement the fact that the flow data permeability is higher in most cases than the Klinkenberg permeability lends weight to the argument that data runs should be carried out for at least two constant mean pressures to ensure that the straight line region of the plot is in fact not influenced by slippage.

A primary aim of this investigation was to examine the result of additional flow data determined characteristics when correlated on a plot of β against K. The data obtained during this investigation together with that of Cornell and Katz[9] is shown plotted on figure 17. A similar plot was used by Cornell and Katz to show that an approximate straight line relationship results. The equation of the straight line was found to be

$$= \frac{4.11 \times 10^{10}}{K^{4/3}} \qquad (11)$$

Subsequently Janicek and Katz recorrelated the data[32] of Cornell and Katz[9] in the following manner. A plot of the formation factor against $1/\phi$ was interpreted to give the linear relationship

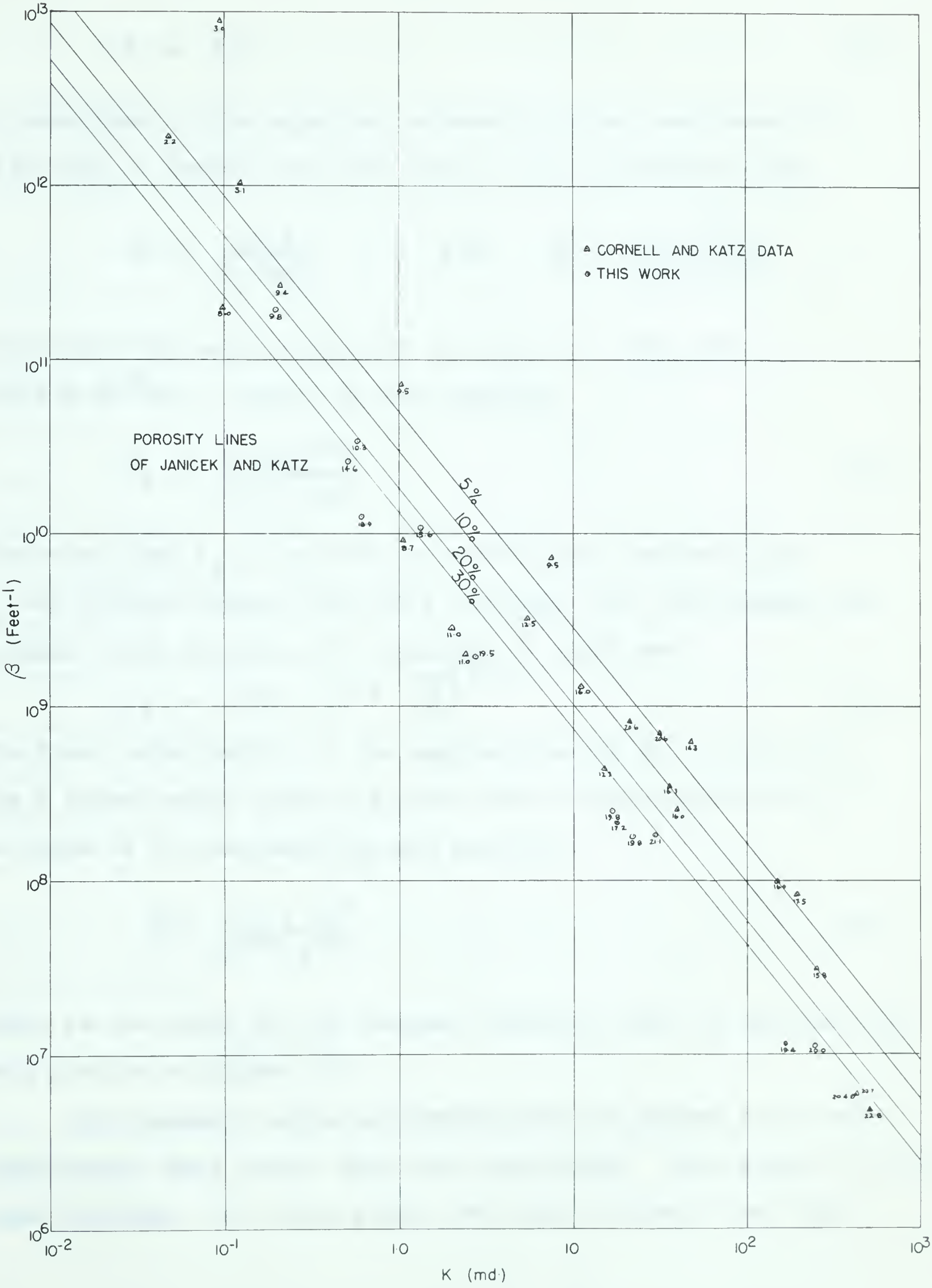

FIGURE 17 CORRELATION OF β FACTOR WITH PERMEABILITY AND POROSITY

$$F = 4/\phi \tag{12}$$

A comparison of the equation proposed by Green and Duwez[14] with that of Cornell and Katz led to the relationship that

$$\alpha = \frac{32\ F}{k_1\ D_E^{\ 2}} \qquad \text{and} \qquad \beta = \frac{32\ F^{3/2}}{k_2\ D_E\ \phi^{1/2}}$$

which with the substitution of $k_1 = 0.5$, $F = 4/\phi$ and $K = 9.411 \times 10^{13}/\alpha$ results in the equation

$$D_E = \frac{8\ (FK)^{1/2}}{9.7 \times 10^6} \tag{13}$$

Observing that k_2 is related to porosity and permeability, k_2 was plotted against K/ϕ and a straight line relationship was assumed to fit the data, the equation of which was

$$k_2 = 2.82 \times 10^{-2} \left(\frac{K}{\phi}\right)^{3/4} \tag{14}$$

The final substitution of the expressions for D_E, k_2 and F in the β relationship expressed above led to the equation for β in terms of the permeability and porosity

$$\beta = \frac{5.5 \times 10^9}{K^{5/4}\ \phi^{3/4}} \tag{15}$$

which is the basis of the constant porosity lines of Janicek and Katz plotted on figure 17.

The porosity lines so developed do not appear to fit the experimental data points with any consistency. They appear to be too close together. For this reason the data of Cornell and Katz,

for the factors k_2, K, Ø and F, was replotted during this study as k_2 against combinations of the other three factors. It was hoped that a grouping, different from that used by Janicek and Katz, would lead to a more consistent set of porosity lines. One of the groupings used was a dimensionless form where k_2 was plotted against Ø/F. Again a straight line can be fitted to the data points. An equation for k_2 can be determined and an expression for β, similar to that above, obtained. This dimensionless relationship lends considerable weight to the porosity and very little to the permeability, while the relationship developed by Janicek and Katz appears to weigh the effect of the permeability very strongly and minimizes the effect of the porosity. Other forms of plotting the data examined were k_2 against KØ, $\sqrt{K\emptyset}$ and KØ/F. These plots all weigh the effect of the permeability and the porosity to varying degrees. The form of the plotted data which was used was that of k_2 against KØ/F resulting in the equation

$$k_2 = 5.62 \left(\frac{K\,\emptyset}{F} \right)^{0.63} \qquad (16)$$

which when substituted with the expression for D_E and F results in the equation

$$= \frac{6.6 \times 10^7}{K^{1.13}\,\emptyset^{2.76}} \qquad (17)$$

This equation is the basis of the set of porosity lines on figure 17a.

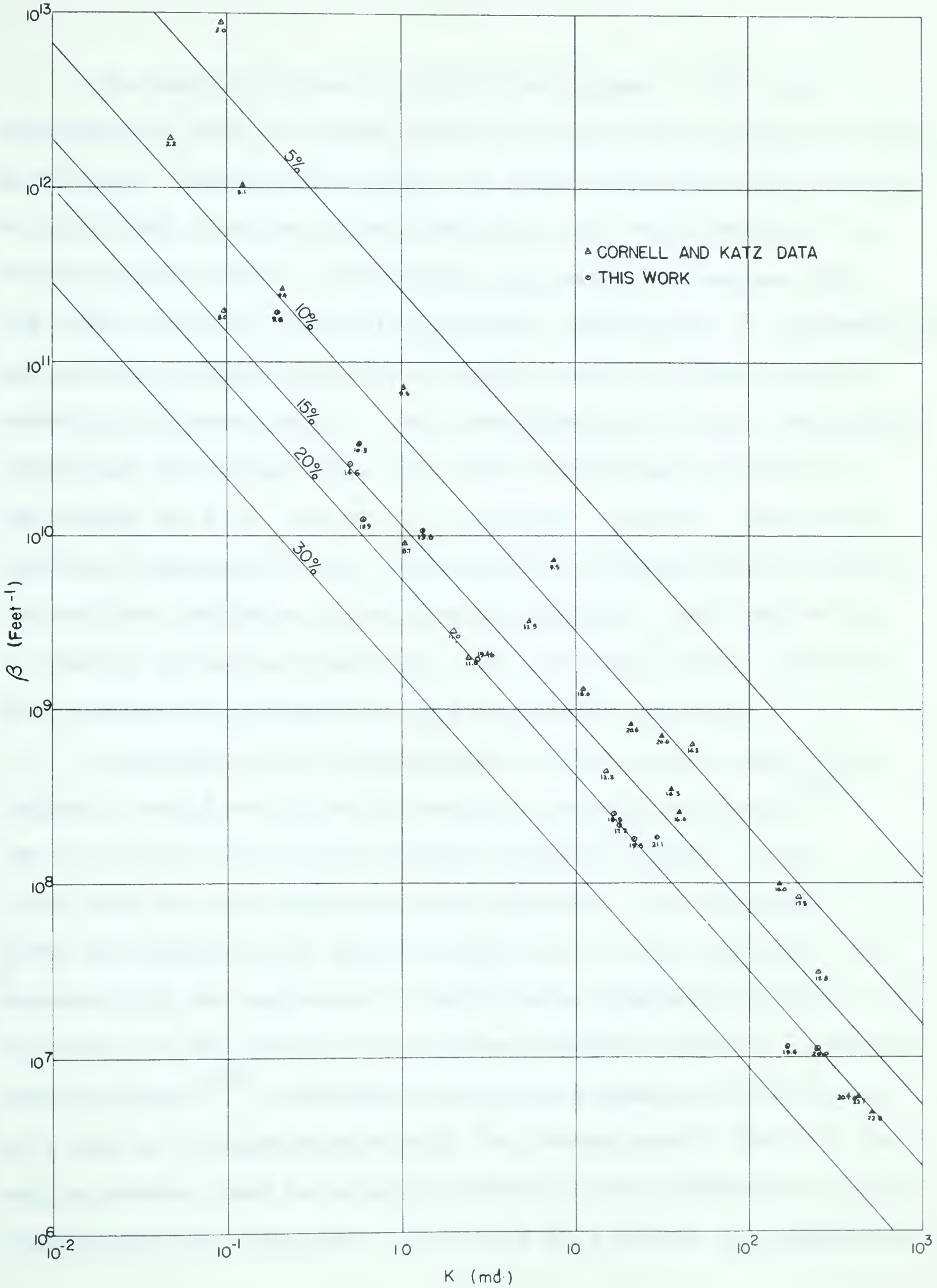

FIGURE 17a CORRELATION OF β FACTOR WITH PERMEABILITY AND POROSITY

The porosity lines so determined appear to fit the experimental data with much more consistency than those predicted previously. However the result is purely empirical and can only be justified if shown to be consistent with experimental flow characteristic data. It is overly optimistic to assume that the three factors, inertial resistance coefficient β, permeability and porosity should completely characterize the flow channel geometry of porous media. The investigation of other measurable properties of porous media, for their modifying influence on the values of K, ϕ, and β, is necessary. Some of those which could be investigated are, the fraction of dead end pore volume, the surface roughness, pore size distribution, and tortuosity. At present it can be generally said that the β factor increases with decreasing permeability and decreasing porosity.

The effect of the temperature on the porous media flow factors α and β was investigated by Greenberg and Weger[15] for the flow of gas through porous sintered metals. They found that as the temperature was increased, the flow data curve was displaced to give a larger value of α, that is, the permeability was decreased. The β factor however appeared to be unchanged as the slope of the curves remained constant. Johnson and Taliaferro[19] conducted controlled temperature flow tests at a series of temperatures with the stated result that for the test procedure used no apparent change in the permeability with temperature was indicated. Flow data at a series of temperatures

for flow through a Cardium sandstone sample were obtained and are shown plotted on figure 18. The plotted data appear to verify the results of Greenberg and Weger with the β factor unchanged and a decreasing permeability with increased temperature.

The factor β is a measure of the energy loss due to the inertial effects becoming significant. Due to the complicated nature of the flow path, the effect will become significant at low velocities of flow. With increased temperature very little change would be expected in the flow path structure, certainly not enough to cause an increase in the energy loss due to the inertial effects. It is reasonable and expected that in the case of the β factor no temperature effect would be apparent.

The permeability, which is the inverse of the factor α, is a viscous resistance coefficient and as such is dependent on the dimensions of the flow channels. With an increased temperature a change in the flow channel dimensions might be expected. The core holder used was a steel holder with the core mounted in a rubber stopper. The stopper was held in the tapered section of the holder as shown in figure 1 with the follower holding the rubber stopper in the tapered section as tightly as possible. The change in the flow characteristic α of the core should not have been due to the method of holding the core but must have been due to rock expansion alone. The result of the increased temperature would be an expansion of the rock causing a reduction in the cross sectional area of the flow channel. This would cause an increase in the flow resistance and result in a reduced

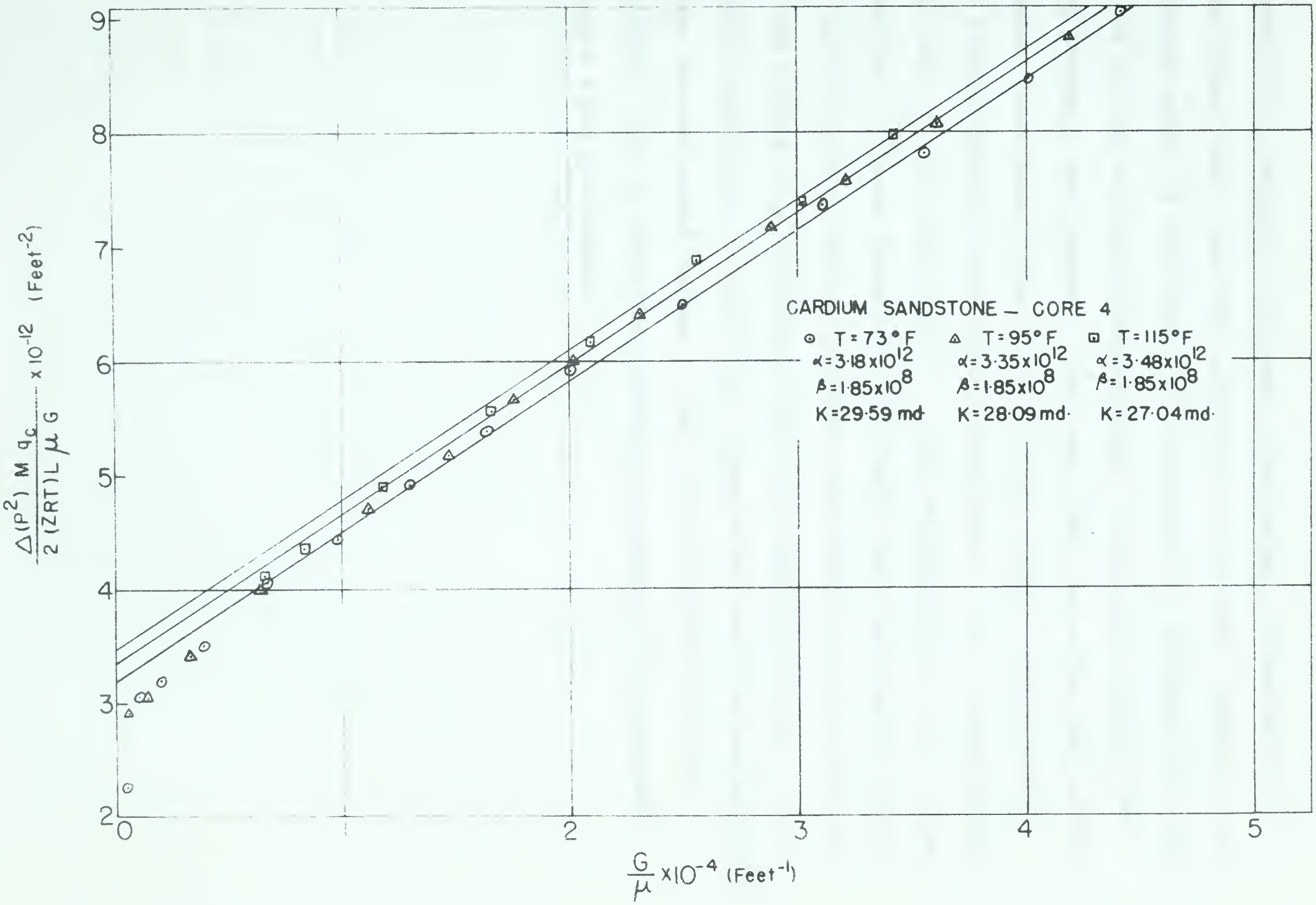

FIGURE 18 FLOW DATA PLOT TO OBTAIN α AND β

permeability, which is what was experienced. Greenberg and Weger state that since the expansion of the metal composing the sintered cores is negligible, the reduction in permeability must be due to the surface irregularities, particularly where the flow passages are narrow. They feel that the major part of the viscous resistance takes place at these narrow openings and any slight change in the size or position of the irregularities will have a very large effect. This explanation is felt to be justified, however there are undoubtedly many such narrow points in the flow paths through a porous rock which will be affected by the slight rock expansion when the temperature rises. The slight decrease in permeability experienced over the temperature range covered could be due to the slight decrease in cross sectional area at these constrictions, causing the increased viscous flow resistance.

CONCLUSIONS AND RECOMMENDATIONS

The plot of β against K with the parameter of porosity shows that there appears to be a relationship relating these variables. The manner in which this relationship may be completely expressed is not apparent other than by the empirical relationship which has been developed. The effects of other factors on the three variables need to be examined to try to find a possible relationship between the variables which is applicable to all porous media. Until such a relationship is developed the modified expression for β , equation (17), together with the friction factor - Reynolds number correlation can be used for gas flow calculations when the permeability and porosity are known.

The effect of gas slippage is considered to be of significance only at low mean pressures; however the flow data plots to obtain the inertial resistance coefficient β and permeability K , depend on the elimination of this effect to predict the correct values of the two factors. Several flow tests for each core, in which experimental data were obtained at different constant mean pressures, would show the flow rate up to which the slippage effect was significant. It is recommended that flow data on cores, covering a wide range of permeability, be obtained at different constant mean pressures. The plots of these data would indicate the flow rates that probably have to be achieved, for any permeability range, before the assumption that the data points fit the straight line, predicted by the flow equation (5), is necessarily true.

A further investigation on the effect of temperature on the flow characteristics of porous rocks needs to be carried out. Changes in the experimental apparatus setup would allow better control of the temperature. A core holder which could be immersed in a constant temperature bath should enable positive control of the temperature to be maintained. With a core holder such as the one used in this study it is necessary that the follower be kept tightly screwed down. This has to be checked on every change of temperature.

The small core samples used in this study were taken from bulk samples of the formation rock. In many cases small cores samples were obtained from immediately adjoining sections of the bulk sample, while the flow characteristic factors determined for each small core sample are significant, they have to be interpreted as applying to the core on which they were determined, thus different permeability and β factor values were found for each small cardium core studied. These factors describe the properties of the particular core, and no one small core can be said to characterize cardium sandstone generally. Characteristic factors based on the average properties of a cardium sandstone reservoir would however be significant as characterizing the bulk rock.

The difficulty that was experienced in mounting large core samples has led to a continuing investigation into different mounting techniques. The use of an epoxy resin material for mounting large core samples has been modified, to

eliminate the penetration of the core by the epoxy resin, which is highly wetting. While the use of this mounting material is of doubtful value for large core samples it can be used successfully for small cores. The methods which are felt to hold the most promise are those in which the core is thinly coated with a non wetting material and then mounted using a non shrink material or other sufficiently strong matieral.

The long core data also points out the need for properly designed equipment, with the proper location of pressure taps and other measuring points. The method of drilling pressure taps along the length of the core needs investigation. The possibility of pressure taps being positioned on the core prior to its mounting might be one way to avoid drilling through the mounting material and into the core.

The Reynolds number - friction factor correlation shown in figures 13 and 14 is based on the definitions expressed by equations (8) and (9). With the Reynolds number so defined, the correlation graphs indicate that for the flow of a gas through porous media, the deviation from purely viscous flow takes place at the same Reynolds number. This Reynolds number value is between 0.08 and 0.10. If permeability and porosity data are available it is possible to determine the mass flow rate at which Darcy's law for gas flow can no longer be used to obtain calculated flow data. The data below a Reynolds number value of approximately 0.03 appear to be influenced by gas slippage to a varying degree. This is indicated by the data points falling below the line defined by the equation $f = 2/N_{Re}$.

NOMENCLATURE

β - coefficient of inertial resistance term of flow equation ($feet^{-1}$)

Δ - difference

P - pressure (pounds force/square inch absolute)

P_m - mean pressure (pounds force/square inch absolute)

M - molecular weight of a gas

g_c - conversion factor (32.17 pounds mass x foot/pounds force x seconds squared)

L - length of porous sample (inches)

Z - compressibility factor of gas

R - gas constant (1543 pounds force x cubic feet/square feet x pound mole x ^oR)

T - absolute temperature ^oR

μ - viscosity of gas (pounds mass/foot second)

G - mass velocity (pounds mass/square foot second)

α - coefficient of laminar term of flow equation ($feet^{-1}$)

K - permeability (millidarcies)

K_a - apparent permeability (millidarcies)

ϕ - porosity

v - velocity (feet/second)

Q - flow rate (cubic feet/hour)

A - cross sectional area of porous sample (square inches)

ρ - density (pounds mass/cubic feet)

F - Electrical resistivity factor; electrical resistance of sample saturated with brine/resistance of quantity of brine of same size and shape as bulk volume of sample.

k_1 - dimensionless geometrical constant in laminar term of flow equation

k_2 - dimensionless geometrical constant in inertial term of flow equation

D_E - effective diameter of pore structure (feet)

N_{Re} - Reynolds number (dimensionless)

f - friction factor

BIBLIOGRAPHY

1. Bakmeteff, B.A. and Feodoroff, N.V., Fluid Flow in Granular Media, Trans. ASME (J. App. Mech.) (1951) 73, 39.

2. Beeson, C.A., The Kobe Porosimeter and the Oilwell Research Porosimeter, Trans. AIME 189 (1950) 313.

3. Brownell, L.E. and Katz, D.L., Flow of Fluids Through Porous Media, Chem. Eng. Prog. 43 (1947) 10, 537.

4. Brownell, L.E., Dombrowski, H.S. and Dickey, C.A., Pressure Drop Through Porous Media, New Data and Revised Correlations, Chem. Eng. Prog. (1950) 46, 415.

5. Bonillas, W.K., Evaluating Low Permeability Cores, Petroleum Engineer, July 1954, B-65.

6. Carman, P.C., Fluid Flow Through Granular Media, Trans. Inst. Chem. Eng. (London 1937), 15, 150.

7. Carman, P.C., Flow of Gases Through Porous Media, Butterworth Scientific Publication, London, 1956.

8. Collins, R.E., Flow of Fluids Through Porous Materials, Reinhold Publishing Corporation, New York, 1961.

9. Cornell, P. and Katz, D.L., Flow of Gases Through Consolidated Porous Media, Ind. Eng. Chem. (1953) 45, 2145.

10. Elenbaas, J.R. and Katz, D.L., A Radial Turbulent Flow Formula, Trans. AIME (1948) 174, 25.

11. Ergun, S. and Orning, A.A., Fluid Flow Through Randomly Packed Columns and Fluidized Beds, Ind.Eng.Chem. (1949) 41, 1179.

12. Ergun, S., Fluid Flow Through Packed Columns, Chem. Eng. Prog. (1952) 48, 89.

13. Fancher, G.H., Lewis, J.A. and Barnes, K.B., Flow of Simple Fluids Through Porous Materials, Ind. Eng. Chem. 1933 (25) 146.

14. Green, L., Jr. and Duwez, P., Fluid Flow Through Porous Metals, Trans. ASME (J. App. Mech.) (1951) 73, 59.

15. Greenberg, D.B. and Weger, E., An investigation of the Viscous and Inertia Coefficients for the Flow of Gases Through Porous Sintered Metals with High Pressure Gradients, Chem. Eng. Sci. (1960) 12, 8.

16. Grunberg, L. and Nissan, A.H., The Permeability of Porous Solids to Gases and Liquids, Inst. of Pet. Journal 20 (1943) 236, 194.

17. Hubbert, M. King, The Theory of Ground Water Motion, Jour. of Geology 8 (1940) 48, 785.

18. Hubbert, M. King, Darcys Law and the Field Equations of Flow of Underground Fluids, Trans. AIME (1956) 207, 222.

19. Johnston, T.W. and Taliaferro, D.B., Flow of Air and Natural Gas Through Porous Media, Tech. Paper 592, USBM 1938.

20. Katz, D.L. et al, Handbook of Natural Gas Engineering, 47, New York, McGraw Hill, 1959.

21. Klinkenberg, K.J., The Permeability of Porous Media to Liquids and Gases, API 1941, 200.

22. Leva, M. et al, Fluid Flow through packed and Fluidized Systems, USBM Bull. 504 (1951) 20.

23. Michels, A. and Gibson, R.O., The Measurement of the Viscosity of Gases. The Viscosity of Nitrogen to 1000 Atmospheres, Proc. Roy. Soc. 134A, 228, (1931).

24. Muskat, M., The Flow of Homogeneous Fluids Through Porous Media, J.W. Edwards Inc. 1946.

25. Muskat, M., Physical Principles of Oil Production, McGraw Hill Book Co. Inc. 1949.

26. Rawlins, E.L. and Schellhardt, M.A., US Bureau of Mines, Monograph 7, 1936.

27. Scheidegger, A.E., The Physics of Flow Through Porous Media, University of Toronto Press, Toronto, 1957.

28. Sage, B.H. and Lacey, W.N., Thermodynamic Properties of the Lighter Paraffin Hydrocarbons and Nitrogen, API New York, 1950.

29. Stewart, C.R. and Owens, W.H., A Laboratory Study of Laminar and TurbulentFlow in Heterogeneous Porosity Limestones, Trans. AIME (1958) 213, 121.

30. Stutzman, L.F. and Thodos, G., Adaption of Friction Factors to the Flow of Fluids Through Consolidated Formations, Trans. AIME (1956) 207, 352, Tech. Note 376.

31. Tek, M.R., Development of a Generalized Darcy Equation, Trans. AIME (1957) 210, 377.

32. Tek, M.R., Coates K.H. and Katz, D.L., The Effect of Turbulence on the Flow of Natural Gas Through Porous Reservoirs, Journ. of Pet. Tech. (July 1962) 799.

APPENDIX I

TABLE 5

GAS FLOW DATA

INDIANA LIMESTONE LONG CORE

Run No	Pressure-PSIA P_1	Pressure-PSIA P_2	T_{flow} (average) $^{\circ}R$	Q_c (SCFH)	$(P_1^2-P_2^2)$ $(PSIA)^2$	G (lbs/ft^2sec)
1	621.3	34.0	535.7	18.25	386000	.00561
2	512.7	25.6	535.4	13.01	262800	.00400
3	415.4	19.9	535.4	8.65	172500	.00272
4	318.7	16.0	535.4	5.33	101500	.00164
5	266.8	14.9	533.1	3.81	71160	.00117
6	215.9	14.1	532.6	2.34	46600	.00075
7	166.1	13.7	532.9	1.55	27600	.00048
8	115.9	13.5	533.3	.78	13400	.00024
9	70.5	13.7	529.2	.39	4970	.00012
10	214.1	124.5	530.5	1.66	45800	.00051
11	313.6	124.9	531.7	4.35	98340	.00134
12	277.4	61.8	531.7	3.90	76950	.00120
13	370.0	62.1	531.7	6.84	136900	.00210

TABLE 6(A)

GAS FLOW DATA

ALUNDUM CORE (TA 7921)
(before pressure taps drilled)

Run No	Pressure-Psia P_1	Pressure-Psia P_2	T_{flow} (average) ^oR	Q_c (SCFH)	$(P_1^2-P_2^2)$ $(Psia)^2$	G (lbs/ft^2sec)	$\frac{1}{p_{avg}}$ (Psi^{-1})	Ka (md.)
1	40.4	17.3	534.7	6.85	1340	.006452	.0347	650.79
2	54.9	22.8	535.7	11.65	2500	.01097	.0257	594.18
3	65.8	28.2	537.4	15.45	3540	.01455	.0213	558.91
4	75.4	33.3	538.9	18.73	4580	.01764	.0184	524.61
5	82.7	37.8	538.9	21.41	5410	.02017	.0166	508.08

TABLE 6(B)

GAS FLOW DATA

ALUNDUM CORE (TA 7921)
(Pressure Taps Drilled Along Length of Core.
Pressure Taps Upstream and Downstream of End Plates.)

Run No	Pressure-Psia P_1	Pressure-Psia P_2	T_{flow} (average) ^oR	Q_c (SCFH)	$(P_1^2-P_2^2)$ $(Psia)^2$	G (lbs/ft^{2}sec)	$\frac{1}{Pavg}$ (Psi^{-1})	Ka (Md.)
1	213.1	138.8	531.5	84.60	26130	7.969×10^{-2}	0.00568	419.8
2	212.5	156.9	530.8	71.58	20540	6.742 "	0.00541	442.43
3	213.7	189.5	530.8	40.75	9760	3.838 "	0.00496	530.86
4	212.5	173.6	530.9	56.90	15040	5.360 "	0.00518	480.72
5	214.2	204.1	530.9	20.12	4220	1.895 "	0.00478	605.94
6	214.1	208.2	530.9	13.47	2490	1.175 "	0.00474	636.59
7	215.1	211.8	530.9	6.53	1380	0.615 "	0.00468	604.41
8	213.6	212.0	530.3	3.24	660	0.305 "	0.00470	624.88
9	21.58	13.85	531.3	1.722	274	0.162 "	0.0564	790.81
10	21.75	14.19	532.0	1.700	272	0.160 "	0.0557	787.80
11	21.47	14.54	532.0	1.560	250	0.147 "	0.0556	787.71
12	21.60	17.02	532.7	1.097	177	0.103 "	0.0518	783.27
13	21.66	21.34	532.7	0.0541	14.10	0.00500 "	0.0465	702.90
14	29.39	22.11	531.7	3.89	643	0.366 "	0.0452	761.2
15	29.41	26.11	531.7	2.18	344	0.205 "	0.0383	799.43
16	28.49	27.63	532.0	0.582	94.5	0.0548 "	0.0362	776.09
17	37.26	16.75	529.2	6.48	1108	0.610 "	0.037	731.47
18	36.51	21.84	529.2	5.09	856	0.479 "	0.0343	743.22
19	36.22	30.09	529.2	2.47	407	0.233 "	0.0302	759.30
20	79.1	38.89	530.2	22.73	4570	2.141 "	0.0169	600.77
21	79.4	56.7	530.2	15.78	3095	1.486 "	0.0158	641.38
22	78.9	67.4	530.9	8.82	1680	0.831 "	0.0137	662.76
23	79.3	77.3	530.9	2.15	313	0.203 "	0.0128	865.93
24	113.3	107.6	530.9	6.49	1250	0.611 "	0.00905	656.3
25	114.2	90.3	530.9	15.98	3190	1.505 "	0.00937	632.71
26	114.5	72.9	530.9	34.22	7800	3.223 "	0.0107	553.44
27	114.3	63.9	530.9	38.31	8980	3.609 "	0.0122	538.39
28	163.8	101.2	530.9	60.92	16590	5.738 "	0.00755	463.93
29	164.2	118.0	529.7	51.15	13030	4.818 "	0.0071	495.67
30	163.7	136.8	529.7	34.96	8080	3.293 "	0.0067	547.03
31	163.3	156.8	530.2	10.29	2060	0.969 "	0.0062	630.81

TABLE 6(C1)

GAS FLOW DATA

ALUMDUN CORE (TA 7921)
(Pressure Taps in End Plates)

Run No	Pressure-Psia P_1	P_2	T_{flow} (Average) ^oR	Q_c (SCF)	$(P_1^2-P_2^2)$ $(Psia)^2$	G (lbs/ft^2sec)	$\frac{1}{Pavg_1}$ (Psi^{-1})	Ka (Md.)
1	63.5	33.1	535	16.66	2940	1.569×10^{-2}	.0207	722.44
2	79.0	45.5	535	23.24	4170	2.189 "	.0161	711.37
3	94.34	57.7	535	31.66	5570	2.982 "	.0142	726.53
4	79.2	45.6	535	24.05	4180	2.265 "	.0160	734.34
5	20.40	13.77	536.3	1.392	227	0.131 "	.0585	784.19
6	23.21	14.07	536.3	2.083	341	0.196 "	.0536	780.81
7	25.44	14.39	536.3	2.68	440	0.247 "	.0502	778.12
8	18.02	13.60	536.5	0.86	140	0.081 "	.0633	785.67
9	33.03	13.17	536.5	4.98	818	0.469 "	.0433	778.71
10	40.80	19.24	536.5	7.70	1295	0.725 "	.0333	760.38
11	51.6	24.81	536.5	11.61	2045	1.094 "	.0262	726.23
12	14.43	13.29	535.4	0.194	31.5	0.0183 "	.0722	784.57
13	13.90	13.31	535.4	0.10	16.1	0.0094 "	.0735	792.82
14	13.48	13.31	535.4	0.0326	4.53	0.0031 "	.0747	919.06
15	77.8	44.4	536.3	23.37	4080	2.201 "	.0163	733.66
16	94.1	58.5	536.3	30.92	5440	2.913 "	.0131	728.78
17	115.9	78.6	536.1	40.42	7250	3.807 "	.0115	714.27
18	140.3	101.4	535.3	53.16	9400	5.007 "	.0083	725.73
19	169.8	130.00	534.4	67.94	11940	6.400 "	.0067	730.79
20	190.2	148.3	534.4	80.23	14170	7.557 "	.0059	728.00
21	214.4	171.5	534.1	93.48	16570	8.805 "	.0052	726.37
22	238.9	194.7	533.5	106.2	19190	10.00 "	.0046	712.85
23	256.44	212.3	533.5	116.2	20680	10.94 "	.0043	723.42
24	226.0	171.1	533.5	121.6	21795	11.45 "	0.005	717.67
25	195.3	142.5	533.5	100.9	17820	9.501 "	0.006	726.48
26	252.4	196.1	533.5	139.7	25270	13.16 "	0.0045	712.42
27	146.2	97.6	533.5	68.25	11860	6.429 "	0.008	735.62

TABLE 6(C2)

GAS FLOW DATA

ALUNDUM CORE (TA 7921)
(pressure taps in end plates)

Run No	Pressure-Psia P_1	Pressure-Psia P_2	T_{flow} (average) ^oR	Q_c (SCFH)	$(P_1^2-P_2^2)$ $(Psia)^2$	G (lbs $ft^2 sec$)	$\frac{1}{Pavg}$ (psi^{-1})	Ka (md.)
1	27.11	13.49	530	3.466	553	3.264×10^{-3}	0.0493	784.0
2	33.34	14.06	530	5.719	914	5.386 "	0.0422	783.2
3	39.3	14.7	530	8.230	1329	7.753 "	0.0370	775.4
4	59.6	19.83	529	18.566	3164	17.49 "	0.0251	729.1
5	83.6	32.50	529	34.99	5933	32.97 "	0.0172	739.2
6	97.1	41.5	529	45.22	7704	42.58 "	0.0144	724.5
7	114.5	54.0	529	59.07	10180	55.63 "	0.0119	727.9
8	133.3	67.9	529	74.57	13160	70.25 "	0.0099	712.2
9	153.3	83.6	529	92.48	16500	87.12 "	0.0084	705.6
10	173.7	99.5	528	110.3	20280	103.9 "	0.0073	684.2
11	164.2	92.6	528	100.3	18380	94.49 "	0.0078	686.1
12	143.8	75.0	529	81.78	15050	77.03 "	0.0091	683.2

TABLE 7

GAS FLOW DATA

CORE #1 CARDIUM SANDSTONE

Run No	Pressure-Psia P_1	Pressure-Psia P_2	T_{flow} (average) ^{o}R	Q_c (SCFH)	$(P_1^2-P_2^2)$ $(Psia)^2$	G (lbs/ft^{2}sec)	$\frac{1}{Pavg}$ (Psi^{-1})	Ka (Md.)
1	66.1	13.96	534.2	2.12	4173	0.804 x 10^{-2}	0.025	23.03
2	80.1	14.40	534.4	3.08	6215	1.167 "	0.0212	22.49
3	93.8	15.04	534.6	4.18	8571	1.584 "	0.0184	22.15
4	115.9	16.60	534.6	6.17	13160	2.339 "	0.0151	21.32
5	138.1	18.95	534.4	8.48	18720	3.214 "	0.0127	20.60
6	153.4	20.97	534.4	10.18	23100	3.859 "	0.0115	20.06
7	174.2	24.05	534.4	12.56	29770	4.761 "	0.0101	19.22
8	189.3	26.65	534.4	14.38	35120	5.451 "	0.0093	18.67
9	204.7	29.40	534.4	16.30	41030	6.178 "	0.0085	18.13
10	218.3	32.00	534.4	17.90	46640	6.785 "	0.0080	17.53
11	233.8	35.13	534.4	19.83	53420	7.516 "	0.0074	16.95
12	242.6	36.98	534.4	20.96	57510	7.945 "	0.0072	16.66
13	234.6	35.32	530.7	20.90	53810	7.922 "	0.0074	17.55
14	271.9	43.3	530.1	26.17	72050	9.920 "	0.0064	16.42
15	310.0	52.3	530.4	31.84	93360	12.07 "	0.0055	15.44
16	361.2	64.5	530.8	39.59	126330	15.01 "	0.0047	14.24
17	412.9	77.7	530.8	47.89	164440	18.15 "	0.0041	13.26
18	460.3	90.0	529.6	55.55	203770	21.06 "	0.0036	12.41
19	513.5	103.9	529.2	64.57	252920	24.78 "	0.0032	11.65
20	810.8	185.6	529.0	116.3	623000	44.07 "	0.0020	8.63
21	754.0	170.2	527.8	106.1	539540	40.22 "	0.0022	9.05
22	700.6	155.5	527.4	97.20	466650	36.84 "	0.0023	9.55
23	641.9	139.3	527.3	86.68	392610	32.86 "	0.0026	10.10
24	589.3	122.2	527.2	76.00	332300	28.81 "	0.00281	10.44
25	527.3	108.4	527.2	67.58	266300	25.62 "	0.00315	11.54

TABLE 8

GAS FLOW DATA

CORE #2 CARDIUM SANDSTONE

Run No	Pressure-Psia P_1	Pressure-Psia P_2	T_{flow} (average) ^oR	Q_c (SCFH)	$(P_1^2-P_2^2)$ $(Psia)^2$	G (lbs/ft^2sec)
1	103.6	13.62	532.8	0.00312	10550	0.1181×10^{-4}
2	133.4	13.62	532.8	0.00348	17200	0.1316 "
3	163.6	13.62	532.8	0.00488	2656	0.1846 "
4	234.0	13.42	529.2	0.00768	5455	0.2912 "
5	317.1	13.43	529.2	0.0128	100390	0.4835 "
6	315.7	13.01	530.7	0.0121	99520	0.4574 "
7	415.3	13.01	530.7	0.0193	172290	0.7305 "
8	521.8	12.96	530.7	0.0287	272130	1.086 "
9	618.9	12.96	530.7	0.0387	382890	1.464 "
10	745.5	13.27	530.2	0.0541	555560	2.047 "
11	896.5	13.29	530.2	0.0748	803480	2.828 "
12	1027.1	13.30	530.2	0.0984	1054680	3.588 "
13	1151.8	13.31	530.8	0.1153	1326540	4.370 "
14	1320.0	13.33	530.9	0.1445	1742090	5.466 "
15	1477.3	13.35	530.9	0.1729	2182210	7.541 "
16	1575.0	13.39	530.9	0.1964	2480290	7.430 "
17	1723.4	13.48	531.2	0.2203	2969890	8.334 "
18	1885.9	13.48	531.2	0.2540	3556440	9.609 "

TABLE 9

GAS FLOW DATA

CORE #3 CARDIUM SANDSTONE

Run No	Pressure-Psia P_1	Pressure-Psia P_2	T_{flow} (Average) ^oR	Q_c (SCFH)	$(P_1^2-P_2^2)$ $(Psia)^2$	G (lbs/ft^2sec)
1	20.59	13.54	540.2	0.100	240.6	$.0379 \times 10^{-2}$
2	32.11	13.55	539.7	0.340	847.5	.1286
3	53.5	13.60	537.9	1.024	2672	.3874
4	18.1	13.65	537.9	2.417	6395	.9144
5	114.2	13.79	537.9	4.594	13850	1.738
6	163.3	14.24	537.9	8.73	26480	3.303
7	188.1	14.59	537.9	11.02	35150	4.169
8	239.3	15.71	537.9	16.24	57020	6.144
9	283.3	17.15	535.0	20.93	79960	7.918
10	338.2	19.41	535.0	28.00	114000	10.59
11	413.6	23.80	534.4	37.41	170500	14.15
12	488.5	29.08	533.1	47.38	237800	17.93
13	577.1	36.03	533.4	59.32	331800	22.44
14	642.4	41.46	533.2	68.63	410900	25.96
15	1216.7	97.7	527.9	158.2	1471000	59.87
16	1107.6	85.8	527.4	139.4	1219500	52.72
17	984.9	74.3	527.4	120.4	964600	45.55
18	843.7	61.2	527.4	97.81	708000	37.00
19	743.0	52.1	527.5	83.46	549300	31.58

TABLE 10(A)

GAS FLOW DATA

CORE #4 CARDIUM SANDSTONE

(T_f = 73°F)

Run No	Pressure-Psia P_1	Pressure-Psia P_2	T_{flow} (average) °R	Q_c (SCFH)	$(P_1^2-P_2^2)$ $(Psia)^2$	G (lbs/ft^2sec)
1	801.8	88.4	531.8	142.1	635100	53.87×10^{-2}
2	736.1	79.7	530.9	128.9	535500	48.87 "
3	665.8	70.3	530.8	113.8	438400	43.14 "
4	601.3	62.0	530.85	99.30	357700	37.64 "
5	499.4	48.6	531.05	77.93	247000	29.54 "
6	430.6	40.1	531.85	63.66	183800	24.13 "
7	370.6	32.76	532.6	51.84	136300	19.65 "
8	314.7	26.48	533.35	41.05	98300	15.56 "
9	260.5	21.21	533.85	30.94	67400	11.73 "
10	206.3	17.36	537.9	21.07	42240	7.987 "
11	147.6	14.84	538.0	12.47	21560	4.727 "
12	101.9	13.87	538.0	6.48	10200	2.456 "
13	74.3	13.61	538.0	3.54	5335	1.340 "
14	44.4	13.54	538.0	1.62	1785	0.614 "

TABLE 10(B)

GAS FLOW DATA

CORE #4 CARDIUM SANDSTONE
(T_f = 95°F)

Run No	Pressure-Psia P_1	P_2	T_{flow} (average) °R	Q_c (SCFH)	$(P_1^2-P_2^2)$ $(Psia)^2$	G ($lbs/ft^2 sec$)
1	86.1	13.63	554.25	4.57	7224	1.732×10^{-2}
2	56.4	13.46	552.2	1.99	3000	0.7543 "
3	138.8	14.42	555.3	10.74	19070	4.071 "
4	211.5	17.24	554.85	21.08	44400	7.990 "
5	301.4	24.23	554.95	36.59	90300	13.87 "
6	364.2	30.97	554.2	48.05	131700	18.21 "
7	415.9	36.56	555.0	57.51	171600	21.80 "
8	458.9	41.9	554.6	66.07	208800	25.04 "
9	510.0	48.3	555.65	76.09	257700	28.84 "
10	603.8	60.1	555.65	94.93	360900	35.98 "
11	809.6	86.5	555.1	138.5	647900	52.49 "
12	721.1	75.2	556.3	119.6	514400	45.35 "
13	656.9	68.1	555.05	106.2	426900	40.27 "

TABLE 10(C)

GAS FLOW DATA

CORE #4 CARDIUM SANDSTONE
(T_f = 115°F)

Run No	Pressure-Psia P_1	P_2	T_{flow} (average) °R	Q_c (SCFH)	$(P_1^2-P_2^2)$ $(Psia)^2$	G $(lbs/ft^2 sec)$
1	260.1	20.23	575.0	27.76	67230	10.52×10^{-2}
2	743.6	76.6	574.8	120.2	546600	45.57 "
3	658.8	66.0	574.8	102.5	429700	38.84 "
4	580.0	55.90	575.45	86.55	333200	32.81 "
5	498.4	45.9	575.3	70.68	246300	26.79 "
6	420.3	36.6	575.45	56.01	175300	21.23 "
7	328.9	26.3	575.0	39.49	107500	14.97 "
8	236.2	18.5	574.65	24.11	55430	9.14 "

TABLE 11

GAS FLOW DATA

CORE #5 CARDIUM SANDSTONE

Run No	Pressure-Psia P_1	Pressure-Psia P_2	T_{flow} (average) ^oR	Q_c (SCFH)	$(P_1^2-P_2^2)$ $(Psia)^2$	G (lbs/ft^2sec)
1	1014.5	86.5	529.2	140.5	1021700	53.36×10^{-2}
2	905.5	75.4	528.7	122.30	814300	46.45 "
3	1096.1	95.0	525.4	155.01	1192400	58.88 "
4	1087.1	94.0	525.4	154.2	1173000	58.57 "
5	809.8	65.7	526.8	106.1	651400	40.30 "
6	694.0	54.3	530.3	87.30	478700	33.16 "
7	616.2	47.40	530.1	74.08	378000	28.14 "
8	537.6	39.21	530.4	62.24	287400	23.64 "
9	461.8	32.14	530.6	50.67	212200	19.25 "
10	359.8	23.53	533.4	35.64	128900	13.54 "
11	306.0	19.96	533.2	28.16	93250	10.70 "
12	133.0	14.04	534.6	7.56	17500	2.87 "
13	213.1	15.77	534.7	16.45	45200	6.25 "
14	97.3	13.73	535.7	3.78	9276	1.44 "
15	60.5	13.60	536.7	1.68	3477	0.64 "
16	25.16	13.56	533.8	0.256	449	0.097 "

TABLE 12

GAS FLOW DATA

CORE #6 STURGEON LAKE SOUTH LIMESTONE

Run No	Pressure-Psia P_1	Pressure-Psia P_2	T_{flow} (average) ^oR	Q_c (SCFH)	$(P_1^2-P_2^2)$ $(Psia)^2$	G (lbs/ft^2sec)	$\frac{1}{Pavg}$ (Psi^{-1})	Ka (Md.)
1	17.93	13.61	531.2	0.00368	136	0.141×10^{-4}	0.0634	1.29
2	22.91	13.61	531.7	0.00849	340	0.324 "	0.0548	1.19
3	30.67	13.61	531.8	0.0172	756	0.657 "	0.0452	1.08
4	38.15	13.61	531.8	0.0269	1270	1.028 "	0.0386	1.005
5	48.00	13.63	528.9	0.0411	2120	1.571 "	0.0324	0.917
6	55.10	13.59	530.2	0.0536	2846	2.048 "	0.0291	0.894
7	64.00	13.57	530.7	0.0711	3914	2.717 "	0.0258	0.864
8	76.5	13.57	530.7	0.0987	5666	3.771 "	0.0221	0.829
9	89.7	13.58	530.7	0.131	7963	5.002 "	0.0194	0.783
10	99.2	13.59	530.7	0.158	9650	6.026 "	0.0177	0.780
11	299.1	13.72	530.7	1.084	89260	41.40 "	0.0064	0.579
12	398.3	13.93	530.7	1.806	158440	69.00 "	0.0049	0.549
13	460.3	14.09	530.7	2.221	211720	84.88 "	0.0042	0.507
14	524.2	14.29	530.7	2.749	274570	105.0 "	0.0037	0.485
15	573.1	14.49	530.9	3.189	328190	121.9 "	0.0034	0.472
16	601.8	14.61	532.5	3.439	361890	131.4 "	0.0032	0.462
17	666.8	14.91	532.5	4.06	444450	155.1 "	0.0029	-
18	711.3	15.15	532.5	4.50	505700	171.95 "	0.0028	-
19	775.8	15.59	532.5	5.17	601600	197.6 "	0.0025	-
20	1456.8	24.15	532.5	13.59	2121800	519.3 "	0.0014	-
21	1370.4	22.68	531.8	12.39	1877400	473.4 "	0.0015	-
22	1283.8	21.30	531.8	11.23	1647700	429.10 "	0.0016	-
23	1198.3	20.07	530.2	10.10	1435500	385.9 "	0.0017	-
24	1123.0	19.12	530.9	9.22	1260700	3.523 "	0.00192	-
25	1006.6	17.70	530.9	7.74	1012900	2.957 "	0.00195	-
26	917.4	16.76	530.2	6.68	841300	2.552 "	0.00214	-
27	830.3	15.98	530.2	5.68	689100	2.170 "	0.00236	-

TABLE 13

GAS FLOW DATA

CORE #7 SOUTH STURGEON LAKE LIMESTONE

Run No	Pressure-Psia P_1	Pressure-Psia P_2	T_{flow} (average) ^oR	Q_c (SCFH)	$(P_1^2-P_2^2)$ $(Psia)^2$	G (lbs/ft^2sec)
1	22.57	13.52	537.2	0.0187	326.7	0.7102×10^{-4}
2	39.98	13.52	537.3	0.0744	1416.	2.823 "
3	61.4	13.52	537.5	0.172	3583	6.54 "
4	92.7	13.52	537.5	0.374	8413	14.20 "
5	207.5	13.57	538.7	1.487	42850	56.43 "
6	308.9	13.62	538.7	2.797	95250	106.12 "
7	469.4	13.81	538.7	5.37	220100	203.76 "
8	604.3	14.08	538.7	7.76	365000	294.44 "
9	761.0	14.55	538.2	10.73	578800	407.13 "
10	910.4	15.19	537.2	13.61	828500	516.41 "
11	1060.7	16.01	536.3	16.87	1124800	640.11 "
12	1202.4	16.95	535.95	19.86	1445500	753.56 "
13	1473.1	19.35	534.1	26.83	2169500	1018.0 "
14	1390.6	18.57	533.2	24.75	1933300	939.1 "
15	1306.0	17.84	533.2	22.28	1705200	845.4 "

TABLE 14

GAS FLOW DATA

CORE #8 BEREA SANDSTONE

Run No	Pressure-Psia P_1	Pressure-Psia P_2	T_{flow} (average) ^oR	Q_c (SCFH)	$(P_1^2-P_2^2)$ $(Psia)^2$	G (lbs/ft^2sec)	$\frac{1}{P_{avg}}$ (Psi^{-1})	Ka (md.)
1	14.68	13.75	530.8	0.133	26.6	0.051×10^{-2}	0.0704	225.90
2	14.19	13.75	530.8	0.0638	12.43	0.024 "	0.0716	231.95
3	19.01	13.85	530.8	0.834	170	0.317 "	0.0609	222.28
4	30.02	14.56	530.8	3.26	690	1.239 "	0.0449	213.74
5	40.17	16.19	530.8	6.11	1352	2.323 "	0.0355	204.51
6	63.6	23.98	526.3	13.66	3465	5.192 "	0.0229	176.30
7	83.3	33.76	527.0	20.96	5801	7.965 "	0.0171	162.06
8	83.4	33.68	527.0	20.82	5818	7.912 "	0.0171	160.51
9	114.7	51.4	527.0	33.30	10510	12.65 "	0.0120	142.36
10	133.2	63.0	529.1	40.89	13760	15.54 "	0.0102	134.54
11	153.5	75.5	529.1	48.93	18080	18.59 "	0.0087	112.62
12	173.5	88.4	529.1	58.00	22290	22.04 "	0.0076	102.86
13	263.2	148.1	527.8	102.6	47340	33.99 "	0.0049	98.35
14	248.3	138.0	527.8	94.67	42590	35.9 "	0.0052	100.82
15	233.5	128.1	527.8	89.40	38110	33.97 "	0.0055	106.27
16	213.5	114.8	527.7	77.62	32400	29.50 "	0.0061	108.41
17	93.4	101.7	527.7	68.13	27070	25.89 "	0.0068	113.80
18	277.1	157.7	527.7	109.2	51930	41.51 "	0.0046	95.59

TABLE 15

GAS FLOW DATA

CORE #9 INDIANA LIMESTONE

Run No	Pressure-Psia P_1	Pressure-Psia P_2	T_{flow} (average) ^oR	Q_c (SCFH)	$(P_1^2-P_2^2)$ $(Psia)^2$	G (lbs ft^2sec)	$\frac{1}{Pavg}$ (Psi^{-1})	Ka (md.)
1	24.45	13.72	532	0.0374	410	0.0142×10^{-2}	0.0524	4.01
2	17.79	13.62	530	0.0128	131	0.0049 "	0.0637	4.25
3	24.36	13.62	530	0.0376	408	0.0143 "	0.0527	4.03
4	38.82	13.63	530	0.114	1321	0.0433 "	0.0381	3.76
5	45.6	13.63	530.1	0.151	1889	0.0574 "	0.0338	3.50
6	113.85	13.73	531.2	0.891	12750	0.339 "	0.0157	3.08
7	156.0	13.89	531.2	1.598	24140	0.607 "	0.0118	2.91
8	216.0	14.34	531.7	2.87	46450	1.091 "	0.0087	2.73
9	263.6	14.57	532.2	4.08	69270	1.550 "	0.0072	2.62
10	310.0	15.57	532.2	5.42	95860	2.060 "	0.0061	2.51
11	395.5	16.77	528.6	7.02	128920	2.668 "	0.0053	2.41
12	412.5	18.47	529.4	8.91	169820	3.386 "	0.0046	2.32
13	459.0	20.28	529.4	10.75	210270	4.085 "	0.0042	2.27
14	511.7	22.67	529.4	12.91	261320	4.906 "	0.0037	2.19
15	558.7	25.15	529.4	14.90	311510	5.662 "	0.0034	2.12
16	609.7	28.12	528.7	17.25	370940	6.555 "	0.0031	2.07
17	707.0	35.56	529.9	21.67	498530	8.235 "	0.0027	1.95
18	670.3	32.82	529.6	20.04	448160	7.615 "	0.0028	2.00
19	642.9	31.01	529.6	18.76	412360	7.129 "	0.0030	2.04
20	687.1	27.44	529.6	20.74	471290	7.882 "	0.0028	1.97

TABLE 16

GAS FLOW DATA

CORE #11 BASAL QUARTZ

Run No	Pressure-Psia P_1	P_2	T_{flow} (average) ^{o}R	(SCFH)	$(P_1^2-P_2^2)$ $(Psia)^2$	G $(lbs/ft^2 sec)$
1	20.50	13.51	536.4	2.53	238	0.924×10^{-2}
2	29.97	13.89	536.4	7.20	705	2.630
3	40.76	15.12	535.0	13.95	1433	5.096
4	55.0	17.83	534.9	22.98	2709	8.395
5	74.9	24.71	534.9	40.05	5002	14.63
6	95.0	34.03	534.6	56.13	7871	20.51
7	113.0	43.2	534.6	71.87	10900	26.26
8	133.3	53.7	534.6	89.54	14880	32.71
9	213.7	97.7	534.4	163.4	36120	59.69
10	192.5	86.0	534.4	144.50	29640	52.79
11	173.2	75.3	534.4	125.9	24330	45.98
12	152.0	64.3	534.4	108.1	18960	39.49

TABLE 17

GAS FLOW DATA

CORE #10 BASAL QUARTZ

Run No	Pressure-Psia P_1	P_2	T_{flow} (average) ^oR	Q_c (SCFH)	$(P_1^2-P_2^2)$ $(Psia)^2$	G (lbs/ft^2sec)
1	20.28	13.7	535.8	1.347	225	0.492×10^{-2}
2	30.69	13.80	535.8	4.38	751	1.601 "
3	40.83	14.2	534.6	8.29	1466	3.031 "
4	63.8	16.4	534.6	18.46	3800	6.748 "
5	83.6	20.3	534.6	29.91	6585	10.930 "
6	103.9	26.3	534.6	42.36	10110	15.49 "
7	125.1	33.9	534.6	55.37	14510	20.24 "
8	143.8	41.1	534.2	68.10	18990	24.90 "
9	166.2	50.0	533.9	83.07	25130	30.37 "
10	183.4	59.0	533.8	94.65	30150	34.60 "
11	203.4	65.2	533.1	110.40	37130	40.37 "
12	225.3	74.4	532.0	125.30	45240	45.81 "
13	243.7	82.4	531.7	138.30	52590	50.57 "
14	262.6	90.6	531.0	151.8	60750	55.44 "

TABLE 18

GAS FLOW DATA

CORE #12 VIKING SANDSTONE

Run No	Pressure-Psia P_1	Pressure-Psia P_2	T_{flow} (average) ^oR	Q_c (SCFH)	$(P_1^2-P_2^2)$ $(Psia)^2$	G (lbs/ft^{2}sec)
1	80.2	13.61	533.2	0.04	6238	1.462×10^{-4}
2	148.5	13.61	533.6	0.126	21860	4.605 "
3	228.1	13.61	534.4	0.272	51830	9.94 "
4	322.1	13.60	534.4	0.491	103560	17.94 "
5	462.9	13.60	535.2	0.917	214060	33.51 "
6	601.8	13.61	535.4	1.424	361930	52.04 "
7	754.5	13.65	534.1	2.051	569100	74.95 "
8	897.8	13.68	535.8	2.706	805900	98.89 "
9	1050.7	13.72	535.9	3.460	1103750	126.4 "
10	1201.5	13.77	535.4	4.225	1443400	154.4 "
11	1298.9	13.81	535.4	4.722	1686900	172.6 "
12	1384.3	13.85	534.75	5.194	1916100	189.8 "
13	1481.3	13.91	534.75	5.721	2194000	209.1 "

TABLE 19

GAS FLOW DATA

CORE #13 VIKING SANDSTONE

Run No	Pressure-Psia P_1	P_2	T_{flow} (average) ^oR	Q_c (SCFH)	$(P_1^2-P_2^2)$ $(Psia)^2$	G (lbs/ft^{2}sec)
1	67.5	13.60	533.7	0.105	4364.2	3.835×10^{-4}
2	116.7	13.60	533.7	0.283	13430	10.34 "
3	262.3	13.59	532.85	1.082	68620	39.52 "
4	367.7	13.62	533.1	1.853	135000	67.69 "
5	508.5	13.67	533.0	3.081	258400	112.6 "
6	664.4	13.77	533.0	4.613	441200	168.5 "
7	818.2	13.93	531.65	6.254	669300	228.4 "
8	879.6	14.01	531.3	6.934	773400	253.2 "
9	1009.6	14.21	530.9	8.477	1019000	309.7 "
10	1119.8	14.36	529.4	9.86	1253800	360.2 "
11	1217.0	14.59	527.8	11.21	1481000	409.5 "
12	1308.0	14.83	527.5	12.35	1711000	451.1 "
13	1409.2	15.16	527.15	13.71	1986000	500.9
14	1493.6	15.46	527.15	14.78	2231000	539.9 "

TABLE 20

GAS FLOW DATA

CORE #14 BELLY RIVER SANDSTONE

Run No	Pressure-Psia P_1	Pressure-Psia P_2	T_{flow} (average) ^oR	Q_c (SCFH)	$(P_1^2-P_2^2)$ $(Psia)^2$	G (lbs/ft^2sec)	$\frac{1}{Pavg}$ (Psi^{-1})	Ka (md.)
1	1428.9	16.84	530.4	19.1	2041600	6.980×10^{-2}	.0014	0.430
2	802.2	14.14	530.6	7.298	643300	2.668 "	.0025	0.510
3	899.6	14.33	530.6	8.849	809100	3.235 "	.0022	0.493
4	1006.6	14.65	530.6	10.68	1013000	3.9050 "	.0020	0.477
5	1098.1	14.99	529.6	12.32	1206000	4.505 "	.0018	0.462
6	424.5	13.72	530.3	2.371	180000	.8668 "	.00456	0.584
7	514.8	13.77	530.8	3.349	265000	1.224 "	.00378	0.562
8	612.2	13.86	530.9	4.538	374500	1.659 "	.00319	0.541
9	703.9	13.97	530.9	5.788	495300	2.116 "	.00279	0.523
10	1192.6	15.43	530.3	13.95	1422000	5.099 "	.00163	0.446
11	1323.0	16.11	529.4	16.460	1750000	6.017 "	.00149	0.429
12	309.1	13.71	530.9	1.328	95380	0.4855 "	.00620	0.615
13	119.5	13.68	532.7	0.236	14090	0.0863 "	.0150	0.738
14	92.4	13.68	533.0	0.145	8350	0.05297 "	.0189	0.764
15	70.1	13.68	533.0	0.0864	4730	0.03157 "	.0239	0.805
16	44.1	13.68	533.7	0.0344	1760	0.01258 "	.0346	0.862
17	31.40	13.68	533.7	0.0173	799	0.006324 "	.0444	1.0334

TABLE 21

EXPERIMENTALLY DETERMINED FLOW CHARACTERISTICS
OF CONSOLIDATED POROUS SAMPLES

INDIANA LIMESTONE LONG CORE

Run No.	$\frac{(P_1^2 - P_2^2)Mgc}{L_B 2ZRT \mu G}$	$\frac{G}{\mu}$	f	Re
1	2.195×10^{13}	4.64×10^{2}	16.9	0.135
2	2.114 "	3.32 "	22.7	0.0965
3	2.050 "	2.27 "	32.2	0.066
4	2.005 "	1.37 "	52.3	0.0398
5	1.977 "	0.98 "	72.0	0.0285
6	1.944 "	0.65 "	106.8	0.0189
7	1.869 "	0.40 "	167	0.0116
8	1.805 "	0.20 "	322	0.00582
9	1.319 "	0.10 "	471	0.00291
10	1.948 "	0.43 "	162	0.0125
11	2.017 "	1.12 "	64.3	0.0326
12	1.991 "	1.00 "	71.1	0.0291
13	2.067 "	1.75 "	42.2	0.0509

TABLE 22(A)

EXPERIMENTALLY DETERMINED FLOW CHARACTERISTICS
OF CONSOLIDATED POROUS SAMPLES

(BEFORE PRESSURE TAPS DRILLED)

ALUNDUM CORE (TA7921)

Run No	$\frac{(P_1^2-P_2^2)Mgc}{L_B 2ZRT\mu G}$	$\frac{G}{\mu}$	f	Re
1	1.435×10^{11}	534.3	20.9	0.0985
2	1.572 "	923.1	13.2	0.170
3	1.671 "	1223.4	10.6	0.225
4	1.781 "	1482.4	9.33	0.273
5	1.836 "	1693.5	8.42	0.312

TABLE 22(B)

EXPERIMENTALLY DETERMINED FLOW CHARACTERISTICS
OF CONSOLIDATED POROUS SAMPLES

ALUNDUM CORE (TA 7921)
(PRESSURE TAPS DRILLED ALONG LENGTH OF CORE.
PRESSURE TAPS UPSTREAM AND DOWNSTREAM OF END PLATES.)

Run No.	$\frac{(P_1^2-P_2^2)\ Mgc}{L_B\ 2ZRT\mu G}$	$\frac{G}{\mu}$	f	Re
1	2.278×10^{11}	66.766×10^{2}	4.64	.756
2	2.115 "	56.395 "	5.10	.639
3	1.763 "	32.069 "	7.48	.363
4	1.947 "	44.804 "	5.91	.508
5	1.544 "	15.822 "	13.3	.179
6	1.518 "	9.805 "	21.1	.111
7	1.549 "	5.134 "	41.1	.0582
8	1.497 "	2.548 "	80.0	.0289
9	1.180 "	1.371 "	117	.0155
10	1.185 "	1.353 "	119	.0153
11	1.187 "	1.241 "	130	.0141
12	1.192 "	0.873 "	186	.00989
13	1.018 "	0.043 "	322	.00487
14	1.227 "	3.096 "	539	.00351
15	1.169 "	1.732 "	919	.00196
16	1.202 "	0.462 "	354	.00052
17	1.277 "	5.170 "	33.6	.0586
18	1.257 "	4.060 "	42.1	.046
19	1.257 "	1.970 "	86.8	.0223
20	1.555 "	1.808 "	117.1	.0205
21	1.457 "	1.253 "	158	.0142
22	1.410 "	6.994 "	27.4	.0792
23	1.079 "	1.704 "	86.2	.0193
24	1.423 "	5.138 "	37.7	.0582
25	1.478 "	12.654 "	15.9	.143
26	1.689 "	27.128 "	8.47	.307
27	1.736 "	30.375 "	7.78	.344
28	2.015 "	48.186 "	5.69	.546
29	1.887 "	40.435 "	6.78	.458
30	1.710 "	27.613 "	8.43	.313
31	1.483 "	8.124 "	24.8	.0920

TABLE 22(C1)

EXPERIMENTALLY DETERMINED FLOW CHARACTERISTICS
OF CONSOLIDATED POROUS SAMPLES

ALUNDUM CORE (TA 7921)
(PRESSURE TAPS IN END PLATES)

Run No	$\frac{(P_1^2-P_2^2)\,Mgc}{L_B\ 2ZRT\,\mu G}$	$\frac{G}{\mu}$	f	Re
1	1.293×10^{11}	1.376×10^{3}	564	.0036
2	1.313 "	1.834 "	430	.0048
3	1.286 "	2.497 "	309	.00653
4	1.272 "	1.898 "	403	.00496
5	1.191 "	0.110 "	6503	.00029
6	1.196 "	0 165 "	4353	.000431
7	1.226 "	0.208 "	3540	.000544
8	1.188 "	0.068 "	10490	.000178
9	1.199 "	0.394 "	1828	.00103
10	1.278 "	0.609 "	1260	.00159
11	1.286 "	0.917 "	842	.0024
12	1.190 "	0.0154 "	46410	.0000403
13	1.177 "	0.0079 "	89480	.0000217
14	1.016 "	0.0026 "	234700	.0000068
15	1.273 "	1.844 "	415	.00482
16	1.282 "	2.446 "	315	.00639
17	1.308 "	2.897 "	271	.00757
18	1.288 "	4.179 "	185	.0109
19	1.279 "	5.329 "	144	.0139
20	1.284 "	6.284 "	123	.0164
21	1.288 "	7.306 "	106	.0191
22	1.321 "	8.287 "	95.1	.0217
23	1.293 "	9.061 "	85.7	.0237
24	1.303 "	9.498 "	82.4	.0248
25	1.287 "	7.900 "	97.8	.0207
26	1.313 "	10.903 "	72.3	.0285
27	1.271 "	5.365 "	127	.014

TABLE 22(C2)

EXPERIMENTALLY DETERMINED FLOW CHARACTERISTICS
OF CONSOLIDATED POROUS SAMPLES

(PRESSURE TAPS IN END PLATES)

ALUNDUM CORE (TA7921)

Run No	$\frac{(P_1^2-P_2^2)Mgc}{L_B 2ZRT \mu G}$	$\frac{G}{\mu}$	f	Re
1	1.191×10^{11}	2.766×10^{2}		
2	1.193 "	4.561 "		
3	1.205 "	6.566 "		
4	1.273 "	14.80 "		
5	1.264 "	27.84 "		
6	1.290 "	35.94 "		
7	1.285 "	46.93 "		
8	1.314 "	59.16 "		
9	1.326 "	73.24 "		
10	1.368 "	87.25 "		
11	1.364 "	79.39 "		
12	1.369 "	64.83 "		

TABLE 23

SUMMARIZED CALCULATIONS OF THE
EXPERIMENTALLY DETERMINED FLOW CHARACTERISTICS
OF CONSOLIDATED POROUS SAMPLES

CORE #1 CARDIUM SANDSTONE

Run No	$\frac{(P_1^2-P_2^2)\ Mgc}{L_B\ 2ZRT\ \mu G}$	$\frac{G}{\mu}$	f	Re
1	4.053×10^{12}	6.767×10^{2}	66.4	.0284
2	4.192 "	9.816 "	47.3	.0412
3	4.217 "	13.32 "	35.1	.0559
4	4.381 "	19.65 "	24.7	.0825
5	4.536 "	26.97 "	18.6	.113
6	4.658 "	32.36 "	15.9	.136
7	4.861 "	39.89 "	13.5	.167
8	5.007 "	45.64 "	12.2	.192
9	5.178 "	51.69 "	11.1	.217
10	5.335 "	56.74 "	10.4	.238
11	5.514 "	62.81 "	9.73	.264
12	5.612 "	66.36 "	9.37	.279
13	5.308 "	66.50 "	8.84	.279
14	5.667 "	83.14 "	7.55	.349
15	6.027 "	101.01 "	6.61	.424
16	6.541 "	125.25 "	5.79	.526
17	7.023 "	151.15 "	5.15	.635
18	7.488 "	174.94 "	4.74	.734
19	7.883 "	205.34 "	4.25	.862
20	10.779 "	360.09 "	3.32	1.515
21	10.255 "	329.59 "	3.45	1.384
22	9.706 "	302.55 "	3.55	1.270
23	9.178 "	270.48 "	3.76	1.135
24	8.875 "	237.84 "	4.13	0.998
25	8.021 "	212.11 "	4.19	.890

TABLE 24

EXPERIMENTALLY DETERMINED FLOW CHARACTERISTICS
OF CONSOLIDATED POROUS SAMPLES

CORE #2 CARDIUM SANDSTONE

Run No	$\frac{(P_1^2 - P_2^2)\ Mgc}{L_B\ 2ZRT\mu G}$		$\frac{G}{\mu}$	f	Re
1	0.695×10^{16}		0.993	130.8	.00552
2	1.040	"	1.106	176.6	.00616
3	1.119	"	1.550	134.9	.00863
4	1.470	"	2.450	112.1	.0136
5	1.624	"	4.053	74.9	.0226
6	1.694	"	3.828	82.7	.0213
7	1.831	"	6.093	56.2	.0339
8	1.939	"	9.021	40.2	.0502
9	2.017	"	12.119	31.1	.0675
10	2.088	"	16.873	23.1	.0939
11	2.174	"	23.176	17.5	.129
12	2.238	"	29.244	14.3	.163
13	2.303	"	35.398	12.2	.197
14	2.399	"	44.110	10.2	.246
15	2.496	"	52.452	8.89	.292
16	2.485	"	59.294	7.83	.330
17	2.637	"	66.154	7.45	.368
18	2.717	"	75.709	6.71	.421

TABLE 25

EXPERIMENTALLY DETERMINED FLOW CHARACTERISTICS
OF CONSOLIDATED POROUS SAMPLES

CORE #3 CARDIUM SANDSTONE

Run No	$\frac{(P_1^2-P_2^2)Mgc}{L_B\ 2ZRT\mu G}$	$\frac{G}{\mu}$	f	Re
1	4.785×10^{12}	0.0032×10^{4}	1181	.00143
2	4.968 "	0.0107 "	366.6	.00478
3	5.23 "	0.0324 "	127.5	.0145
4	5.29 "	0.0764 "	54.7	.0342
5	6.03 "	0.145 "	32.8	.0648
6	6.06 "	0.275 "	17.4	.123
7	6.36 "	0.347 "	14.5	.155
8	6.99 "	0.510 "	10.8	.228
9	7.76 "	0.659 "	9.19	.295
10	8.16 "	0.880 "	7.32	.393
11	9.13 "	1.174 "	6.14	.525
12	10.08 "	1.486 "	5.36	.664
13	11.18 "	1.852 "	4.77	.828
14	11.95 "	2.138 "	4.41	.956
15	18.50 "	4.856 "	3.01	2.171
16	17.50 "	4.292 "	3.22	1.919
17	16.10 "	3.727 "	3.41	1.666
18	14.62 "	3.044 "	3.79	1.361
19	13.33 "	2.607 "	4.04	1.166

TABLE 26(A)

EXPERIMENTALLY DETERMINED FLOW CHARACTERISTICS
OF CONSOLIDATED POROUS SAMPLES

CORE #4 CARDIUM SANDSTONE (T_f = 73°F)

Run No	$\frac{(P_1^2-P_2^2)\ Mgc}{L_B\ 2ZRT\mu G}$	$\frac{G}{\mu}$	f	Re
1	9.502×10^{12}	4.407×10^{4}	2.32	2.564
2	8.459 "	4.013 "	2.27	2.335
3	7.869 "	3.555 "	2.39	2.068
4	7.371 "	3.108 "	2.56	1.808
5	6.505 "	2.449 "	2.86	1.425
6	5.922 "	2.003 "	3.19	1.165
7	5.396 "	1.635 "	3.56	0.951
8	4.917 "	1.298 "	4.08	0.755
9	4.469 "	0.979 "	4.92	0.570
10	4.069 "	0.664 "	6.61	0.386
11	3.506 "	0.393 "	9.62	0.229
12	3.203 "	0.205 "	16.84	0.119
13	3.072 "	0.112 "	29.57	0.0652
14	2.246 "	0.051 "	47.47	0.0297

TABLE 26(B)

EXPERIMENTALLY DETERMINED FLOW CHARACTERISTICS
OF CONSOLIDATED POROUS SAMPLES

CORE #4 CARDIUM SANDSTONE (T_f = 95°F)

Run No	$\frac{(P_1^2-P_2^2)Mgc}{L_B\ 2ZRT\mu G}$	$\frac{G}{\mu}$	f	Re
1	3.049×10^{12}	0.141×10^{4}	23.31	.0820
2	2.928 "	0.062 "	50.91	.0361
3	3.408 "	0.331 "	11.10	.193
4	4.042 "	0.648 "	6.72	.377
5	4.716 "	1.122 "	4.53	.653
6	5.238 "	1.471 "	3.84	.856
7	5.682 "	1.756 "	3.49	1.022
8	6.018 "	2.015 "	3.22	1.172
9	6.417 "	2.314 "	2.99	1.346
10	7.178 "	2.877 "	2.69	1.674
11	8.835 "	4.193 "	2.27	2.439
12	8.075 "	3.611 "	2.41	2.101
13	7.587 "	3.217 "	2.54	1.872

TABLE 26(C)

EXPERIMENTALLY DETERMINED FLOW CHARACTERISTICS
OF CONSOLIDATED POROUS SAMPLES

CORE #4 CARDIUM SANDSTONE (T_f = 115°F)

Run No	$\frac{(P_1^2-P_2^2)\ Mgc}{L_B\ 2ZRT\mu G}$	$\frac{G}{\mu}$	f	Re
1	4.344 x 10^{12}	0.830 x 10^4	5.64	.483
2	7.975 "	3.539 "	2.43	2.059
3	7.376 "	3.025 "	2.63	1.760
4	6.783 "	2.560 "	2.86	1.489
5	6.169 "	2.096 "	3.17	1.219
6	5.562 "	1.664 "	3.60	0.956
7	4.862 "	1.177 "	4.45	0.685
8	4.109 "	0.7174 "	6.26	0.417

TABLE 27

EXPERIMENTALLY DETERMINED FLOW CHARACTERISTICS
OF CONSOLIDATED POROUS SAMPLES
CORE #5 CARDIUM SANDSTONE

Run No	$\frac{(P_1^2-P_2^2)Mgc}{LB\ 2ZRT\mu G}$	$\frac{G}{\mu}$	f	Re
1	14.72×10^{12}	4.348×10^{4}	3.13	2.170
2	13.50 "	3.805 "	3.28	1.899
3	15.73 "	4.808 "	3.02	2.399
4	15.55 "	4.783 "	3.00	2.387
5	12.63 "	3.321 "	3.51	1.657
6	11.20 "	2.735 "	3.78	1.365
7	10.45 "	2.328 "	4.15	1.162
8	9.47 "	1.961 "	4.46	.979
9	8.61 "	1.601 "	4.97	.799
10	7.41 "	1.128 "	6.07	.563
11	6.79 "	0.892 "	7.03	.445
12	4.75 "	0.241 "	18.21	.120
13	5.61 "	0.522 "	9.93	.275
14	5.02 "	0.120 "	38.65	.060
15	4.24 "	0.0535 "	73.21	.0267
16	3.61 "	0.0082 "	406.7	.0041

TABLE 28

EXPERIMENTALLY DETERMINED FLOW CHARACTERISTICS
OF CONSOLIDATED POROUS SAMPLES

CORE #6 STURGEON LAKE SOUTH LIMESTONE

Run No	$\frac{(P_1^2 - P_2^2)\ Mgc}{L_B\ 2ZRT\mu G}$	$\frac{G}{\mu}$	f	Re
1	7.270 x 10^{13}	0.012 x 10^2	4637	.00017
2	7.838 "	0.027 "	2222	.00038
3	8.604 "	0.056 "	1176	.00079
4	9.246 "	0.087 "	813	.00123
5	10.152 "	0.133 "	584	.00187
6	10.448 "	0.173 "	462	.00244
7	10.805 "	0.230 "	360	.00324
8	11.257 "	0.318 "	271	.00448
9	11.916 "	0.422 "	216	.00595
10	11.983 "	0.508 "	181	.00716
11	16.153 "	3.490 "	35.4	.00492
12	17.025 "	5.753 "	22.7	.00811
13	18.467 "	7.064 "	20.0	.00995
14	19.304 "	8.720 "	16.9	.0123
15	19.840 "	10.092 "	15.0	.0142
16	20.240 "	10.855 "	14.3	.0153
17	20.956 "	12.787 "	12.5	.0180
18	21.350 "	14.154 "	11.5	.0199
19	22.200 "	16.217 "	10.5	.0228
20	29.097 "	41.620 "	5.35	.0586
21	28.340 "	38.025 "	5.70	.0536
22	27.534 "	34.583 "	6.10	.0487
23	26.913 "	31.286 "	6.58	.0441
24	25.979 "	28.71 "	6.93	.0405
25	25.030 "	24.12 "	7.94	.0340
26	24.064 "	20.89 "	8.82	.0294
27	23.261 "	17.82 "	9.99	.0251

TABLE 29

EXPERIMENTALLY DETERMINED FLOW CHARACTERISTICS
OF CONSOLIDATED POROUS SAMPLES

CORE #7 STURGEON LAKE SOUTH LIMESTONE

Run No	$\frac{(P1^2-P2^2)\ Mgc}{LB\ 2ZRT\mu G}$	G	f	Re
1	3.476×10^{13}	5.95	1075	.000091
2	3.788 "	23.64	295	.000361
3	4.132 "	54.7	139	.000835
4	4.461 "	118.6	69.2	.00181
5	5.680 "	468.9	22.3	.00716
6	6.693 "	878.5	14.0	.0134
7	8.018 "	1677.9	8.79	.0256
8	9.157 "	2412.0	6.99	.0368
9	10.46 "	3318.6	5.80	.0506
10	11.79 "	4193.3	5.17	.0640
11	12.89 "	5175.1	4.58	.0790
12	14.02 "	6064.3	4.25	.9025
13	15.51 "	8135.4	3.51	.124
14	15.08 "	7537.1	3.68	.115
15	14.63 "	6807.0	3.95	.104

TABLE 30

EXPERIMENTALLY DETERMINED FLOW CHARACTERISTICS
OF CONSOLIDATED POROUS SAMPLES

CORE #8 BEREA SANDSTONE

Run No	$\frac{(P_1^2-P_2^2)Mgc}{LB\ 2ZRT\mu G}$	G	f	Re
1	4.134×10^{11}	0.428×10^{2}	1688	.00085
2	4.026 "	0.205 "	3433	.00041
3	4.199 "	2.684 "	273	.00534
4	4.368 "	10.49 "	72.8	.0209
5	4.566 "	19.64 "	40.6	.0391
6	5.299 "	44.05 "	21.0	.0877
7	5.767 "	67.46 "	14.9	.134
8	5.823 "	67.005 "	15.2	.133
9	6.567 "	107.02 "	10.7	.213
10	6.950 "	130.89 "	9.28	.261
11	7.628 "	156.54 "	8.52	.312
12	7.928 "	185.34 "	7.48	.369
13	9.520 "	326.82 "	5.09	.651
14	9.286 "	301.76 "	5.38	.601
15	8.808 "	285.28 "	5.40	.570
16	8.633 "	247.90 "	6.09	.494
17	8.223 "	217.75 "	6.60	.434

TABLE 31

EXPERIMENTALLY DETERMINED FLOW CHARACTERISTICS
OF CONSOLIDATED POROUS SAMPLES

CORE #9 INDIANA LIMESTONE

Run No	$\frac{(P_1^2-P_2^2)Mgc}{L_B\ 2ZRT\ \mu G}$	G	f	Re
1	2.329×10^{13}	0.120×10^{2}	1968	.000683
2	2.191 "	0.0412 "	5392	.000235
3	2.323 "	0.1211 "	1945	.00069
4	2.480 "	0.367 "	685	.00209
5	2.670 "	0.486 "	557	.00277
6	3.044 "	2.856 "	108	.0163
7	3.196 "	5.112 "	63.4	.0291
8	3.424 "	9.156 "	37.9	.0521
9	3.581 "	12.983 "	28.0	.0739
10	3.725 "	17.218 "	21.9	.098
11	3.890 "	22.265 "	17.7	.127
12	4.034 "	28.273 "	14.5	.161
13	4.133 "	34.044 "	12.3	.194
14	4.269 "	40.794 "	10.6	.232
15	4.403 "	47.003 "	9.50	.268
16	4.529 "	54.326 "	8.45	.309
17	4.814 "	67.931 "	7.19	.387
18	4.689 "	62.919 "	7.56	.358
19	4.605 "	58.835 "	7.94	.335
20	4.762 "	65.100 "	7.42	.371

TABLE 32

EXPERIMENTALLY DETERMINED FLOW CHARACTERISTICS
OF CONSOLIDATED POROUS SAMPLES

CORE #10 BASAL QUARTZ

Run No	$\frac{(P_1^2-P_2^2)\ Mgc}{LB\ 2ZRT\mu G}$	G	f	Re
1	3.600×10^{11}	0.0414×10^{4}	157	.0119
2	3.692 "	0.125 "	53.4	.0359
3	3.816 "	0.254 "	27.1	.073
4	4.445 "	0.567 "	14.2	.163
5	4.752 "	0.917 "	9.36	.264
6	5.150 "	1.298 "	7.17	.373
7	5.650 "	1.696 "	6.02	.488
8	6.016 "	2.085 "	5.21	.599
9	6.522 "	2.540 "	4.64	.730
10	6.865 "	2.892 "	4.29	.831
11	7.253 "	3.373 "	3.89	.970
12	7.816 "	3.833 "	3.68	1.102
13	8.218 "	4.221 "	3.52	1.214
14	8.674 "	4.629 "	3.39	1.331

TABLE 33

EXPERIMENTALLY DETERMINED FLOW CHARACTERISTICS
OF CONSOLIDATED POROUS SAMPLES

CORE #11 BASAL QUARTZ

Run No	$\frac{(P_1^2-P_2^2)\ Mgc}{LB\ \ 2ZRT\mu G}$	G	f	Re
1	2.184×10^{11}	0.078×10^{4}	98.4	.0196
2	2.275 "	0.221 "	36.2	.0556
3	2.393 "	0.428 "	19.7	.108
4	2.744 "	0.705 "	13.7	.177
5	2.906 "	1.228 "	8.32	.309
6	3.261 "	1.719 "	6.67	.433
7	3.524 "	2.198 "	5.64	.553
8	3.858 "	2.736 "	4.96	.689
9	5.113 "	4.969 "	3.62	1.251
10	4.754 "	4.404 "	3.80	1.108
11	4.480 "	3.838 "	4.10	.966
12	4.069 "	3.300 "	4.34	.831

TABLE 34

EXPERIMENTALLY DETERMINED FLOW CHARACTERISTICS
OF CONSOLIDATED POROUS SAMPLES

CORE #12 VIKING SANDSTONE

Run No	$\frac{(P_1^2-P_2^2)Mgc}{L_B\ 2ZRT\mu G}$	$\frac{G}{\mu}$	f	Re
1	3.457×10^{14}	12.3	286	.00505
2	3.834 "	38.6	101	.0158
3	4.191 "	83.0	51.5	.0341
4	4.625 "	149.4	31.5	.0613
5	5.084 "	277.4	18.7	.114
6	5.505 "	428.3	13.1	.176
7	6.007 "	614.4	9.96	.252
8	6.380 "	804.6	8.08	.330
9	6.803 "	1024.2	6.77	.421
10	7.253 "	1243.1	5.95	.510
11	7.563 "	1385.6	5.56	.569
12	7.799 "	1520.9	5.23	.624
13	8.077 "	1668.9	4.93	.685

TABLE 35

EXPERIMENTALLY DETERMINED FLOW CHARACTERISTICS
OF CONSOLIDATED POROUS SAMPLES

CORE #13 VIKING SANDSTONE

Run No	$\frac{(P_1^2 - P_2^2)Mgc}{L_B \, ZZRT\mu G}$	G	f	Re
1	8.883×10^{13}	32.3	161	.00673
2	10.126 "	86.8	68.3	.0181
3	13.508 "	330.6	23.9	.0689
4	15.461 "	563.9	16.0	.118
5	17.705 "	932.2	11.1	.194
6	20.107 "	1388.4	8.48	.289
7	22.467 "	1872.9	7.02	.390
8	23.409 "	2072.0	6.61	.432
9	25.156 "	2526.1	5.83	.526
10	26.623 "	2930.2	5.32	.611
11	27.706 "	3326.0	4.88	.693
12	28.986 "	3654.2	4.64	.762
13	30.208 "	4043.2	4.37	.843
14	31.386 "	4343.7	4.23	.905

TABLE 36

EXPERIMENTALLY DETERMINED FLOW CHARACTERISTICS
OF CONSOLIDATED POROUS SAMPLES

CORE #14 SALT & PEPPER SANDSTONE

Run No	$\frac{P_1^2-P_2^2)Mgc}{L_B\ 2ZRT\mu G}$	G	f	Re
1	2.184×10^{14}	5.609×10^{3}	6.16	0.452
2	1.840 "	2.192 "	13.28	0.177
3	1.903 "	2.649 "	11.36	0.214
4	1.965 "	3.185 "	9.76	0.257
5	2.029 "	3.669 "	8.75	0.296
6	1.603 "	0.721 "	35.16	0.0581
7	1.664 "	1.016 "	25.90	0.0819
8	1.731 "	1.372 "	19.96	0.111
9	1.790 "	1.744 "	16.24	0.141
10	2.101 "	4.133 "	8.04	0.333
11	2.188 "	4.859 "	7.12	0.392
12	1.521 "	0.406 "	59.24	0.0327
13	1.266 "	0.0725 "	276.2	0.00585
14	1.222 "	0.0446 "	433.6	0.00359
15	1.161 "	0.0266 "	691.3	0.00214
16	1.083 "	0.0106 "	1618	0.000853
17	0.9783 "	0.00533 "	2906	0.000429

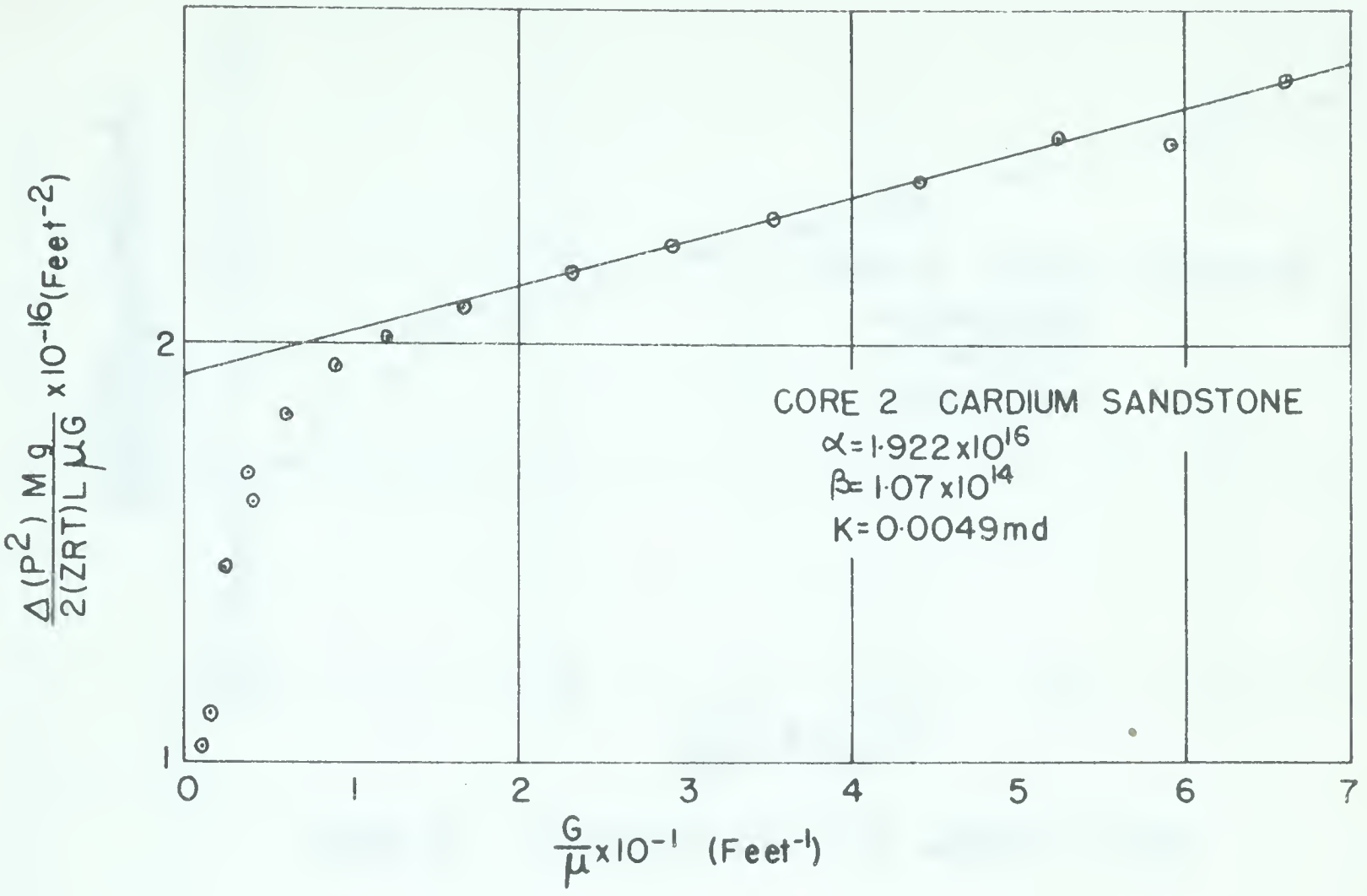

FIGURE 19 FLOW DATA PLOT TO OBTAIN α AND β

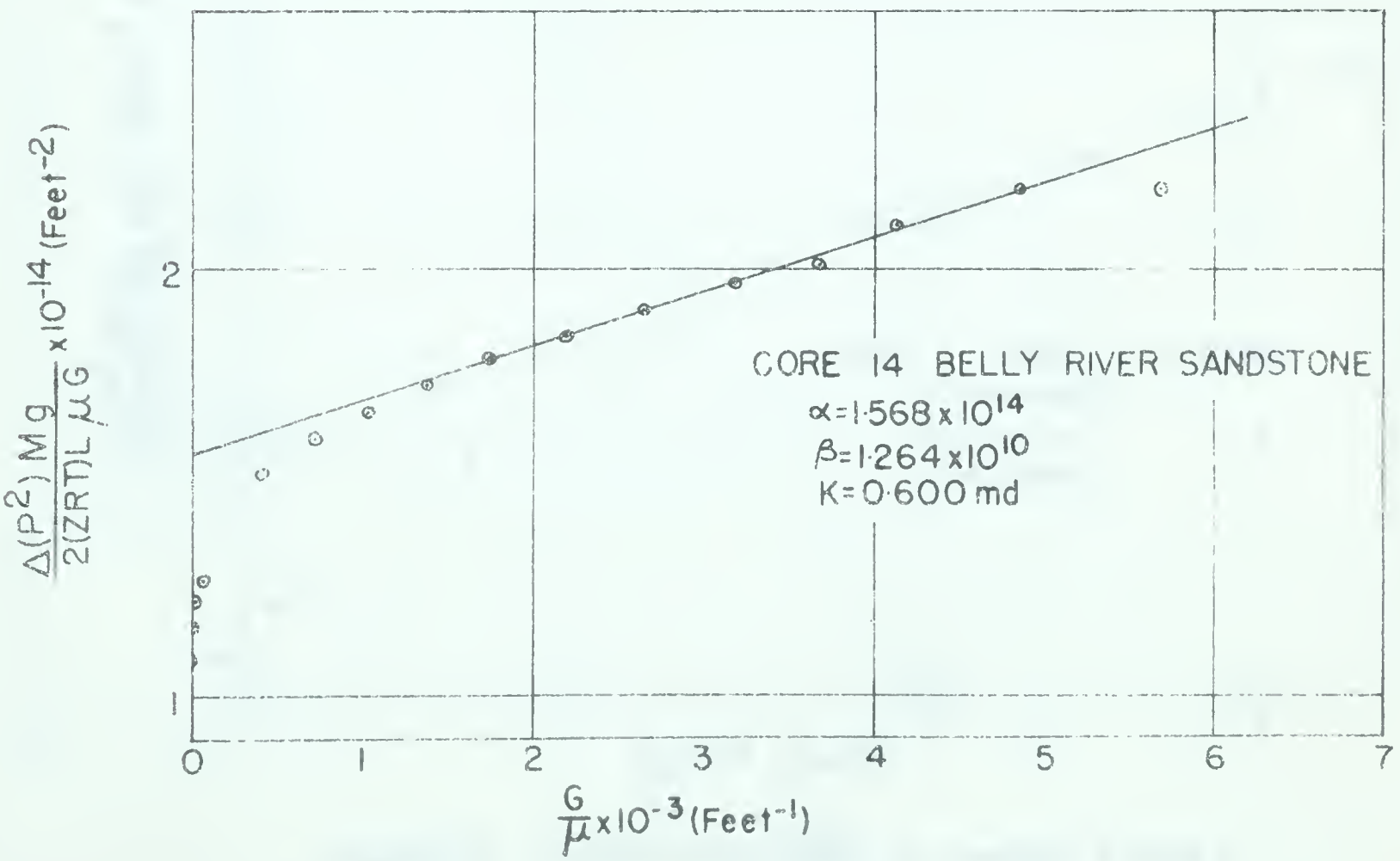

FIGURE 20 FLOW DATA PLOT TO OBTAIN α AND β

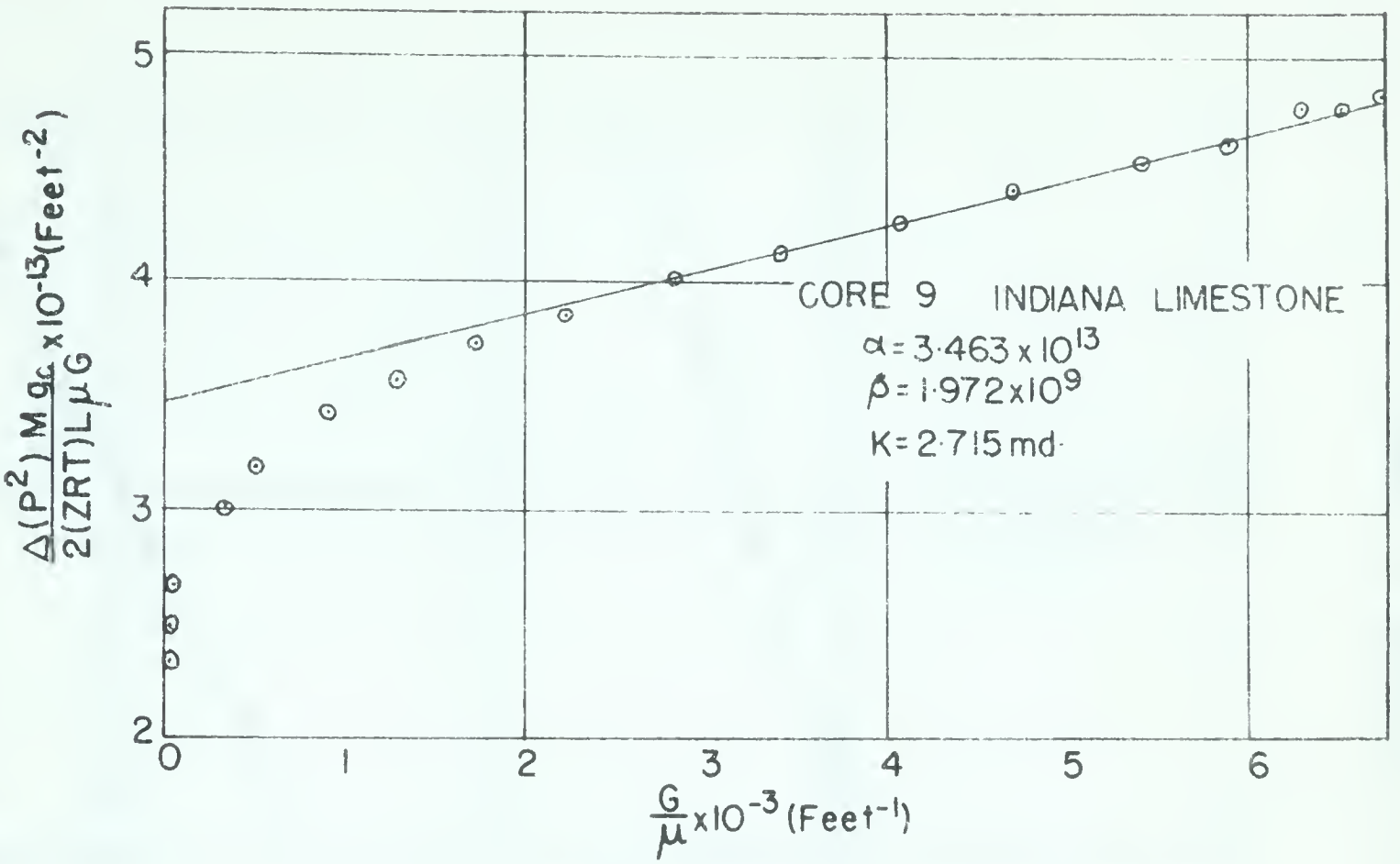

FIGURE 21 FLOW DATA PLOT TO OBTAIN α AND β

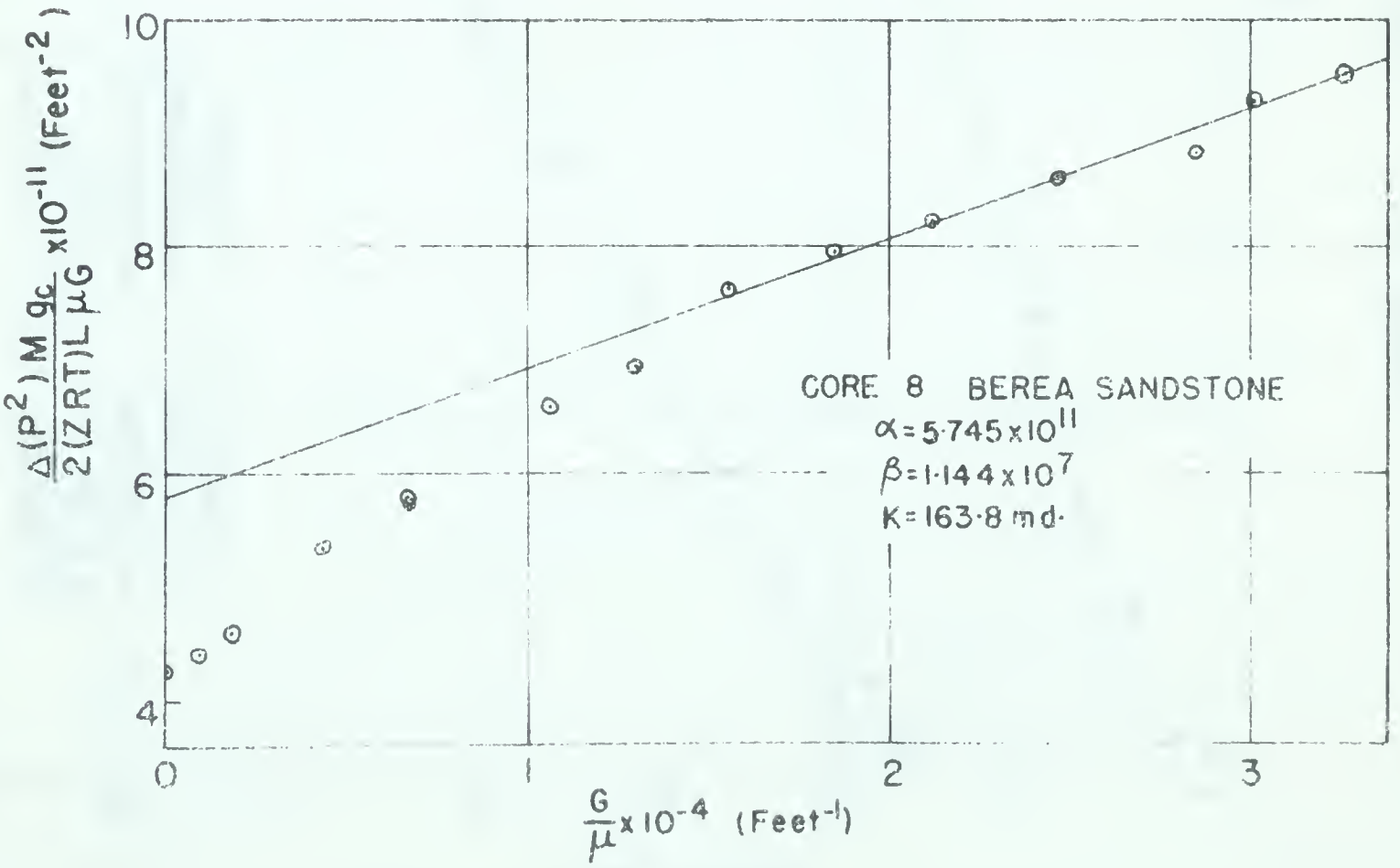

FIGURE 22 FLOW DATA PLOT TO OBTAIN α AND β

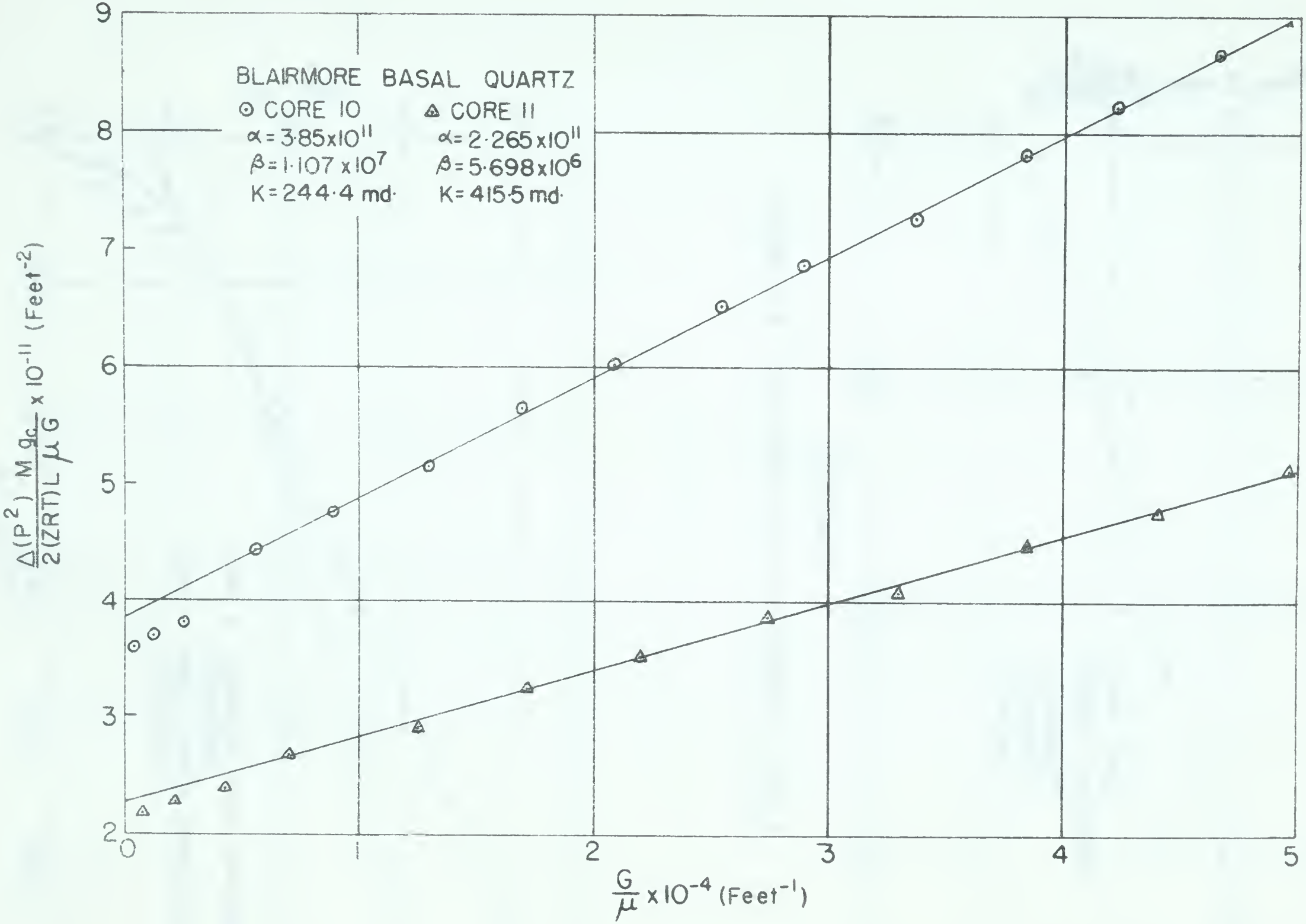

FIGURE 23 FLOW DATA PLOT TO OBTAIN α AND β

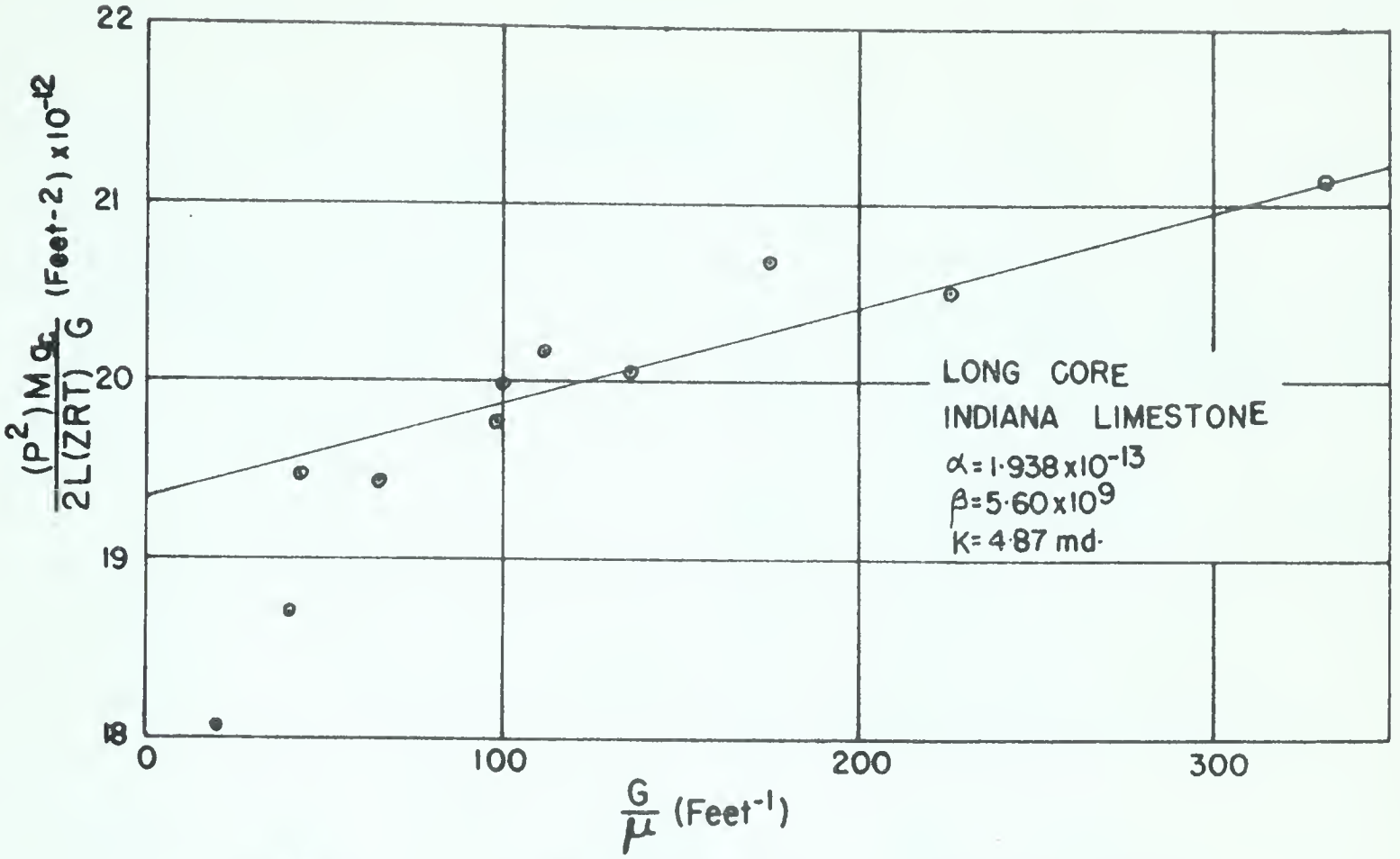

FIGURE 24 FLOW DATA PLOT TO OBTAIN α AND β

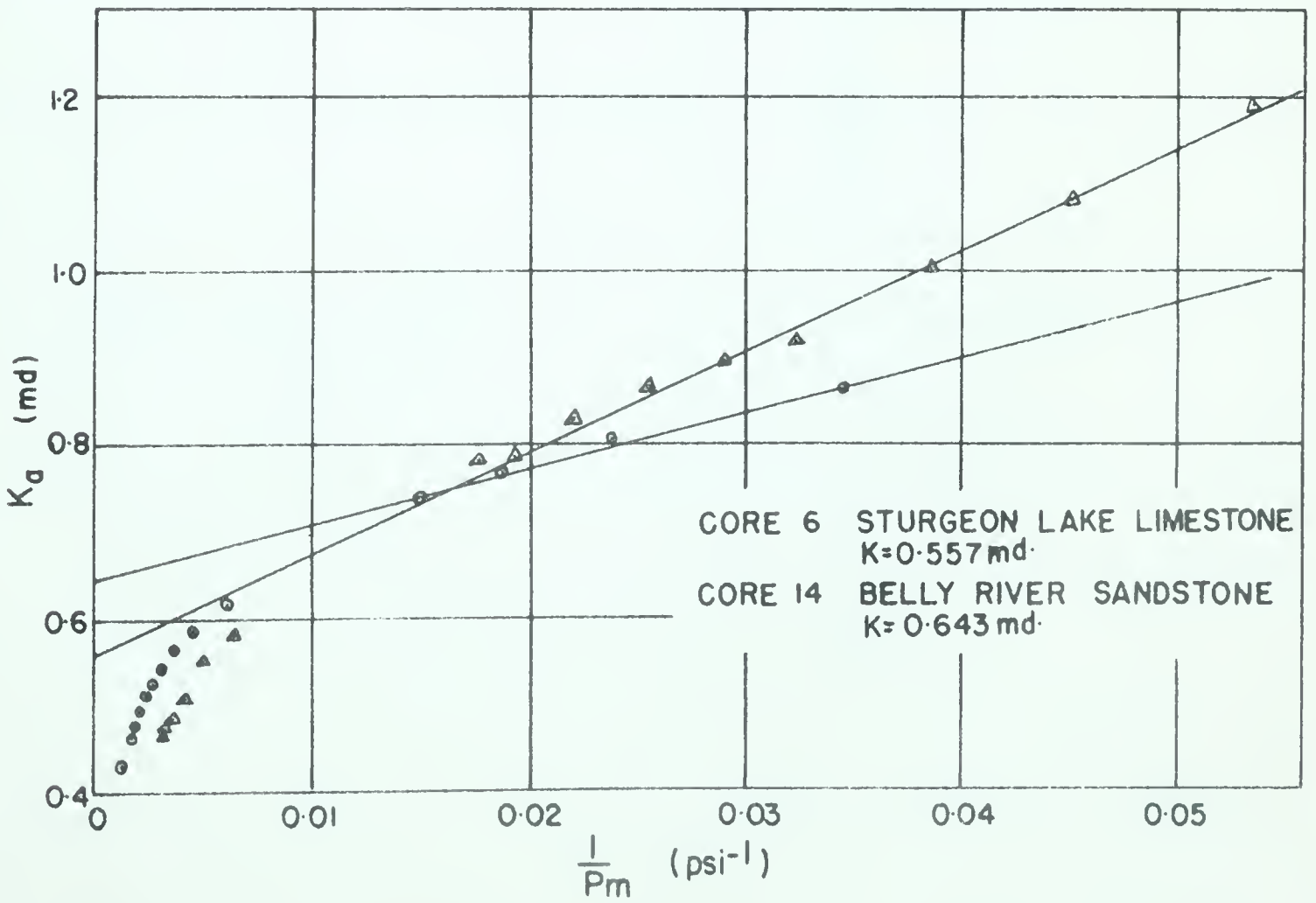

FIGURE 25 KLINKENBERG PERMEABILITY PLOT

APPENDIX II

EQUATIONS

$$Q_m = \frac{2\,Q_c\,P_b}{(P_1 + P_2)} \cdot \frac{T_f}{T_b}$$

Q_m = flow rate at mean pressure and flowing temperature
Q_c = flow rate at standard conditions, 14.65 psia and 60°F.
P_b = pressure base = 14.65 psia
T_f = average flowing temperature in °R
T_b = temperature base = 60°F.
P_1 = upstream pressure
P_2 = downstream pressure

$$K_a = \frac{Q_m}{A}\,\frac{L}{P_1 - P_2} = 2Q_c\,\frac{P_b}{(P_1^2 - P_2^2)} \cdot \frac{\mu L}{A} \cdot \frac{T_f}{T_b}$$

K_a = darcies
μ = cp
Q = cc/sec
L = cm
P = atm
A = cm^2
T = °R

$$K_a = 0.25573\,\frac{Q_c\,T_f\,\mu\,L}{(P^2)\,A}$$

K_a = millidarcies
T_f = °R
μ = micropoise
L = in
A = in^2
P = psia
Q_c = SCFH

$$\frac{M_{gc}}{2(ZRT)\mu L} = 52.0956 \times 10^{6} \cdot \frac{1}{ZT_f \mu L} \quad \frac{lb_m}{lb_f^2 \text{ sec}}$$

Z = compressibility
T_f = ^oR
μ = micropoise
L = in

$$G = \frac{Q_c \rho}{A} = .04 \frac{Q_c \rho}{A} \quad \frac{lb_m}{ft^2 \text{ sec}}$$

Q = SCFH
ρ = lb_m/ft^3
A = in^2
L = psia

$$\frac{\Delta(P^2)}{G} = 20736 \frac{\Delta(P^2)}{G} \quad \frac{lb_f^2 \text{ sec}}{lb_m \text{ ft}^2}$$

$$\frac{G}{\mu} = 148.8 \times 10^{5} \frac{G}{\mu} \quad \frac{1}{ft}$$

$$G = \frac{lb_m}{ft^2 \text{ sec}}$$

μ = micropoise

$$Q_c = Q \times \text{Meter Correction factor} \times \frac{P_M}{T_M} \times 35.495$$

Q = CFH
P_M = Meter inlet pressure in psia
T_M = Meter inlet temperature ^{o}

$P_M = P_{Atm.} + P_{\text{meter inlet (psig)}}$ - Partial Pressure of water

Sample Calculation

Measured Flow Data

Core #13 - Viking Sandstone

Area = 0.8101 in^2 Length = 1.4669 in Porosity = 10.28%
Volume Rate = 2.113 CFH
Temperature (meter) = 533.1 ^oR Vapor pressure = 0.8203 in Hg
Pressure (atmospheric) = 73.3 cm Hg = 13.567 psi
Flowing fluid - nitrogen
Temperature (average flowing) = 533.1 ^oR
$\mu_{(avg.\ T.\ and\ P.)}$ = 178.6 micropoise
P_1 = 367.7 psia
P_2 = 13.62 psia
P_{base} = 14.65 psia
T_{base} = 520 ^oR

Calculations

1. $Q_{(SCFH)} = Q_{(meter)} \times$ Meter Correction Factor $\times \frac{P_{meter}}{T_{meter}} \times \frac{T_{base}}{P_{base}}$

$Q_{(SCFH)}$ = 1.853 SCFH

2. $G = 0.04 \frac{Q_{(SCFH)}\rho}{A} = 1.694 \times 10^{-2} \frac{lb_m}{ft^2\ sec}$

3. $\frac{\Delta(P^2)}{G} = 20736 \frac{\Delta(P^2)}{G} = 4.136 \times 10^{11} \frac{lb_f^2\ sec}{lb_m\ ft^2}$

4. $\frac{Mg_c}{2(ZRT)\mu L} = 52.0956 \times 10^6 \times \frac{1}{Z\mu LT_f} = 3.738 \times 10^2 \frac{lb_m}{ft\ sec^2}$

5. $\frac{Mg_c\ \Delta(P^2)}{2(ZRT)\mu LG} = 15.461 \times 10^{13}\ feet^{-2}$

6. $\frac{G}{\mu} = 148.8 \times 10^5 \quad \frac{G}{\mu} = 564 \text{ feet}^{-1}$

7. $N_{Re} = \left(\frac{\beta}{\alpha}\right)\left(\frac{G}{\mu}\right) = 0.118$

8. $f = \frac{\Delta(P^2)\ Mg_c}{\beta(ZRT)\ LG^2} = 16.0$

APPENDIX III

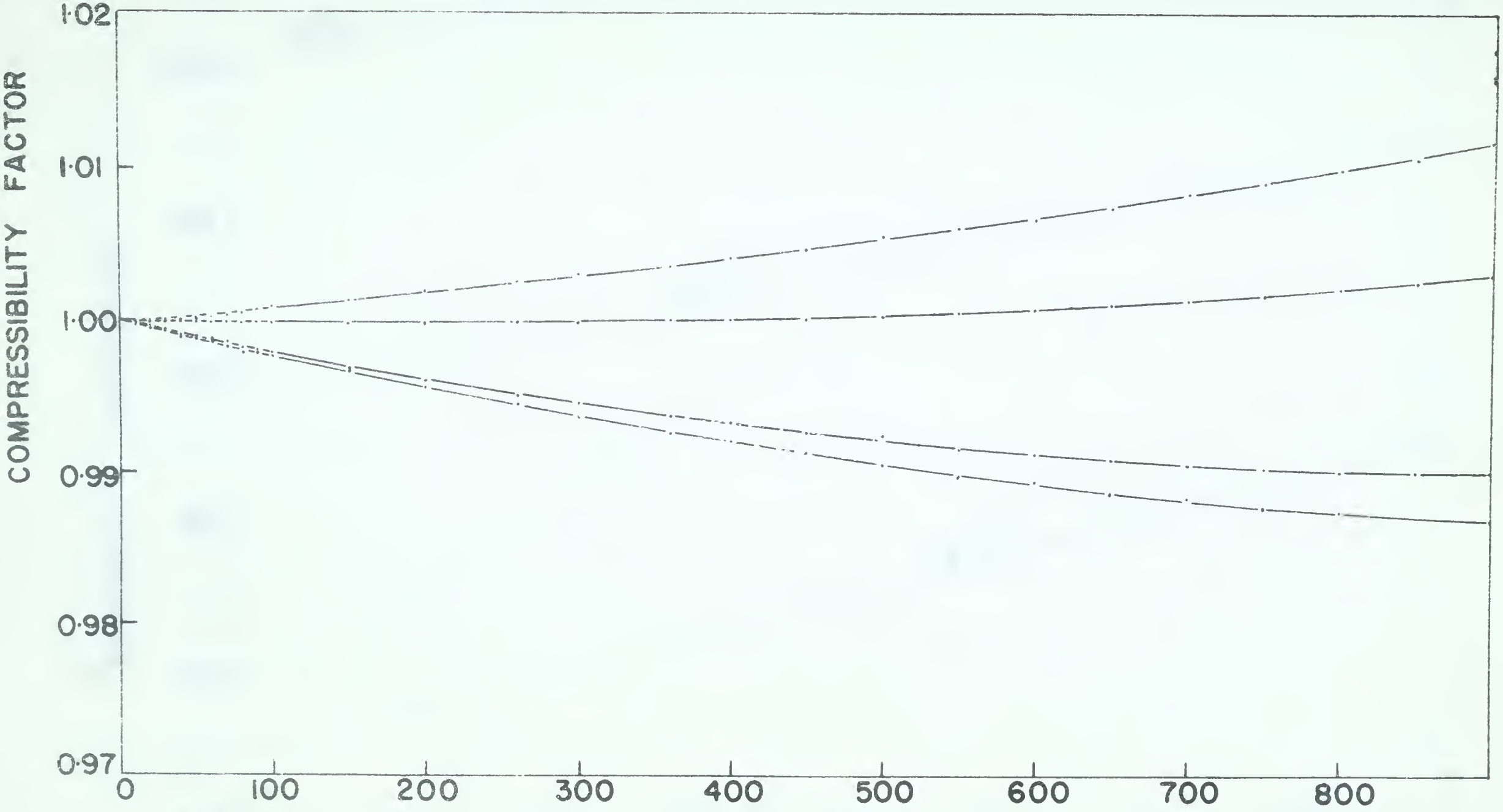

FIGURE 26 COMPRESSIBILITY FACTOR OF NITROGEN
(from Sage and Lacey 26)

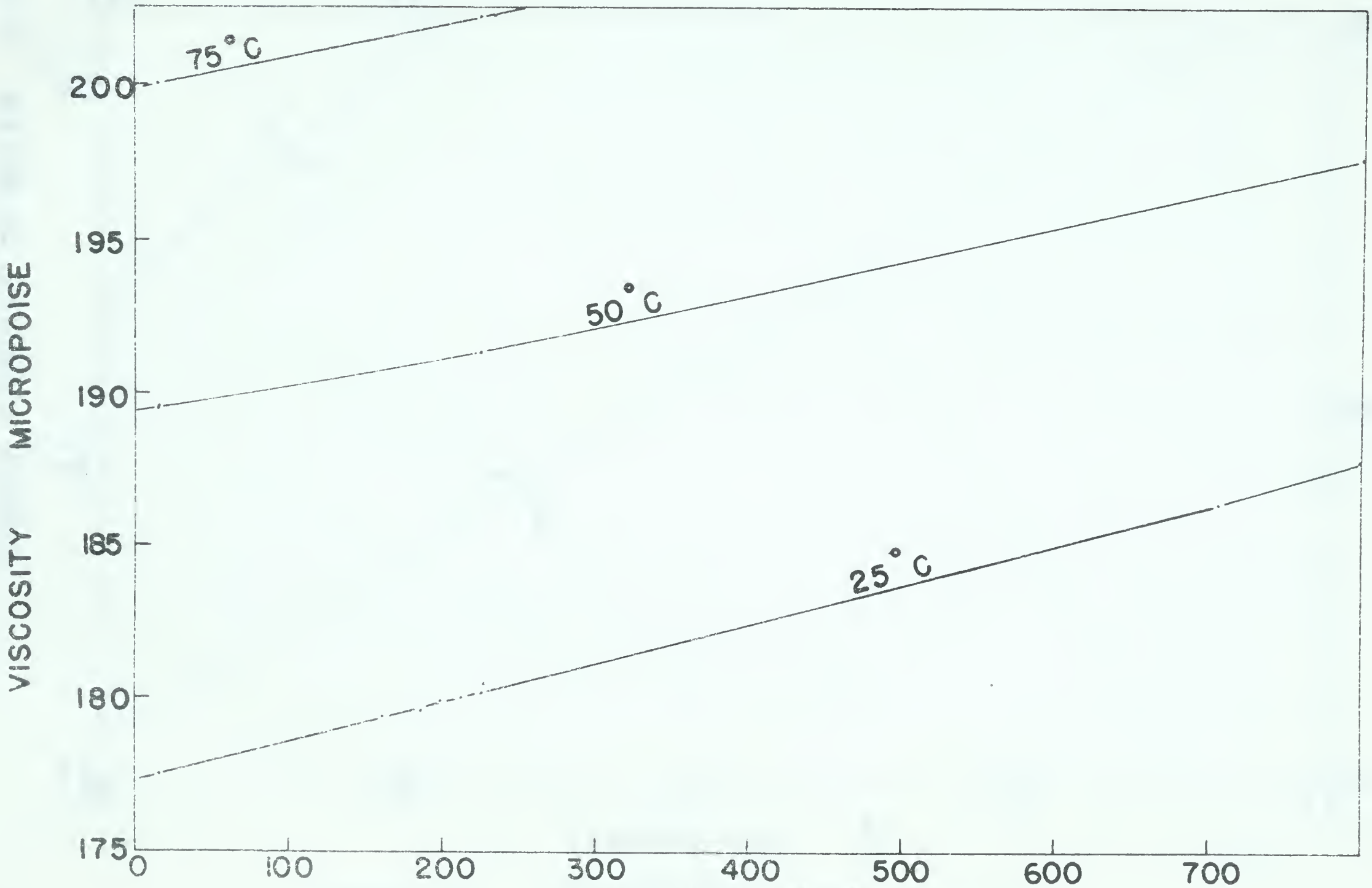

FIGURE 27 VISCOSITY OF NITROGEN
(from Michels and Gibson [22])

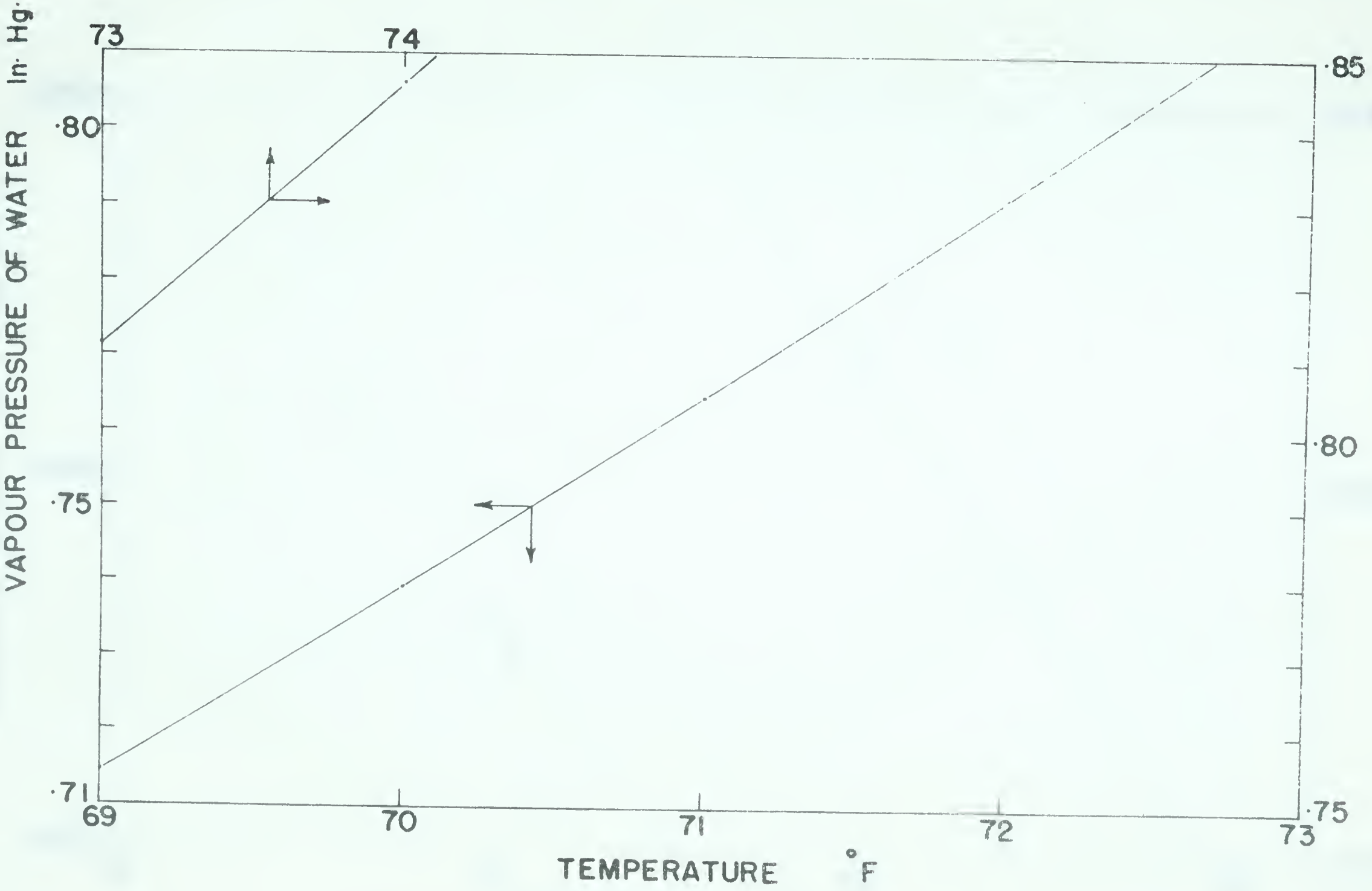

FIGURE 28 VAPOUR PRESSURE OF WATER
(Chem. Eng. Handbook)

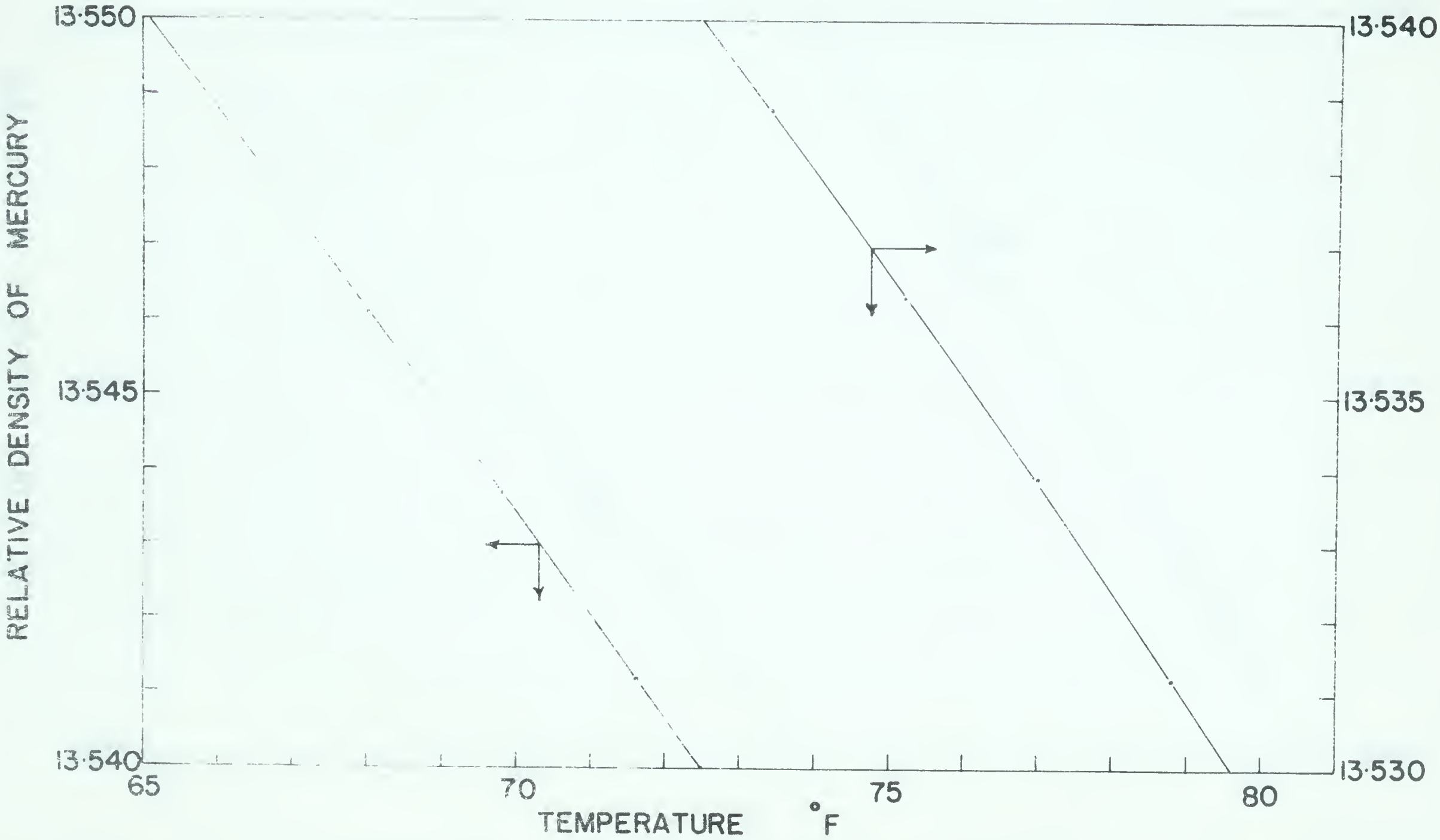

FIGURE 29 RELATIVE DENSITY OF MERCURY
(from Handbook of Chemistry and Physics [33])

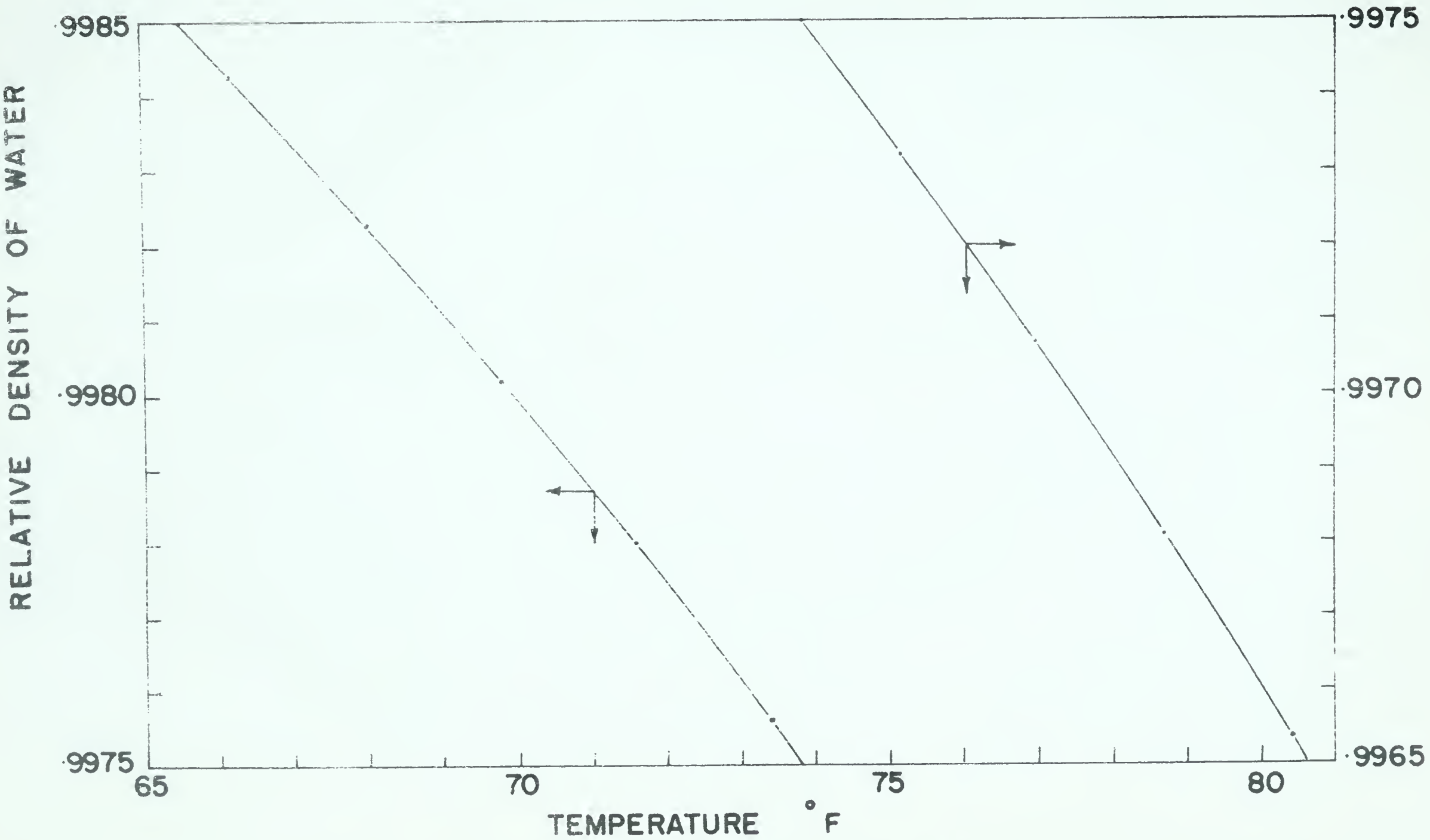

FIGURE 30 RELATIVE DENSITY OF WATER

B29805